MAY 1986

EPA REGIONAL OXIDANT MODEL:
ROM1 EVALUATION FOR 3-4 AUGUST 1979

ATMOSPHERIC SCIENCES RESEARCH LABORATORY
OFFICE OF RESEARCH AND DEVELOPMENT
U.S. ENVIRONMENTAL PROTECTION AGENCY
RESEARCH TRIANGLE PARK, NORTH CAROLINA 27711

EPA REGIONAL OXIDANT MODEL:
ROM1 EVALUATION FOR 3-4 AUGUST 1979

by

Kenneth L. Schere
Meteorology and Assessment Division
Atmospheric Sciences Research Laboratory
Research Triangle Park, North Carolina 27711

ATMOSPHERIC SCIENCES RESEARCH LABORATORY
OFFICE OF RESEARCH AND DEVELOPMENT
U.S. ENVIRONMENTAL PROTECTION AGENCY
RESEARCH TRIANGLE PARK, NORTH CAROLINA 27711

NOTICE

The information in this document has been subject to the United States Environmental Protection Agency's peer and administrative review and has been approved for publication as an EPA document. Mention of trade names or commercial products does not constitute endorsement or recommendation for use.

AFFILIATION

Mr. Schere is on assignment to the Meteorology and Assessment Division, Atmospheric Sciences Research Laboratory, from the National Oceanic and Atmospheric Administration, U.S. Department of Commerce.

ABSTRACT

The first generation U.S. Environmental Protection Agency Regional Oxidant Model (ROM1) has been tested and evaluated for O_3 predictions on a two-day test case episode in the northeast U.S. during 3-4 August 1979. The period was characterized by relatively high O_3 concentrations in the southern Great Lakes area where clear skies persisted. Intermittent periods of relatively high O_3 levels existed near some of the eastern seaboard cities where partly cloudy skies alternated with clouds and showers in the vicinity of a stationary frontal zone. The highest observed hour-average O_3 level monitored at a surface site during the period was 159 ppb.

The ROM1 incorporates some simplifying assumptions and algorithms as compared to the second generation version, ROM2, which is in preliminary testing stages now and will eventually become the production version of the model. Among these simplifications are the assumptions of flat terrain as well as temporally and spatially constant grid cell sizes. Also, preliminary versions of the chemical kinetic mechanism and source emissions inventory have been used. Evaluation results for this test episode showed that the ROM1 had approximately a 6% average underprediction of O_3 when all hours and surface monitoring sites were considered. When the data were restricted to only those observed and predicted pairs of O_3 values greater than 50 ppb the average performance improved to a 1% underprediction. The evaluation aspect concerned with estimating maximum daily O_3 values showed an 8% average underprediction of the maximum value for the restricted data subset. An analysis of individual O_3 plumes during the episode showed average model performance for predicting the plume maximum concentration level to lie between 22% underprediction and 38% overprediction.

CONTENTS

Abstract iii
Figures vi
Tables viii
Acknowledgements ix

1. Introduction 1
2. Test Episode: 3-4 August 1979 8
   Meteorological conditions 8
   Air quality conditions 12
   ROM1 initial and boundary concentrations 21
3. Results of Model Simulation for O_3 25
   Hourly data comparisons 25
   Maximum values analysis 54
4. Summary and Conclusions 93

References 99
Appendices

A. Listing of Surface Monitoring Stations 100
B. Maximum O_3 Values at Surface Monitoring Stations 110

Glossary 118

FIGURES

Number		Page
1	ROM grid resolution in the NEROS study region.	2
2	Surface weather map for 3 August 1979.	9
3	Surface weather map for 4 August 1979.	10
4	Maximum hourly values of O_3 observed at surface monitoring sites on 3 August 1979	13
5	Maximum hourly values of O_3 observed at surface monitoring sites on 4 August 1979	14
6	NEROS aircraft sampling flight paths on 3 August 1979.	17
7	NEROS aircraft sampling flight paths on 4 August 1979.	18
8	Flight paths and mixed layer O_3 concentrations during 3-4 August 1979	19
9	Histogram of observed O_3 concentrations at surface monitoring sites on 3-4 August 1979	27
10	Histogram of O_3 concentrations predicted by ROM1	29
11	Histogram of residual O_3 concentrations	31
12	Time-series over the 3-4 August 1979 simulation period	34
13	Histogram of observed O_3 concentrations (where obs. and pred. O_3 > 50 ppb)	43
14	Histogram of O_3 concentrations predicted by ROM1 (where obs. and pred. O_3 > 50 ppb)	44
15	Histogram of residual O_3 concentrations (where obs. and pred. O_3 > 50 ppb)	46
16	Time-series over the 3-4 August 1979 simulation period (where obs. and pred. O_3 > 50 ppb)	49
17	Scatterplot of (a) c_{p0}^{max} vs. c_{ob}^{max} and (b) $c_{p0}(h_{ob}^{max})$ vs. c_{ob}^{max} . . .	56
18	Scatterplot of (a) d_{B0}^{max} vs. c_{ob}^{max} and (b) d_{A0}^{max} vs. c_{ob}^{max}	58
19	Projected 12-hour forward trajectories on 3 August 1979 from selected urban source areas	63
20	Projected 12-hour forward trajectories on 4 August 1979 from selected urban source areas	64

Number		Page
21	Contours of hour-averaged predicted O_3 concentrations in ROM1 layer 1 on 3 August 1979 at (a) 1400 h and (b) 1600 h, LST . . .	66
22	Contours of hour-averaged predicted O_3 concentrations in ROM1 layer 1 on 4 August 1979 at (a) 1400 h and (b) 1600 h, LST . . .	68
23	Predicted and observed maximum O_3 concentrations (ppb) downwind of Toronto on 3 August 1979	71
24	Time-series of predicted and observed O_3 concentrations at monitoring site ORO on 3 August 1979	73
25	Predicted and observed maximum O_3 concentrations (ppb) downwind of Detroit and Cleveland on 3 August 1979	74
26	Time-series of predicted and observed O_3 concentrations at monitoring site SR2 on 3 August 1979	76
27	Predicted and observed maximum O_3 concentrations (ppb) downwind of New York on 3 August 1979	77
28	Time-series of predicted and observed O_3 concentrations at monitoring site GRW on 3 August 1979	79
29	Predicted and observed maximum O_3 concentrations (ppb) downwind of Toronto on 4 August 1979	81
30	Time-series of predicted and observed O_3 concentrations at monitoring site ORO on 4 August 1979	82
31	Predicted and observed maximum O_3 concentrations (ppb) downwind of Detroit on 4 August 1979	84
32	Time-series of predicted and observed O_3 concentrations at monitoring site PTR on 4 August 1979	85
33	Predicted and observed maximum O_3 concentrations (ppb) downwind of New York and Philadelphia on 4 August 1979	87
34	Time-series of predicted and observed O_3 concentrations at monitoring site MER on 4 August 1979	88
35	Time-series of predicted and observed O_3 concentrations at monitoring site VIN on 4 August 1979	90

TABLES

Number		Page
1	Summary of NEROS aircraft sampling flights -- 3-4 August 1979. . .	16
2	Set of initial and boundary species concentrations used in ROM1. .	26
3	Summary of ROM1 hourly results for 3-4 August 1979	38
4	Summary of ROM1 hourly results for 3-4 August 1979 where observed and predicted O_3 > 50 ppb	51
5	Summary of ROM1 results for local maximum values for 3-4 August 1979.	61
6	Summary of ROM1 results for global maximum values for 3-4 August 1979.	91

ACKNOWLEDGMENTS

Discussions with Dr. Robert Lamb were very helpful in the interpretation of ROM1 evaluation data and in assessing the results. Appreciation is also extended to Mr. Larry Bergman of Computer Sciences Corporation and Mr. Dale Coventry for developing the computer graphics programs for this project.

SECTION 1

INTRODUCTION

The United States Environmental Protection Agency's Regional Oxidant Model (ROM) has been under development and testing for a number of years. The model formulation and developmental tests have been thoroughly documented in a series of reports (Lamb, 1983, 1984, 1985). The ROM attempts to simulate all of the important physical and chemical processes that affect the generation and dispersion of photochemical smog on regional scales (up to 1000 km). In the present configuration of the ROM domain, the model's horizontal resolution is approximately 18.5 km. In the vertical there are 3 1/2 layers. The first and second layers encompass most of the planetary boundary layer above the surface of the earth and the third layer is the cloud layer extending from cloud base to near the tops of any cumulus-type clouds. Layer 0 is a shallow layer adjacent to the surface designed to treat sub-grid scale effects in the ROM. It is handled in a diagnostic manner within the model.

The horizontal spatial extent of the first ROM application is shown in Figure 1. This model domain includes the areas covered by special field monitoring projects during the summers of 1979 and 1980. During these projects highly resolved air quality, meteorological, and source emissions data bases were developed for the study area, hereafter referred to as the NEROS region (Northeast Regional Oxidant Study). The field projects conducted in the NEROS region included those of the 1980 Northeast Corridor Regional Modeling Project (NECRMP), focusing on the larger urban areas bordering the Atlantic coast, as well as the regionally-oriented NEROS projects (Possiel and Freas, 1982; Vaughan, 1985). The specific episode studied in this report occurred during 3-4 August 1979, during the first NEROS field project. Meteorological and air quality details of this episode are described in the next section.

The ROM version used in this modeling study is the first generation model (ROM1). Several aspects of the ROM1 modeling system are in preliminary or simpler form as compared to that described in the full ROM documentation (Lamb, 1983, 1984, 1985). These aspects include the following considerations:

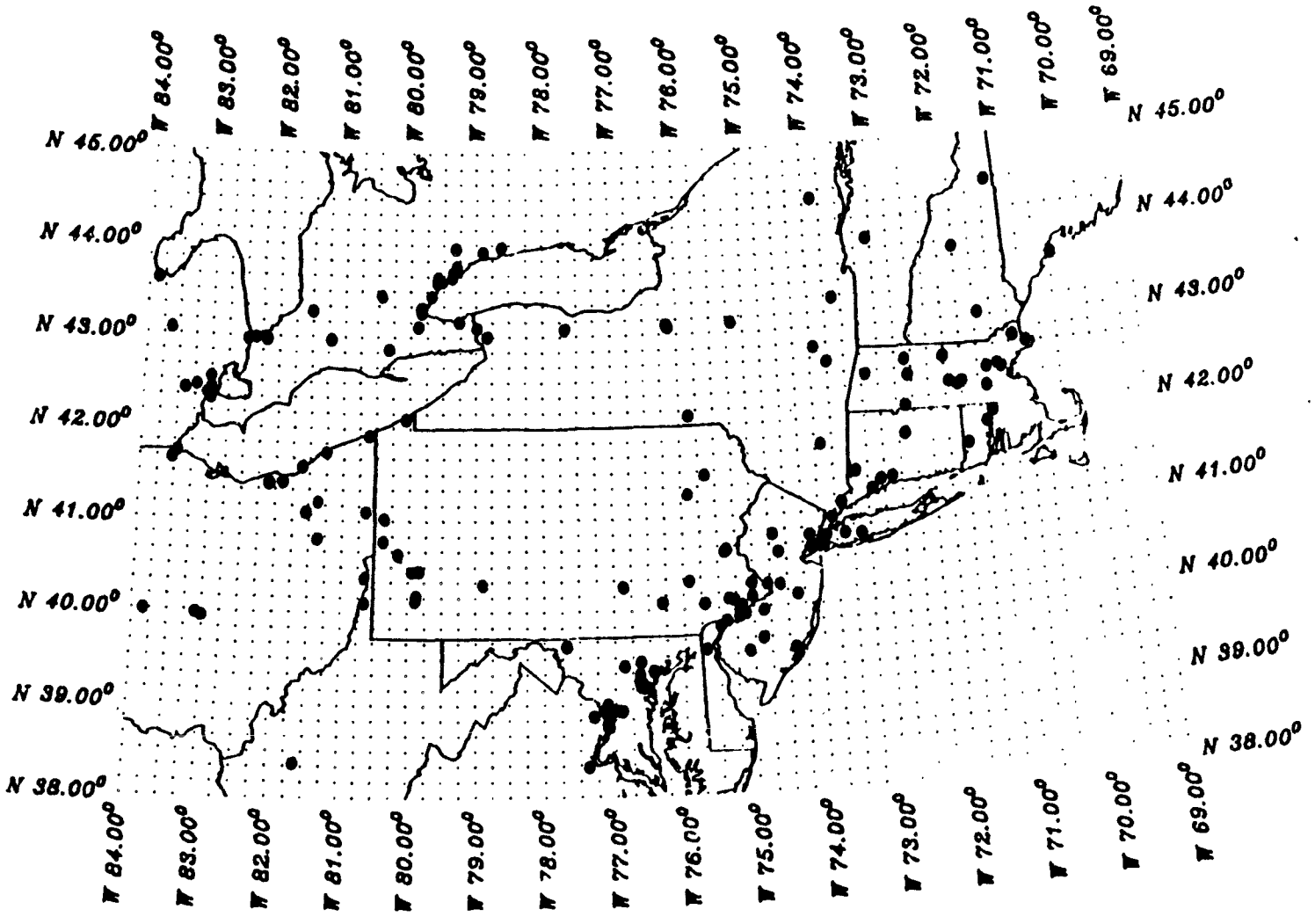

Figure 1. ROM grid resolution in the NEROS study region. O_3 monitoring stations operating during the 3-4 August 1979 period are indicated by dots.

(1) The source emissions inventory is the preliminary one developed during the NECRMP project. It does not contain biogenic sources of hydrocarbon species. Eventually, the newer NAPAP (National Acid Precipitation Assessment Program) emissions inventory, including biogenic emissions, will be used in ROM studies of the NERUS region.

(2) The wind fields generated to drive the horizontal advection component of the model are derived, for all 3 model layers, from objective interpolation of measured surface and upper air winds. Later wind field processors for layer 1 will include a predictive hydrodynamic model of winds in the nighttime boundary layer.

(3) Vertical cloud flux parameters are now pre-specified in the ROM1. Later versions will incorporate a cloud flux module that calculates vertical flux velocities based on a computed moist convection level for each grid cell.

(4) A single wind field interpolation (realization) for each hour of model simulation is used for each of the ROM1's three prognostic layers. The wind processor currently under development provides multiple wind realizations for each hour with a probability-weighted likelihood of occurrence for each.

(5) The vertical dimension of all grid cells in any given layer in ROM1 is constant in space and time. Also, a flat surface is assumed to exist beneath the model domain. The relevant vertical dimensions are 40 m for layer 0, 400 m for layer 1, 800 m for layer 2, and 800 m for layer 3. The next model version will provide for terrain relief at the surface (no flat surface assumption made) and for spatially and temporally variable cell heights across the domain. The vertical size of any given cell will be a function of the locally occurring physical phenomena.

The model features described above that are not yet implemented will become part of the second generation regional model, ROM2, scheduled to

become operational shortly. The final major difference between ROM1 and ROM2 is in the chemical kinetic mechanism. ROM1 contains a 23-species, 36 reaction step mechanism developed by Dr. Ken Demerjian of EPA, while ROM2 will contain a 28-species, 70 reaction step mechanism, Carbon Bond IV (CB-IV), developed by Dr. Gary Whitten of Systems Applications, Inc. The CB-IV mechanism contains an explicit reaction pathway for the biogenic hydrocarbon species, isoprene. This will allow the ROM2 to accommodate biogenic species in the source emissions inventory; ROM1 has no provision for biogenic species.

This report discusses the evaluation of ROM1 results for O_3 predictions on the 3-4 August 1979 episode in the NEROS region. The evaluation has been structured in a manner designed to elicit the ROM1's performance for prediction of hourly and maximum O_3 concentrations. The primary function of the Regional Oxidant Model is to evaluate the effects of various emission control strategies on the maximum O_3 concentrations generated by these precursor emissions. Ideally, the model would be tested on two data bases separated by a number of years encompassing actual changes in emission inventories and the resulting air quality. This goal is not yet attainable because of a scarcity in regional scale emission inventory data for previous years, although in the future such a test should be possible. At present our confidence in the ROM1's ability to replicate the spatial and temporal O_3 patterns resulting from the base year precursor source emissions inventory is a necessary step in the evaluation process. This step is necessary because the non-linear physical and chemical reaction effects that result in the production of ambient O_3 concentrations preclude one from assuming that changes in precursor emissions may be linearly mapped into changes in the resulting O_3. It is necessary to verify photochemical models in an absolute sense for model predictions as well as relatively for source emissions changes. The sufficient condition for evaluating the Regional Oxidant Model must await the establishment of multiple base year emission inventories separated in time by a number of years to verify actual ambient air quality changes with respect to emissions changes.

The present task therefore is to evaluate the absolute magnitudes and patterns of O_3 concentrations predicted by the ROM1. The planned procedures for model evaluation for ambient simulations have been documented

in a previous report (Schere and Fabrick, 1985). We will follow the protocol discussed therein to the extent that the available data and resources permit. The evaluation procedure includes several levels of analysis. The first level explores the observed data set to bring out the important features, both on temporal and spatial scales. This includes an analysis of the existing meteorological conditions during the simulation period to provide a background context in which the air quality conditions evolve. Next the spatial and temporal patterns of O_3 concentrations from surface monitors and aircraft sampling are studied to highlight the significant phenomena occurring in the modeling domain. It is these features that the model should be able to replicate during the simulation.

The next level of analysis explores the comparison between ambient O_3 observations and the model-predicted concentrations. First, the comparison is made for all hourly observations at all monitoring sites. This analysis brings out gross features of model performance including any systematic trends in model bias. Subsets of the full data set are used to explore particular aspects of the comparisons, such as whether the model predicts O_3 concentrations more accurately at higher values than lower values. Next, comparisons are made between maximum daily O_3 concentrations at surface monitoring sites and model predictions of O_3 maxima. These comparisons are performed in a number of ways. First, daily maxima at all surface monitoring locations are matched with model predictions at those locations. The analysis on these data pairs is conducted with statistical tests and graphical analyses such as scatterplots and is designed to elicit the ability of the model to predict O_3 maxima over the entire modeling domain. Of course, over the size area contained in a regional modeling domain the areas of maximum O_3 are generated from different precursor source emissions regions and are affected by different meteorological influences. Therefore, in an effort to isolate the model performance for a given source area, O_3 plumes are individually identified and the model's ability to predict maximum O_3 concentrations within the plume is evaluated. Both types of maximum values analyses are necessary in conjunction with assessing the ROM1 as a tool for emission control

strategy assessment. Examining all daily O_3 maximum values together illustrates the potential effects of a control strategy on the entire region while individual plumes will highlight any O_3 reductions from the controls on a particular urban source area.

The inherent uncertainty in model predictions on the regional scale should be factored into an analysis of the results from the Regional Oxidant Model. This uncertainty evolves from measurement and estimation errors in model input parameters as well as uncertainty from the empirical parameterizations used throughout the modeling system. Perhaps the greatest area of uncertainty though is in the horizontal transport portion of the model. Lamb (1983) discusses this aspect of model uncertainty. Basically the heart of the problem is that there does not exist a unique transport field that can be determined for a model simulation based on the existing wind monitoring network. In fact, on the 1000-km regional scale it would be impractical to design a network dense enough to unambiguously determine the transport for the model.

In the analyses of model results presented here for the entire model domain at once (i.e. all receptor locations considered together) this transport uncertainty is not considered. Thus if the simulated transport field carries a plume of O_3 in a slightly different direction from the actual field such that a monitoring site that was directly affected by the plume appears to have been bypassed in the simulation, a large underpredictive bias will result. The converse situation will result in an overpredictive bias. In the analysis for individual plume maximum O_3 concentrations the transport uncertainty is considered in that the observed and predicted plumes of O_3 from major source areas are identified separately by the observations and predictions. Maximum O_3 values are matched in such a way as to compensate for the transport uncertainty.

The second generation, ROM2, modeling system will include an objective method of interpolating winds from the existing observation network that will produce a family of legitimate wind field "realizations", each with

an assigned probability of occurrence. This will enable the model evaluation analysis to directly consider the effects of inherent transport uncertainty. The single wind field used in the ROM1 simulation is considered the field with the greatest probability of occurrence.

Figure 1 shows the extent of the ROM1 domain in the NEROS application. There are 60 cells in the E-W direction and 42 cells in the N-S direction. The dimensions of each individual grid cell are 15 minutes of longitude (E-W) and 10 minutes of latitude (N-S), or about 18.5 km square cells. There are approximately 200 SAROAD air monitoring sites measuring hourly ambient O_3 concentrations within the NEROS region, although at any given day and hour only a subset of these sites generally is actively measuring. The locations of the SAROAD monitoring stations measuring O_3 during the 2 day modeling episode are shown in the figure. Appendix A contains a list of those stations (as well as others) along with their grid coordinates.

SECTION 2

TEST EPISODE: 3-4 AUGUST 1979

The data base used here to test and evaluate the O_3 simulation results from ROM1 corresponds to that of 3-4 August 1979. This 2-day period occurred during the 1979 NEROS summer field study which included enhanced meteorological and air quality measurements in the northeast United States. A detailed description of the NEROS data base is not included here, but a summary can be found in the ROM evaluation protocol report (Schere and Fabrick, 1985) and further details are in the reports of Possiel and Freas (1982), Freas (1983), Vaughan (1985), and others. This section discusses the meteorological conditions prevalent during the test period as well as the observed surface O_3 monitoring data.

Meteorological Conditions

On 2 August 1979, a weak area of low pressure traveled northeast from the Illinois-Indiana area through Michigan into Ontario. The trailing cold front moved eastward just off the Atlantic coast by the morning of 3 August, and became stationary. A low pressure area developed on the stationary front near the coast of Virginia and widespread cloudiness and showers were prevalent along the Atlantic seaboard, traveling generally from the mid-Atlantic coast on 3 August to the northeast coast on 4 August. A large area of high pressure built into the eastern U.S. from the midwest after the passage of the cold front. Aside from being slightly drier the newer air mass was not substantially different than the older air mass. Highest temperatures throughout the NEROS study area were generally from the mid to upper 80's (°F). Figures 2 and 3 show the 7a.m. (EST) surface weather map features for the U.S. for the 2 day period under study.

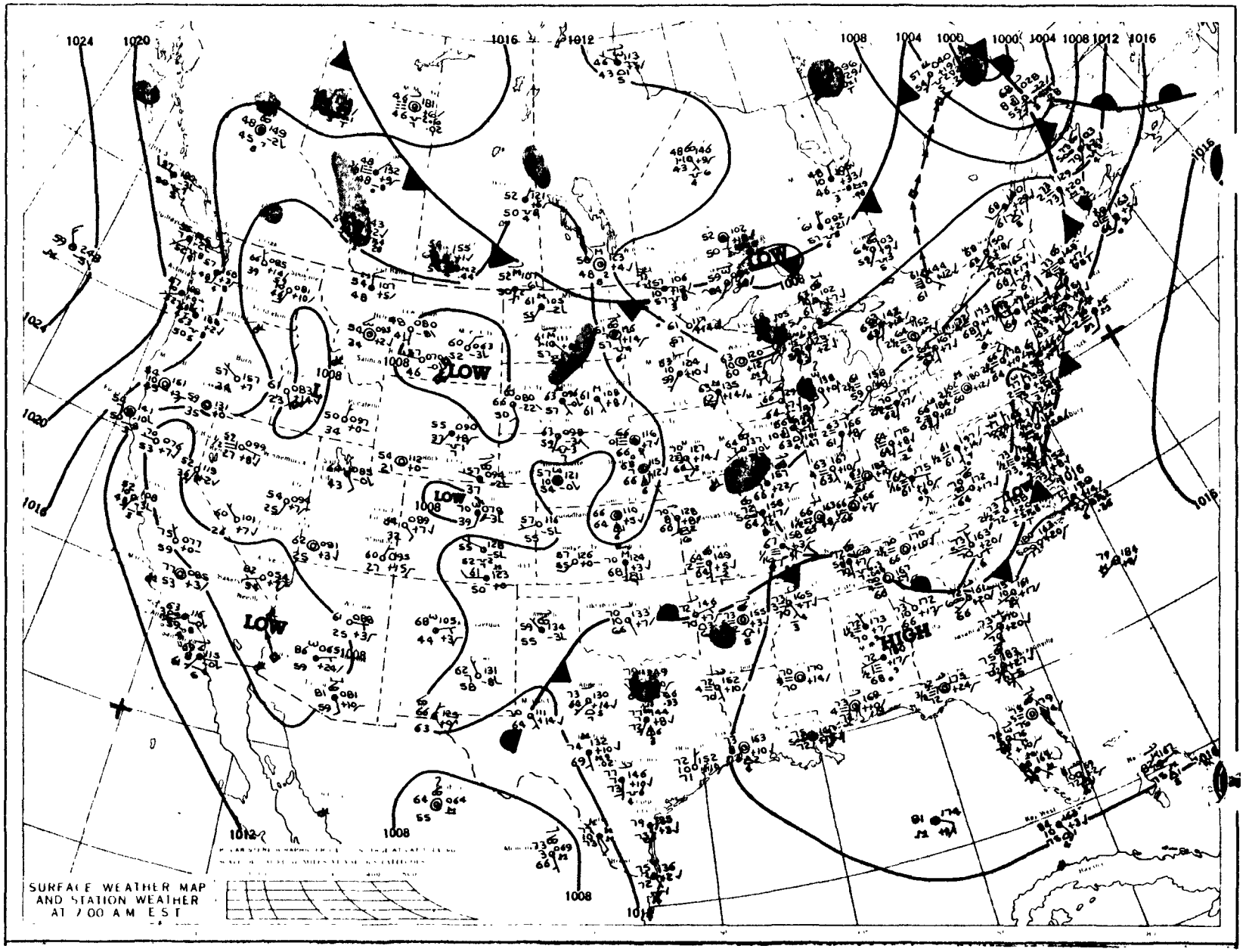

Figure 2. Surface weather map for 3 August 1979.

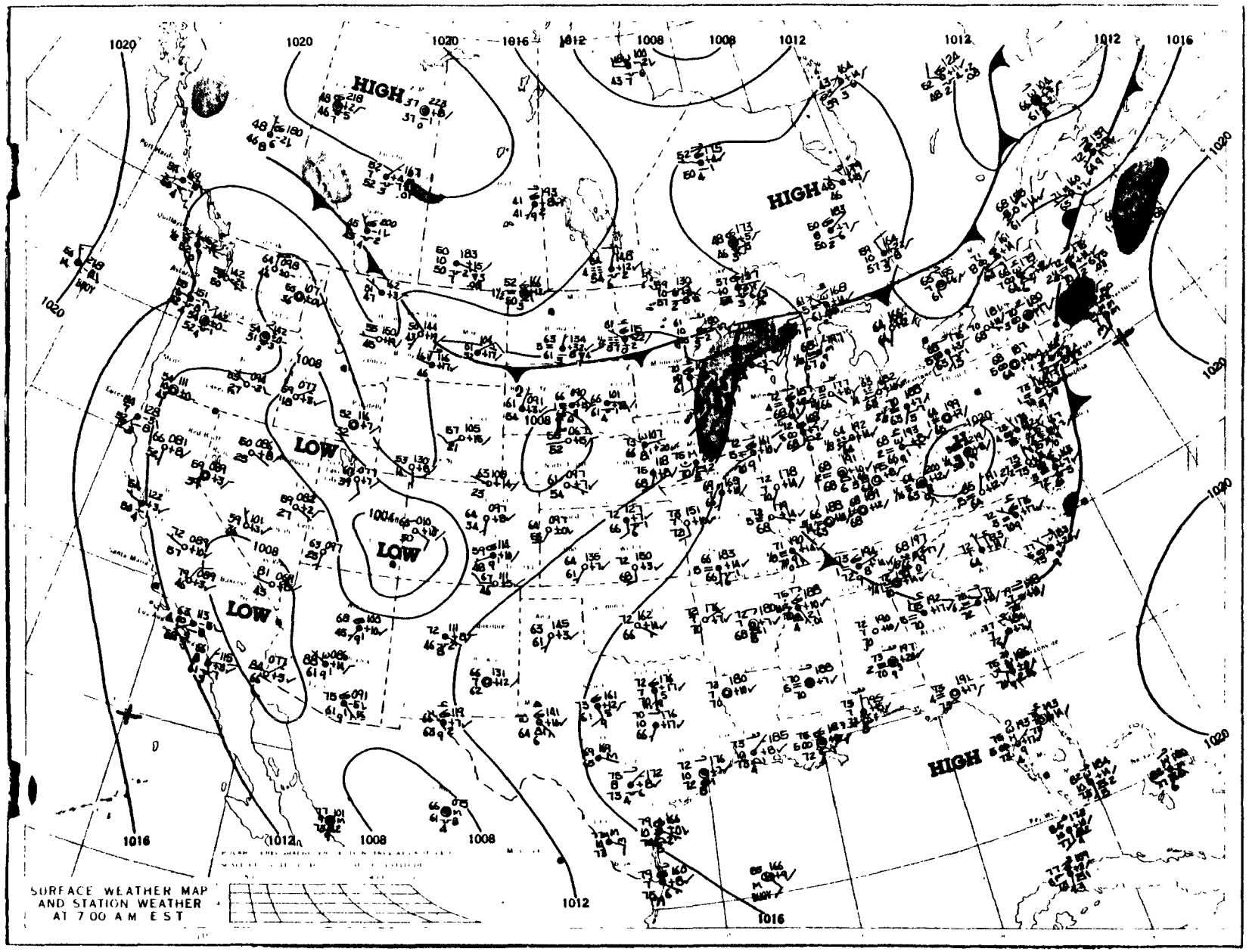

Figure 3. Surface weather map for 4 August 1979.

The atmospheric pressure gradient aloft was very weak, with accompanying low wind speeds. On 3 August, the 500 mb flow was generally from the SW ranging in speed from 5 m/s over Virginia to 20 m/s over New York and New England. On 4 August, the 500 mb flow was from the W through SW at speeds of 5-10 m/s over the NEROS region. Surface winds were of lighter speed and similar direction.

Examining the surface observation record from selected stations during this period shows the western part of the NEROS region (Ohio, western Pennsylvania and New York, Ontario) to be generally cloud-free or with scattered high cirrus-type clouds. Haze was reported at many ground stations. The eastern seaboard cities were generally under heavy cloud cover with occasional showers. For instance, Washington, D.C. reported ceiling heights of 2000 to 6500 feet above ground on 3 August, with rain showers. By the next day the cloudy area had moved north and Washington was generally clear with some haze. On 3 August, Bridgeport, Connecticut showed generally clear skies, although to the south and east heavier cloudiness was reported. The next day Bridgeport was under low clouds with showers. In contrast the station reports from Buffalo, New York and Detroit, Michigan reported mostly clear skies throughout the period.

In assessing the impact of the synoptic meteorological features on the photochemical smog potential over the NEROS study area it seems clear that the area of greatest interest would be the Ohio valley through the Great Lakes into Ontario for this 2 day period. Wind speeds were light but of persistent direction here and skies were clear. The eastern seaboard cities were under partially clear skies for only part of the period, or not at all. Surface wind directions were quite variable here also. The effects of these meteorological conditions would be to suppress the photochemical potential in the East , although for brief periods during the daytime when skies cleared there would be a local increase in the potential.

Air Quality Conditions

Figures 4 and 5 display the maximum values of hourly averaged O_3 measured at the U.S. SAROAD monitoring stations in and just outside of the ROM1 model domain and the Ontario stations within the domain for 3 August and 4 August, respectively. The surface stations are not distributed evenly across the region. They tend to be clustered in the vicinity of urban areas, leaving large portions of the model domain with little or no surface monitored O_3 data. Scarcity of data is especially apparent in the region stretching from the Ohio Valley northeast through central and northern New York state, except for the Pittsburgh area. Model performance in the central section of the grid will therefore be difficult to judge, except in a gross sense. The Northeast corridor of cities is well represented, as is, to a lesser degree, the industrialized areas near the Great Lakes.

The 3-4 August 1979 period was not a major episode for O_3, although values exceeded 100 ppb in selected areas. On 3 August, despite the cloud cover over the mid-Atlantic seaboard some O_3 values reached between 100 and 115 ppb in the Washington and Philadelphia areas and between 120 and 130 ppb in the New Jersey, New York and Connecticut area, where there was less cloud cover on that day. Measured O_3 values around 100 ppb were found downwind of Detroit and Toronto. Other measured values in the vicinity of the Great Lakes and Ohio Valley were not high, except for near the southeast shore of Lake Erie, where Conneaut, Ohio recorded 159 ppb as the daily maximum. The diurnal record of measured O_3 at that station is an interesting one. Hourly concentrations at Conneaut from 0800 to 1200 h, LST are 29, 40, 82, 100 and 132 ppb. The very rapid rise in concentration between 0900 and 1000 h might suggest the entrainment of O_3 from a plume aloft rather than from local photochemical generation near the surface. Measured O_3 data from aircraft flights during the NEROS study should help determine the validity of this premise.

On 4 August, the overcast and rainy conditions along the Atlantic coast from New York northward did, in fact, seem to suppress O_3 generation. South of New York however, relatively high levels were measured near the Philadelphia

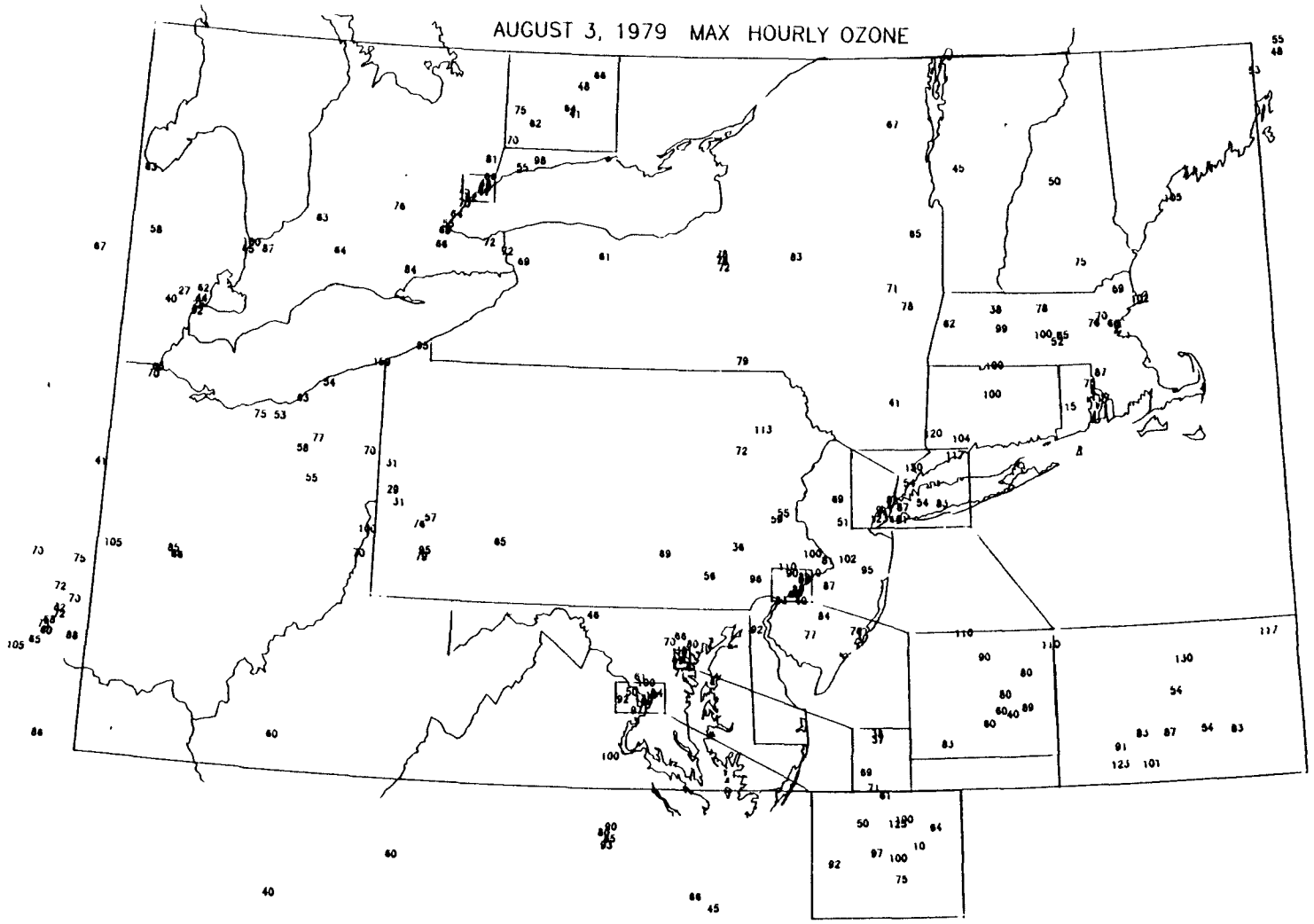

Figure 4. Maximum hourly values of O_3 observed at surface monitoring sites on 3 Aug. 1979.

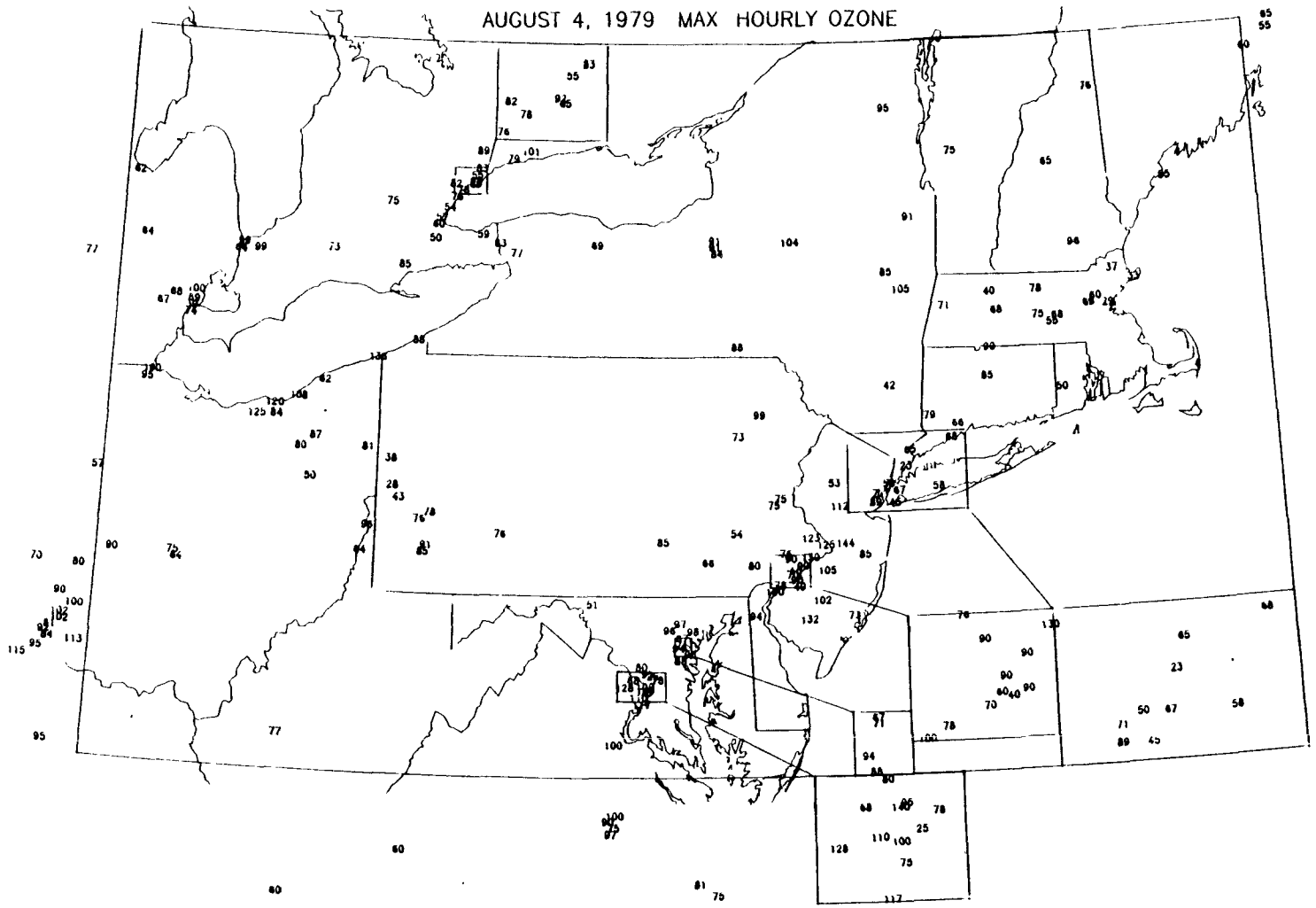

Figure 5. Maximum hourly values of O_3 observed at surface monitoring sites on 4 Aug. 1979.

area (143 ppb) and Washington, D.C. (139 ppb) where skies had cleared. Several observation stations along the south shore of Lake Erie reported maximum O_3 levels from 120-135 ppb. Most other areas of the NEROS region reported low values, except for a few observations near 100 ppb downwind of Detroit and Toronto.

Numerous aircraft transects were made over the NEROS region during the 3-4 August period. Participating aircraft included those from Washington State University (WSU), Research Triangle Institute (RTI), and Brookhaven National Lab (BNL). A listing of the flights made is given in Table 1 and the approximate flight paths are shown in Figures 6 and 7 for 3 August and 4 August, respectively. The temporal progression of flights from west to east reflects the Lagrangian sampling strategy of attempting to follow an area of high pollutant concentrations over the Midwest as it is transported east. Flights outside of the Lagrangian sampling were made as well.

The aircraft O_3 measurements were made mostly within the boundary layer, within 2 km of the earth's surface. The sampling altitude corresponds generally to layers 2 and 3 of ROM1. Aircraft observations have the advantage of being more representative of the boundary layer than measurements made only at the surface, but also have the disadvantage (from the perspective of Eulerian modeling) of being very short-lived at any one location. The aircraft measurements of O_3 help determine the regional background O_3 burden. Flight A, the RTI aircraft transect over the Ohio-Lake Erie region during midday on 3 August showed 60-70 ppb of O_3 in the upper portion of the troposphere and 70-80 ppb of O_3 in the lower portion. Slightly lower values (by about 5-10 ppb) were seen on the return portion of the RTI flight that night, flight C. The remaining flights made on 3 August, flights B and D by WSU, showed somewhat higher background O_3 values in the central portion of the NEROS region. The range here was 70-90 ppb O_3 during the afternoon and late evening, with higher values to the north in an area of relatively high O_3 near the Great Lakes. The general boundary layer O_3 pattern on 3 August was constructed by Clarke et al. (1983) from the aircraft measurements made on that day, and is reproduced here in Figure 8. It shows the area of high O_3 concentrations mainly over

TABLE 1. SUMMARY OF NEROS AIRCRAFT SAMPLING FLIGHTS - 3-4 AUGUST 1979

Flight	Date	Operator	Start Time (h, LST)	End Time (h, LST)	Start Location	End Location
A	3 Aug. 1979	RTI	11:54	13:59	39°48'N 82°40'W	43°55'N 79°25'W
B	3 Aug. 1979	WSU	17:09	19:37	39°18'N 81°32'W	43°20'N 78°10'W
C	3 Aug. 1979	RTI	22:31	00:42	43°55'N 79°25'W	39°48'N 82°40'W
D	3 Aug. 1979	WSU	23:07	02:25	43°07'N 77°40'W	40°07'N 76°18'W
E	4 Aug. 1979	BNL	07:03	09:35	42°51'N 76°19'W	39°05'N 78°45'W
F	4 Aug. 1979	RTI	12:47	15:21	39°08'N 82°05'W	42°56'N 82°35'W
G	4 Aug. 1979	BNL	13:18	15:32	39°28'N 77°26'W	41°23'N 73°50'W
H	4 Aug. 1979	WSU	17:20	19:15	40°07'N 76°18'W	41°10'N 80°40'W
I	4 Aug. 1979	RTI	20:43	23:06	42°56'N 82°35'W	39°08'N 82°05'W

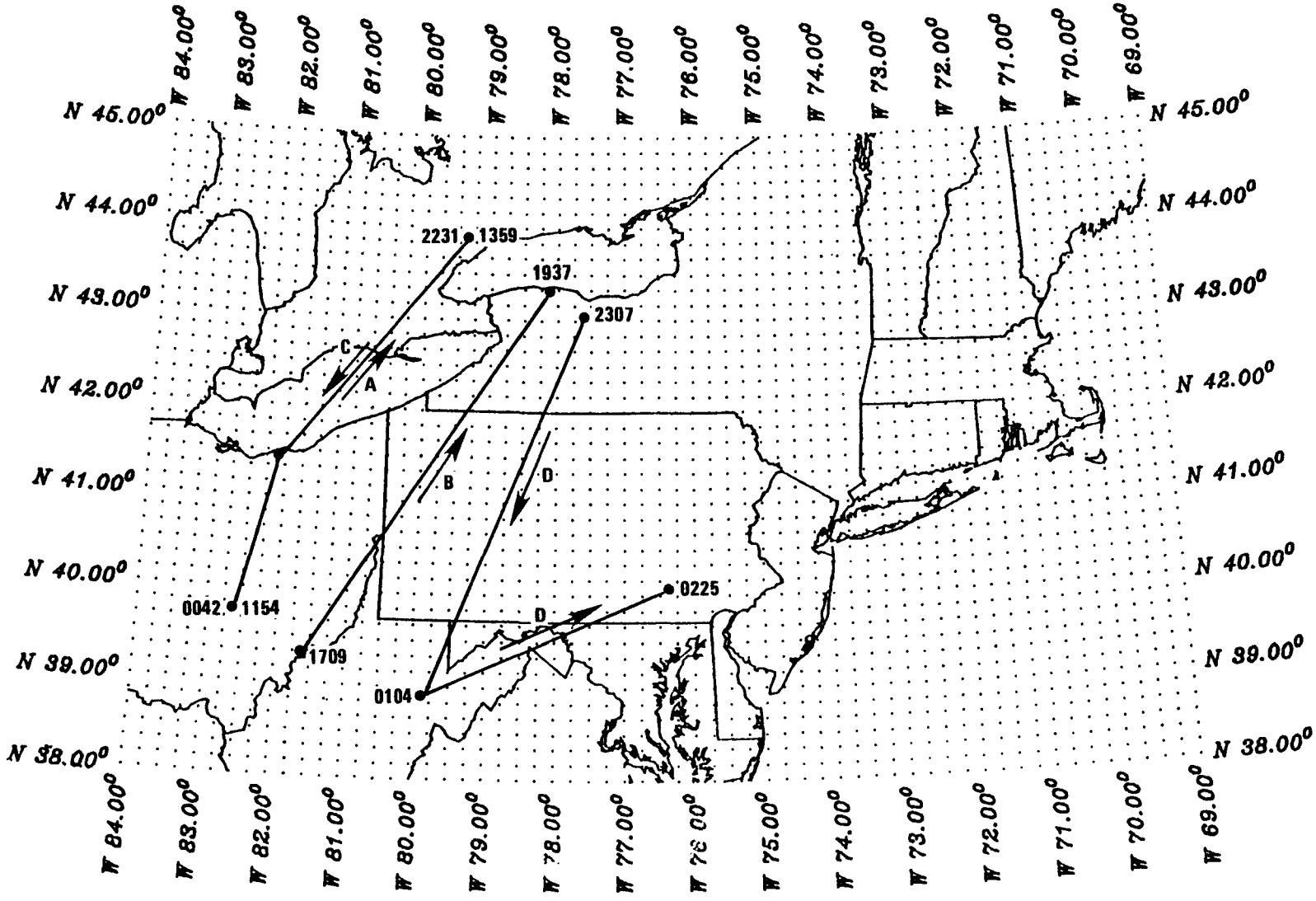

Figure 6. Approximate aircraft sampling flight paths conducted during the NEROS study on 3 August 1979.

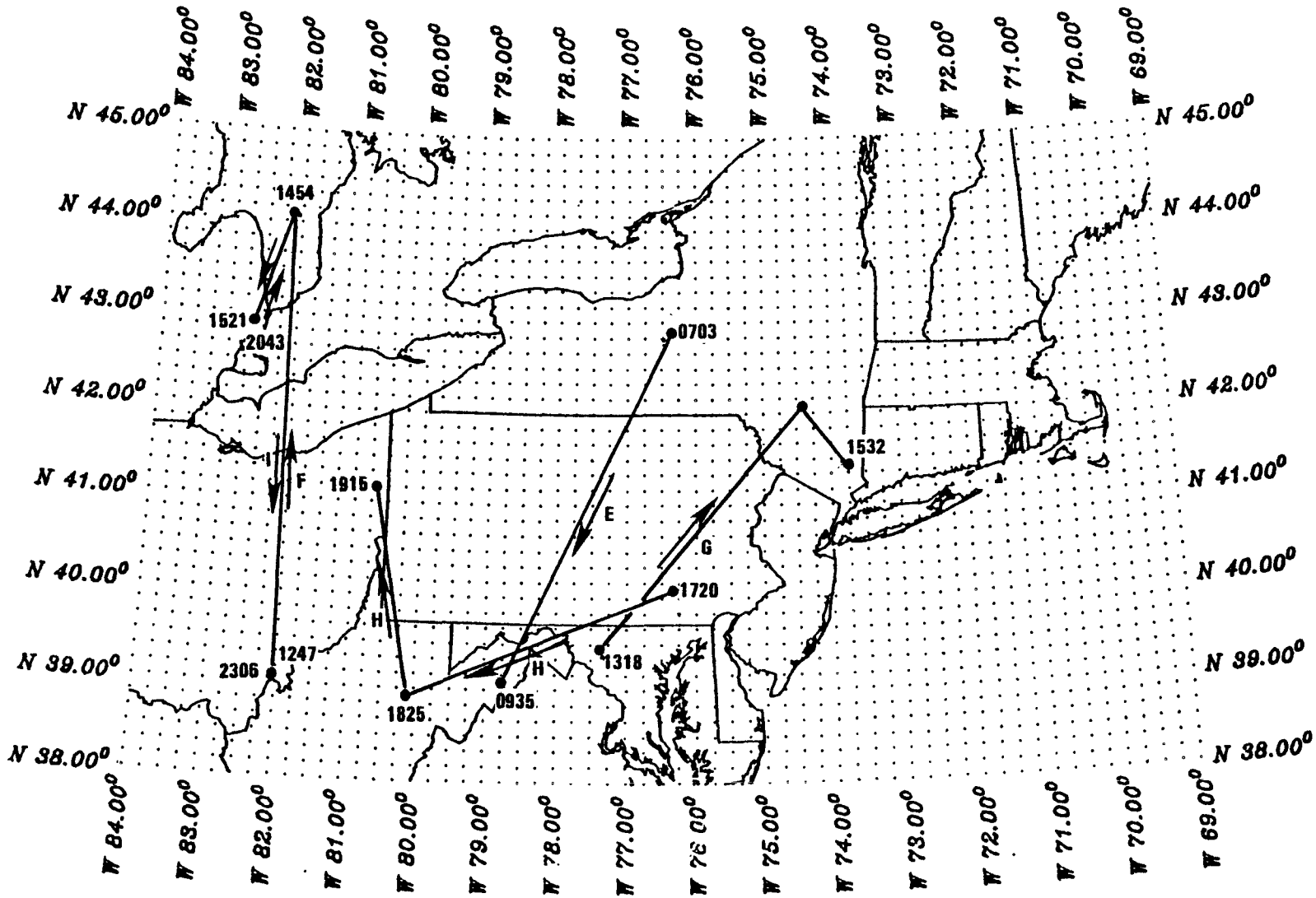

Figure 7. Approximate aircraft sampling flight paths conducted during the NEROS study on 4 August 1979.

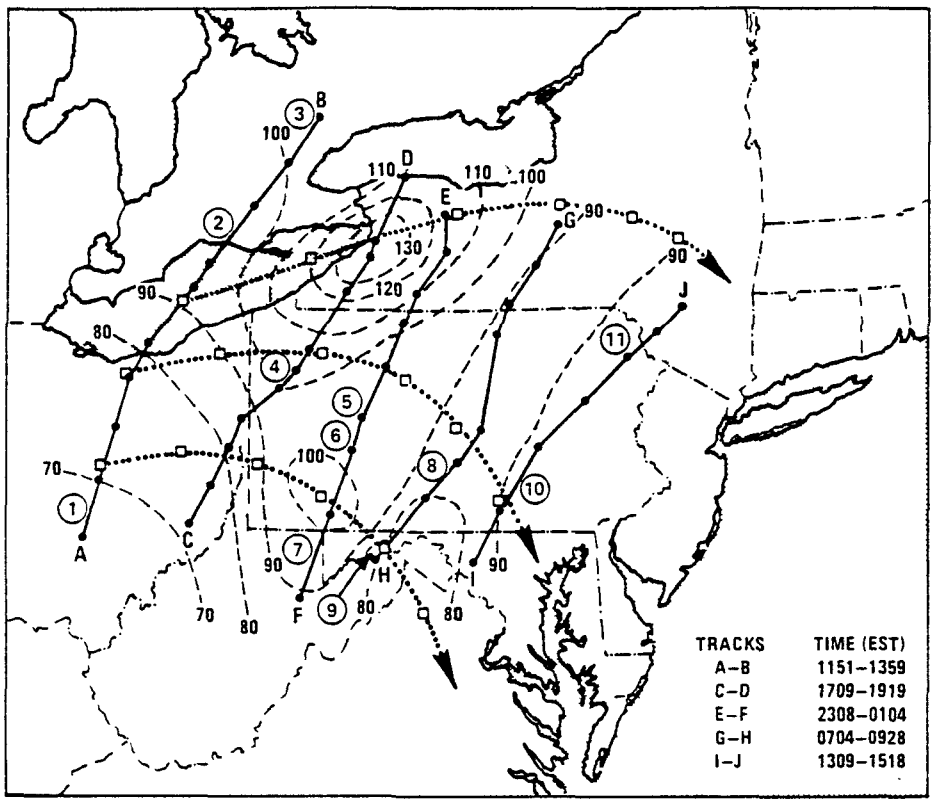

Figure 8. Aircraft sampling flight tracks and O_3 concentrations (ppb) near the center of the mixed layer (dashed lines) during the 3-4 August 1979 period. (from Clarke et al., 1983)

western New York and Pennsylvania, with the highest point values between 160 and 170 ppb. This is just to the east of the surface monitoring site at Conneaut, Ohio where a maximum surface value of 159 ppb was recorded the same day. The aircraft data add further evidence to a verification of the premise that there existed an area of elevated O_3 concentrations aloft in the boundary layer to the south and east of the Lake Erie shoreline and possibly over the lake itself on 3 August. The timing and location of this area of high O_3 concentrations indicates that it was not generated on this day, but rather advected here from another time and location, quite possibly from Detroit and the heavy industrial areas to the west of Lake Erie. The wind flow over this region the previous day had been from the west and southwest directions, with a stronger westerly component immediately behind the weak cold front that passed through on 2 August. Clarke et al. (1983) suggest that the higher pollutant loading seen here may have originated as far west as Chicago, given the results of a back trajectory analysis.

The first aircraft transect made on the morning of 4 August was a particularly interesting one because it sampled in an area of the NEROS region that is sparse in surface monitoring locations. Flight E seen on Figure 7 was conducted by BNL and proceeded from a point south of Syracuse, NY to easternmost West Virginia. On this flight O_3 values in the boundary layer were seen to fluctuate in the range of 70-80 ppb over New York and Pennsylvania and 60-70 ppb over Maryland and West Virginia. A similar pattern of concentrations was seen on the return flight (G) that afternoon. The transect for flight G proceeded from south to north and to the east of transect E. Again no pronounced increases in O_3 concentration during the flight were observed here, and the general boundary layer values were 70-80 ppb. The WSU aircraft conducted a late afternoon flight on 4 August consisting of 2 legs. The first leg of flight H proceeded from southeast Pennsylvania to West Virginia. Boundary layer O_3 concentrations along this leg were in the 70-80 ppb range. The second leg of the flight went north from West Virginia to northeast Ohio. Here the concentrations of O_3 were more in the 50-70 ppb range within the boundary layer. The RTI aircraft made 2 north-south transects along the same path on 4 August. An afternoon flight from southern Ohio to Lake Huron

showed O_3 concentrations of 70-80 ppb generally in the boundary layer, with a few exceptions. Concentrations of around 90 ppb were detected southeast of Columbus and also west of Akron. The aircraft apparently encountered an O_3 plume southeast of Detroit over Lake Erie extending into southwestern Ontario. Concentrations of 90-150 ppb O_3 were detected in the plume. The relative compactness of the plume and the distance downwind of Detroit indicate that the plume probably represents photochemical activity from that city on 4 August. The return flight occurring during late evening along the same path showed a broad O_3 plume now northeast of Detroit with peak concentrations of 120 ppb extending over about a 35 km cross-section. South of this plume O_3 concentrations were generally in the 65-75 ppb range with an increase to about 90 ppb in southeast Ohio.

In general, the aircraft sampling during this 2-day episode over the NEROS region indicated widespread boundary layer O_3 levels of 70-80 ppb with some areas slightly higher or lower than this range at times. The aircraft sampling showed the presence of 2 pronounced O_3 plumes during the period in the areas covered by the transects. The first was a large area of O_3 from an aged plume over western New York on 3 August (see Figure 8) and the second was an urban-scale plume, probably from Detroit, over western Ontario on 4 August. Aircraft sampling downwind of other major urban source areas in the NEROS region was either insufficient or nonexistent in order to detect O_3 plumes.

Section 3 presents detailed comparisons of the hourly averaged surface O_3 concentrations and the corresponding model predictions. Measurements of O_3 concentrations aloft from aircraft monitors are also used in the analysis to help resolve particular features of the concentration pattern.

ROM1 Initial and Boundary Concentrations

Any mass-conservative grid model of atmospheric air pollution, including ROM1, is sensitive to the initial field of mass within the

modeling domain as well as the mass flux across inflow boundaries during the simulation. The initial mass field specified as a model input can remain within the model domain and exert considerable influence on simulation results for hours or days, depending upon the spatial scale of the model, wind transport speeds, and source emissions distributions and flux rates. In urban scale modeling the initial field is typically advected out of the modeling domain within a few hours after the start of simulation. Monitoring networks on this scale are often sufficient to adequately specify the initial concentrations of the major pollutant species of interest. On the larger regional scale however more problems are encountered in specifying a proper initial concentration field.

One major concern is the density of monitoring stations over a 1000-km regional scale model domain. Figure 1 demonstrates that the density of O_3 monitors in the standard U.S. SAROAD network is not uniform. Major urban areas are covered fairly well but large areas of the domain are unmonitored. Interpolation across such large distances may not be reliable. Aircraft sampling may help to some degree, but the transects available are relatively few and those taken near model initialization time are fewer still. The density of monitors for species other than O_3, such as NO_x and hydrocarbons, is considerably less than that for O_3, making the initialization problem worse because these precursor species are important in the photochemical generation of O_3. The uncertainty in the initial concentration estimates is further compounded by the transport speeds. Days may elapse before the initial mass field is completely flushed out of a regional model domain. For instance, in a 1000-km model domain with a lateral transport wind speed of 5 m/sec it would be 55 hours before the initial mass is completely transported out. In the interim simulation period errors in the initial field specification would propagate through the chemical interactions to the model species predictions.

The first attempt at simulating the 3-4 August 1979 period with the ROM1 included an estimate of the initial concentration field at 00 h, LST on 3 August over the model domain. Five "categories" of grid cells were determined, based mainly on land use, where the same set of initial concentration values

were used in all cells of a given category. The categories ranged from a remote or wilderness class to an urban-industrial class. Ambient observations of O_3 near model initialization time were studied for each class of cells and estimates of the initial O_3 value within each class were made. Data observations of NO_x were very sparse and those of hydrocarbons were essentially non-existent, so estimates of these concentration values were made for each category of grid cells based on chemical equilibrium considerations of all the reactive species. It became clear in examining the simulation results for the 2-day episode using this method of model initialization that it would not be possible to distinguish between model O_3 results based on precursor source emissions input to the simulation or model results as artifacts of the specified initial field. For example, the large area of O_3 over western New York (see Figure 8) appeared in the simulation results primarily because of heavy initial mass loadings of O_3, NO_x, and hydrocarbons over the Ohio-Lake Erie vicinity. In attempting to evaluate model results for O_3 we are interested primarily in analyzing the model's ability to generate O_3 patterns from the given source emissions distribution because the ROM1 will eventually be asked to judge the effects on O_3 of proposed changes in the source emissions input function. The effects of initial conditions must therefore be minimized in any simulations performed with a regional model.

We minimize the influence of initial conditions by specifying tropospheric background "clean" conditions throughout the model domain. In conjunction with this procedure it will be necessary to begin model simulation at a relatively "clean" period of time throughout the domain also, such as after the passage of a cold front with an attendant air mass exchange. In future work with ROM2 we will use this initialization procedure at the start of a long period (1-4 weeks) simulation. This longer period will also insure a minimal dependence of model results on initial concentrations.

For the 2-day episode at hand, however, the simulation was performed again with tropospheric clean initial conditions in order to judge the model's ability to produce O_3 from the source emissions function. This is done with the knowledge that the initial ambient field did not in fact, contain clean

conditions. Surface and aircraft monitoring showed areas with higher O_3 values, including the large O_3 plume in the eastern Great Lakes area. Other plumes though, formed during the 2-day period, should be included in the simulation. Interpretation of model performance here must be done with this understanding of the potential omissions in the initial mass field. With this newly acquired appreciation of the effects of initial conditions all future simulations will begin at a clean period and proceed for one week or more in time. It was, however, still thought useful to analyze the results of this short test episode as an exercise in some of the model evaluation techniques that will be used in longer term simulations.

Boundary concentrations, both at the lateral edges and the top of the modeling region, are handled similarly to the initial concentrations for this 2-day episode. That is, tropospheric background values are used at all boundaries for all times. The combination of the clean initial and boundary concentrations here produced simulation results reflecting these clean concentrations, except where source emissions injections into the model domain raised the level of pollutants above background. The background tropospheric O_3 concentration specified in ROM1 was around 40 ppb, and model results show this O_3 value through large sections of the domain during the simulation. Actual ambient boundary layer O_3 values of 60-80 ppb O_3 were measured by most of the aircraft sampling performed during the 3-4 August period. Therefore there is an inherent underpredictive bias of 30-40 ppb of O_3 introduced into this model simulation because of the inconsistency in background values. Future applications of the regional model will provide for day/night temporal variations in the lateral boundary concentrations.

SECTION 3

RESULTS OF MODEL SIMULATION FOR O_3

The ROM1 model was run for the 48-hour period of 3-4 August 1979 using data from the NEROS and SAROAD data bases. Before the model itself was started the series of required preprocessors was run to provide the necessary model inputs to the ROM1 (Schere and Fabrick, 1985). The model was initialized throughout its entire domain with a set of tropospheric background species concentrations which were computationally adjusted for chemical equilibrium. These concentrations are shown in Table 2. The same set of concentrations was used for both lateral inflow and top boundary concentrations throughout the model simulation period. These chemical species correspond to those in the 36 reaction Demerjian chemical kinetic mechanism contained in ROM1.

The evaluation of the ROM1 results here for O_3 occurs in several stages. First we compare model predictions, interpolated to the surface SAROAD station locations, with observed values over all hours and receptor sites. The model predictions, which are available every 30 minutes, have been averaged into 1-hour intervals to correspond with the hourly averaged surface data. Next, an analysis of the maximum concentrations at receptor locations is made, and finally a close look at individual plumes from large source areas within the domain is performed. Aircraft observations of O_3 concentrations in urban plumes, where available, are included in the analysis. We ignore the first 6 hours of predictions from the model because of the strong influence of initial conditions in this period. Therefore the first hour that comparisons of observed and predicted data are made is 0600-0700 h, LST on 3 August and the last hour of the evaluation period is 2300-2400 h, LST on 4 August.

Hourly Data Comparisons

Figure 9 presents a histogram of the hourly O_3 values observed by the surface monitoring stations in the ROM1 domain during the model evaluation period. There is a pronounced peak in the observations at very low values of

TABLE 2. SET OF INITIAL AND BOUNDARY SPECIES CONCENTRATIONS USED IN ROM1

Species	Concentration (ppb)	Species	Concentration (ppb)
NO	.00658	H_2O_2	.002571
NO_2	1.824	O	2.180×10^{-9}
O_3	36.9	NO_3	.01345
olefins	.3087	OH	7.953×10^{-6}
paraffins	.3919	HO_2	.003544
aldehydes	.04323	HO_2NO_2	.002115
aromatics	.1224	RO	1.254×10^{-9}
CO	99.98	RO_2	.001722
HNO_2	.001939	R2O	1.196×10^{-10}
HNO_3	.1523	$R1O_2$	7.089×10^{-7}
PAN	4.931×10^{-5}	$R2O_2$	1.526×10^{-4}
RNO_3	1.803×10^{-8}		

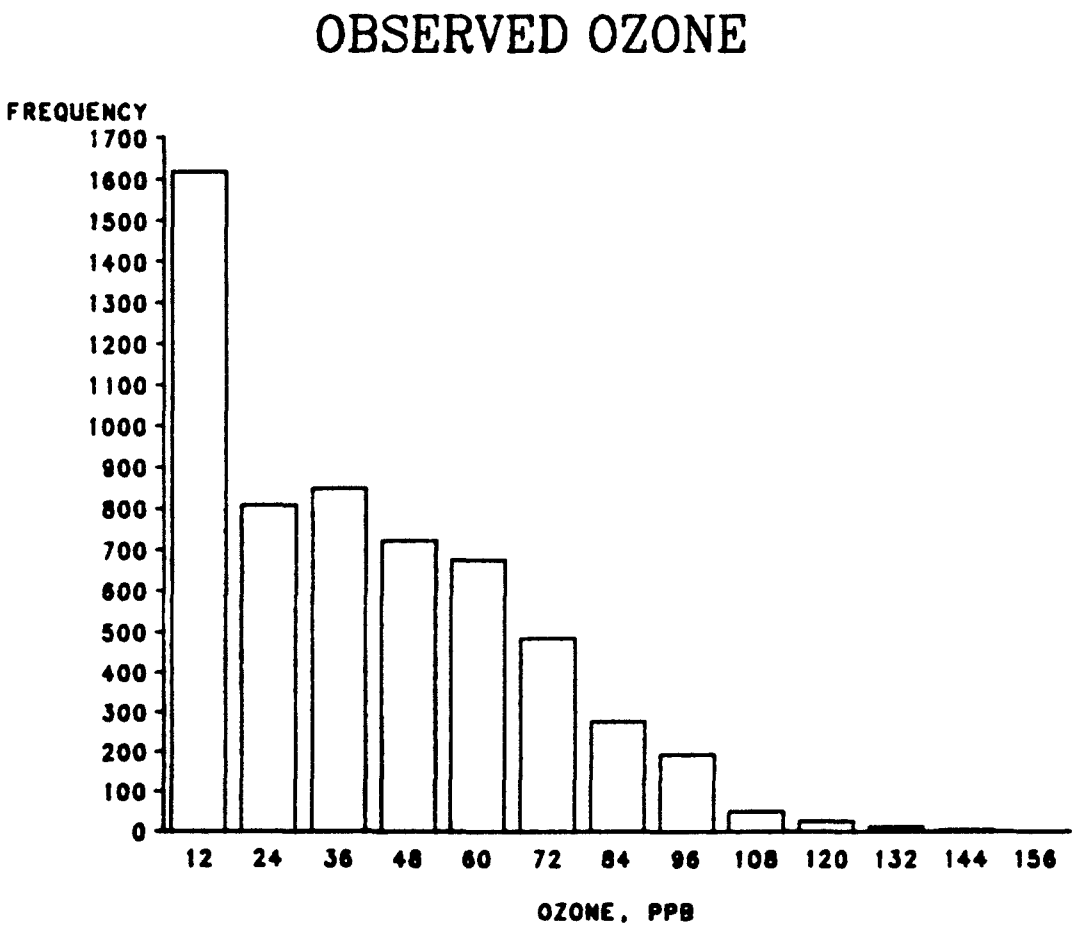

Figure 9. Histogram of observed O_3 concentrations at surface monitoring sites on 3-4 August 1979.

O_3, between 0 and 18 ppb. The magnitude of this peak might be confusing. These low values are generally occurring at night and are the result of near surface depletion of O_3 by ground deposition and chemical reaction. Instrument sensitivity at such low concentration levels must also come into question. Beyond these values, a broad peak in the distribution up to about 65 ppb is seen, beyond which the frequency distribution drops off gradually to the maximum values, near 160 ppb.

Figures 10a and 10b present the histograms of hourly predicted O_3 values interpolated to the surface monitoring site locations from the ROM1 layers 0 and 1, respectively. These distributions appear more normally-shaped (Gaussian) than the observed distribution and have sharp peaks in the 25-45 ppb vicinity. This concentration range spans the specified background value for O_3 of 37 ppb which is used by ROM1 for lateral and top boundary concentrations.

Apparently this background value dominates the ROM1 predictions at grid locations of the surface monitoring sites over many of the simulation hours. The peak in the layer 0 distribution appears in the 25-35 ppb range while the peak in layer 1 predictions is 35-45 ppb. This slight shift toward lower values in layer 0 reflects the effects of ground deposition and the sub-grid scale processes that chemically deplete O_3 in the surface layer. In general, the layer 0 ROM1 concentrations are a few ppb less than the corresponding layer 1 concentrations over the grid.

The residual or bias in the concentration predictions, d, is defined as the difference between the observed and predicted O_3 concentrations. That is, for layer 0, $d_0 = c_{ob} - c_{p0}$, and for layer 1, $d_1 = c_{ob} - c_{p1}$. The histograms of d_0 and d_1 for the model simulation period are shown respectively in Figures 11a and 11b. The peak value in both figures appears slightly on the negative, or overpredictive, side of the Gaussian shaped distributions. The negative peaks in these figures are artifacts of the model. These overpredicted concentrations correspond to very low ambient O_3 values observed mostly at night. The majority of surface monitoring stations are located in or near urban areas and are thus sensitive to rapid spatial or temporal changes in

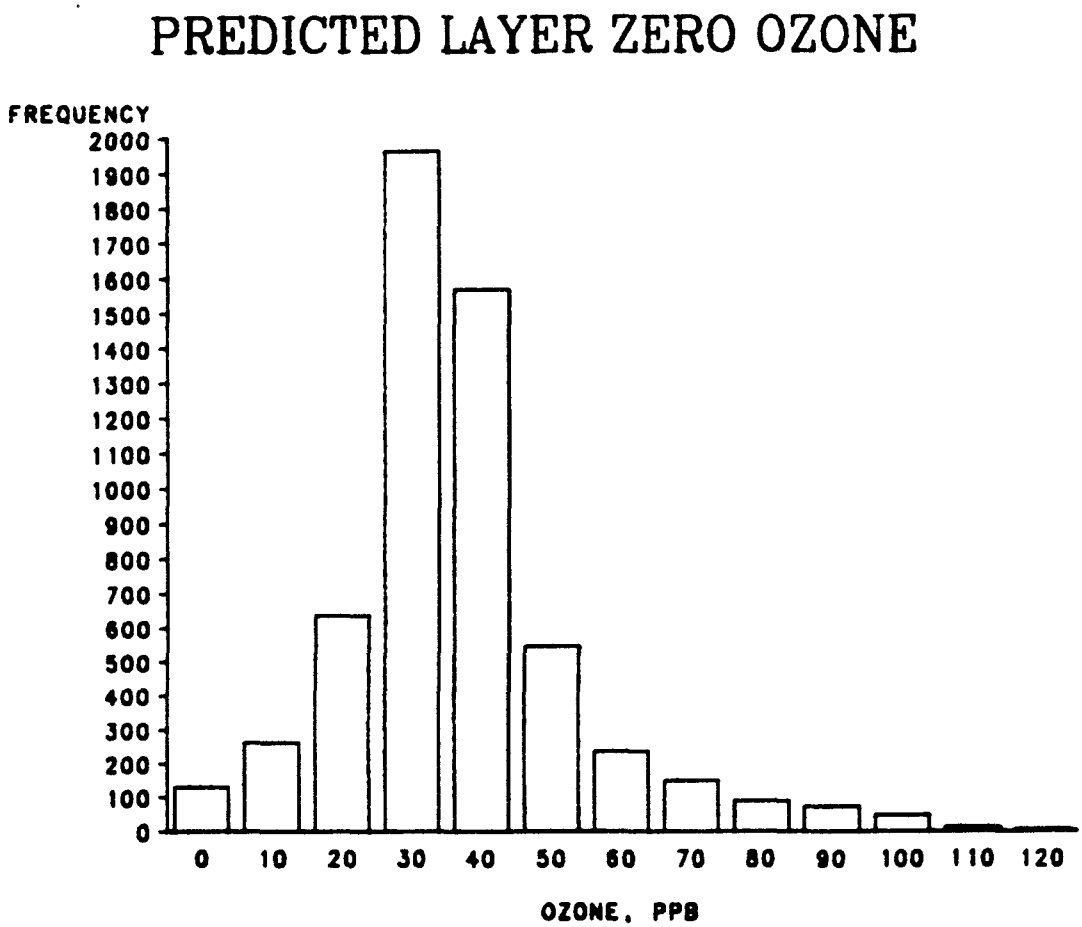

Figure 10a. Histogram of O_3 concentrations predicted by ROM1 at monitoring site locations for 3-4 August 1979 (ROM1 layer 0).

PREDICTED LAYER ONE OZONE

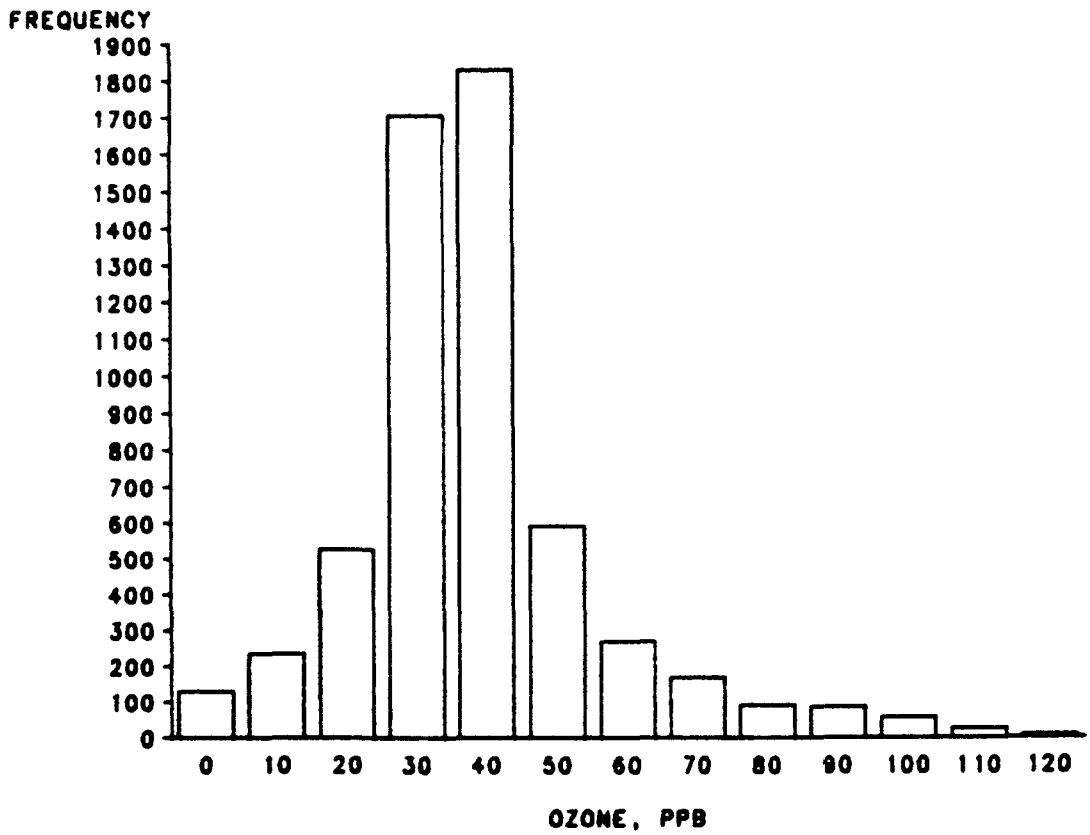

Figure 10b. Histogram of O_3 concentrations predicted by ROM1 at monitoring site locations for 3-4 August 1979 (ROM1 layer 1).

OBSERVED MINUS PREDICTED OZONE, LEVEL ZERO

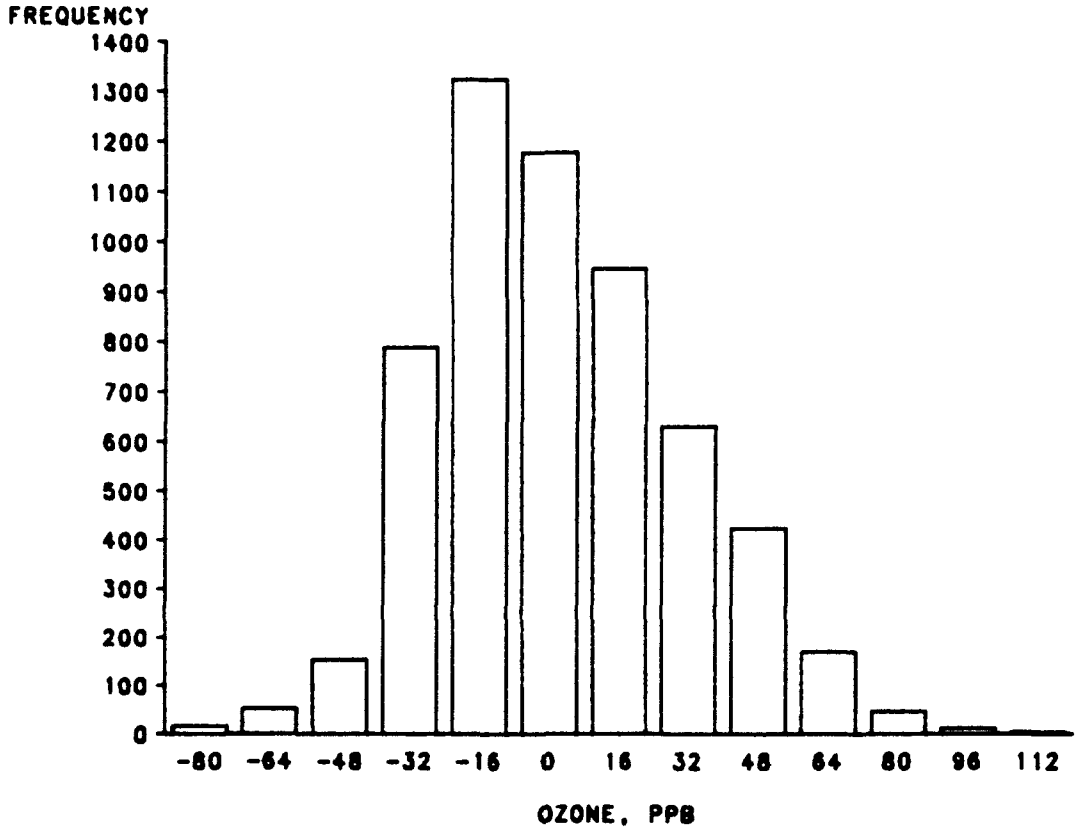

Figure 11a. Histogram of residual O_3 concentrations at monitoring site locations for 3-4 August 1979, ROM1 layer 0.

OBSERVED MINUS PREDICTED OZONE, LEVEL ONE

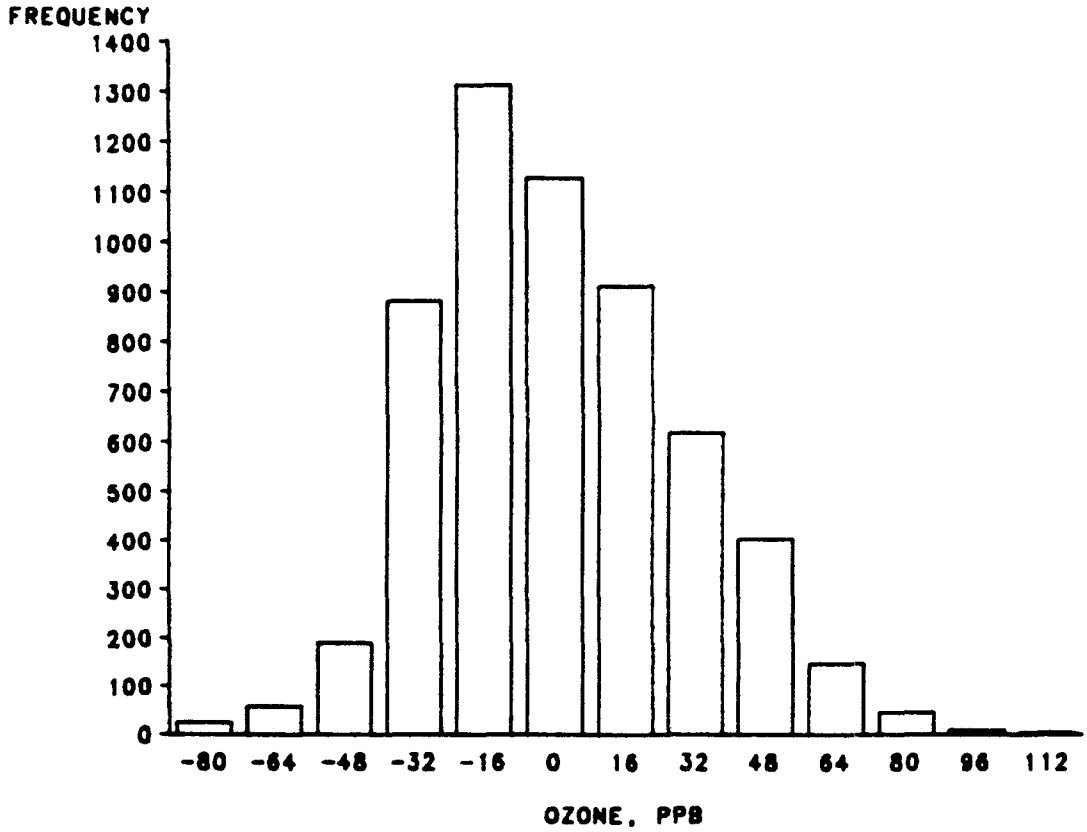

Figure 11b. Histogram of residual O_3 concentrations at monitoring site locations for 3-4 August 1979, ROM1 layer 1.

emissions patterns, especially the titration of O_3 by NO_x sources. On the other hand the ROM1 predictions are volumetric averages over the 20 km X 20 km X H size of the grid cell (where H is the depth of the grid cell). Therefore, the sub-grid scale effects from urban area sources are typically only a small perturbation on the volumetric average predicted cell concentration. This will lead to overprediction under these circumstances and is reflected in the negative peak in the histograms. The majority of daytime residuals corresponds to underpredictions and we speculate at this point that they would be aligned with higher O_3 concentrations. A discussion of the trends in magnitude of the bias with ambient concentration level is given later in the discussion of concentration maxima.

The average bias in layer 0 O_3 predictions over all surface monitoring locations is shown in Figure 12a as a function of time. The first data point, at 6 hours after the start of model simulation, corresponds to the hour period 06-07 h, LST on 3 August 1979. The 95% confidence interval about each average bias point is also shown. Figure 12b presents the same information, except as the percent bias of the observed O_3 concentration. Figure 12c is another way of showing this information in a time series. It is a box plot of the bias among the surface monitoring locations where the middle of each box is the median, the top edge is the 75th percentile, the bottom edge is the 25th percentile, and the minimum and maximum points are the bottom and top, respectively, of the vertical projections from the box. All three time series show a distinct diurnal trend in the average bias, with underpredictions averaging 30-32% during the midday hours and overpredictions averaging as much as 100+ % at night. These large overpredictions correspond to relatively modest bias values, 10 to 25 ppb, as seen from Figure 12a. At those times of high overpredictions, the bias and percent bias figures imply observed and predicted O_3 values on the order of 20 and 40 ppb, respectively, confirming an earlier premise made from analyzing the histograms that the ROM1 overpredictions correspond to quite low ambient concentrations.

From Figure 12c it is seen that the median underpredictions on the first day of simulation peak at about 20 ppb and on the second day at nearly 30 ppb,

BIAS AVERAGE ALL RECEPTORS, LAYER ZERO

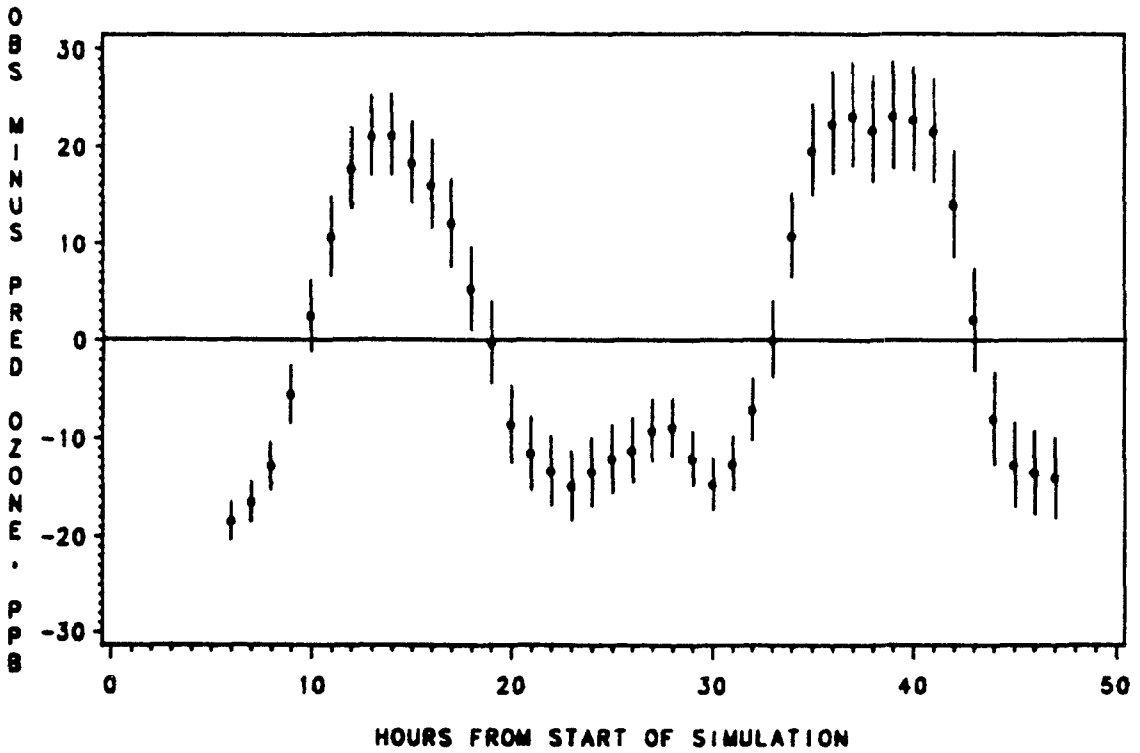

Figure 12a. Time-series over the 3-4 August 1979 simulation period of average bias over all surface receptor locations.

PERCENT BIAS AVERAGE ALL RECEPTORS, LAYER ZERO

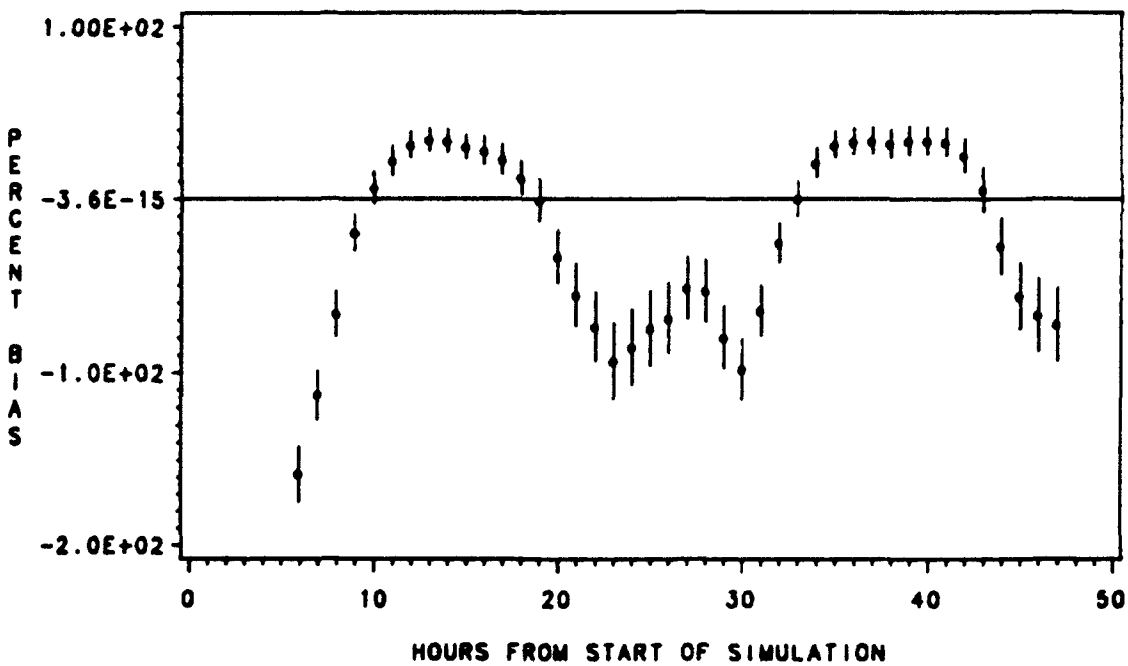

Figure 12b. Time-series over the 3-4 August 1979 simulation period of average percent bias over all surface receptor locations.

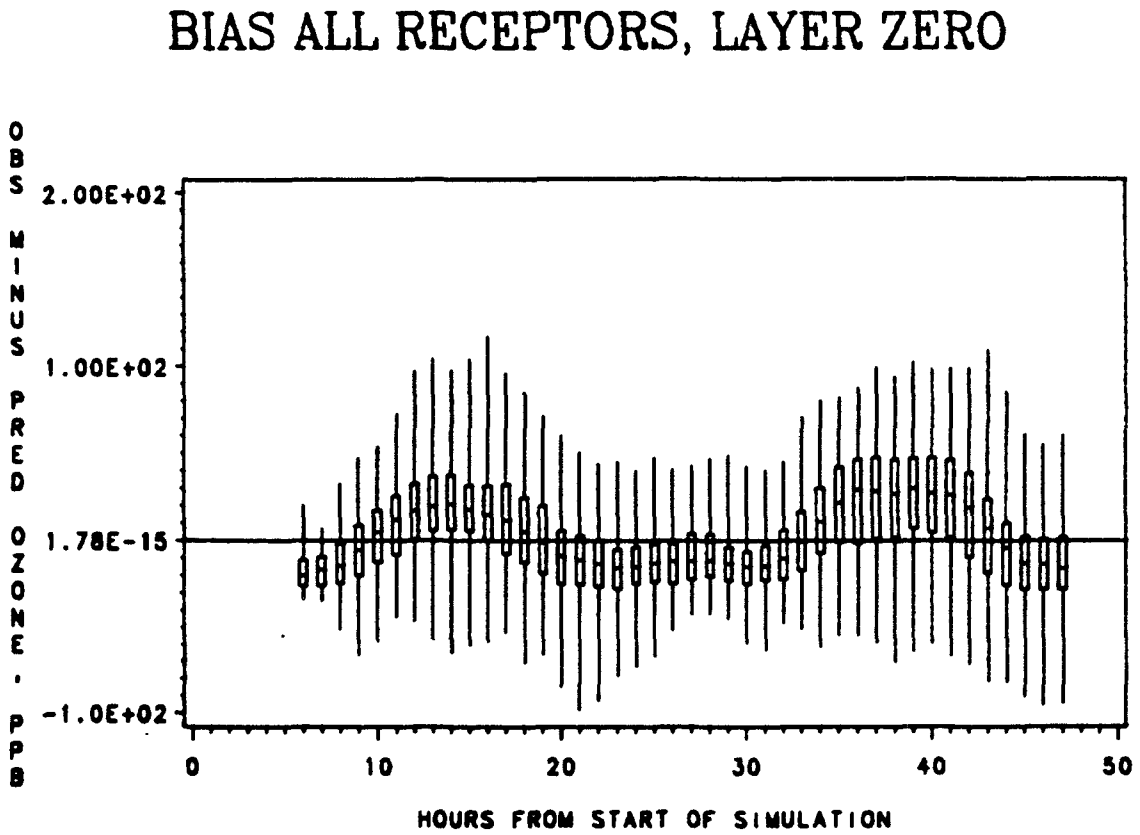

Figure 12c. Time-series over the 3-4 August 1979 simulation period of a box-plot distribution of bias over all surface receptor locations.

both during the daylight hours when O_3 is expected to reach its daily maximum values. Taken together with the percent underpredictions these bias values imply that the O_3 observations during the midday period on 3 August at the monitoring site locations are in the 60-65 ppb range, while the layer 0 predictions are in the 40-45 ppb range. On 4 August the corresponding observed and predicted ranges are 65-70 ppb and 40-45 ppb, respectively. The layer 0 predictions are at a level generally near the specified background and initial O_3 concentrations, indicating their influence over the grid locations corresponding to the surface monitoring sites. It should be reiterated here that the surface monitoring sites are not regularly spaced in the NEROS region, but are concentrated near urban areas. The underprediction during this period may be the result of the model's inability to correctly replicate all of the sub-grid processes, transport inaccuracies, or other problems. A closer look at some specific areas of the grid will be examined later. Figure 12a indicates that there are only four hours during the simulation period when the average bias is not significantly different from zero. These hours occur during transitional time periods on both days of simulation. Although not shown here, the corresponding time series plots from ROM1 layer 1 results are very similar to those discussed for layer 0.

A tabulation of hourly averaged parameters for the simulation period is given in Table 3. Parameter abbreviations are defined in the Glossary and their significance is discussed in Schere and Fabrick (1985). For each hour displayed there are 'n' monitoring station locations used in the averages. The values in the table confirm the very low observed O_3 concentrations at night. The diurnal range in O_3 concentrations is considerably greater in the observations than in the model predictions, where a variation of only 10-15 ppb is shown. The bias values confirm the data presented in Figure 12 with negative values at night and positive values during the day. The absolute values of bias (gross error) are all consistently rather high, indicating that the hours with average bias near zero actually contain a wide variation of individual values with opposite signs. The episodic average value of observed O_3 for all hours at the surface monitoring sites was 38.9 ppb and the corresponding model predictions for ROM1 layers 0 and 1 were 36.6 and 38.1 ppb,

TABLE 3. SUMMARY OF ROM1 HOURLY RESULTS FOR 3-4 AUGUST 1979

DATE	HOUR	n	$R_{\overline{c}_{ob}}$ (ppb)	$R_{\overline{c}_{p0}}$ (ppb)	$R_{\overline{c}_{p1}}$ (ppb)	$R_{\overline{d}_0}$ (ppb)	$R_{\overline{\lvert d_0 \rvert}}$ (ppb)	$R_{S_{d0}}$ (ppb)	$R_{\overline{d}_1}$ (ppb)	$R_{\overline{\lvert d_1 \rvert}}$ (ppb)	$R_{S_{d1}}$ (ppb)
79215	06	111	11.6	30.0	32.0	-18.4	19.0	10.1	-20.3	20.9	10.5
	07	110	14.6	31.1	32.5	-16.4	17.1	10.7	-17.8	18.4	11.0
	08	134	19.4	32.2	33.5	-12.8	15.9	14.2	-14.2	17.0	14.4
	09	140	28.4	33.8	35.2	- 5.5	15.0	17.6	- 6.8	15.2	17.6
	10	142	38.0	35.5	37.0	2.6	17.8	21.8	1.0	17.6	21.8
	11	144	47.8	37.1	38.5	10.7	21.6	24.6	9.3	21.1	24.6
	12	148	56.4	38.6	40.1	17.6	24.8	25.5	16.3	24.3	25.6
	13	147	61.3	40.2	41.6	21.1	25.8	25.0	19.7	25.1	25.1
	14	148	62.8	41.6	43.0	21.2	26.6	25.7	19.8	25.8	25.8
	15	150	60.1	41.8	43.0	18.3	25.0	25.5	17.1	24.3	25.8
	16	149	57.0	40.9	42.8	16.1	25.0	27.7	14.1	24.2	27.9
	17	150	52.4	40.2	41.9	12.1	24.1	27.7	10.5	23.9	28.0
	18	148	44.1	38.7	40.3	5.3	21.2	26.1	3.7	21.1	26.4
	19	145	35.4	35.6	37.6	- 0.2	20.7	25.5	- 2.1	21.2	25.9
	20	142	25.7	34.2	35.4	- 8.5	20.0	23.5	- 9.8	20.7	23.8
	21	133	20.9	32.4	33.8	-11.5	19.5	21.8	-12.9	20.4	22.1
	22	126	18.1	31.4	32.9	-13.3	19.1	19.8	-14.8	20.2	20.5
	23	122	15.9	30.7	31.9	-14.8	20.1	19.1	-16.0	21.1	19.5
79216	00	114	15.7	29.1	30.5	-13.4	19.2	18.2	-14.8	20.1	18.8
	01	114	16.2	28.2	29.4	-12.0	18.5	18.6	-13.3	19.4	19.1

TABLE 3. (continued)

DATE - HOUR	n	$R_{\overline{c}_{ob}}$ (ppb)	$R_{\overline{c}_{p0}}$ (ppb)	$R_{\overline{c}_{p1}}$ (ppb)	$R_{\overline{d}_0}$ (ppb)	$R_{\overline{\lvert d_0 \rvert}}$ (ppb)	$R_{S_{d0}}$ (ppb)	$R_{\overline{d}_1}$ (ppb)	$R_{\overline{\lvert d_1 \rvert}}$ (ppb)	$R_{S_{d1}}$ (ppb)
02	114	16.4	27.6	28.8	-11.2	17.6	17.6	-12.4	18.6	18.1
03	121	17.8	27.0	28.1	- 9.2	16.8	17.6	-10.3	17.6	18.0
04	129	16.7	25.6	27.0	- 8.9	16.2	16.9	-10.3	17.1	17.4
05	121	15.1	27.2	28.5	-12.1	16.2	14.9	-13.4	17.2	15.5
06	129	15.0	29.7	31.9	-14.7	17.5	14.9	-16.9	19.5	16.2
07	137	19.5	32.1	34.0	-12.6	17.0	16.2	-14.5	18.6	17.3
08	150	27.7	34.8	36.5	- 7.1	17.0	19.1	- 8.8	18.0	20.0
09	140	38.1	38.1	39.5	0.0	18.8	23.0	- 1.4	19.2	23.4
10	143	51.6	40.9	42.4	10.8	22.5	26.0	9.2	22.3	26.3
11	144	62.5	42.9	44.4	19.6	28.6	28.3	18.1	28.1	28.6
12	135	67.5	45.1	46.7	22.4	32.4	30.3	20.8	31.9	30.6
13	142	68.9	45.7	47.4	23.2	33.6	31.7	21.5	33.0	32.0
14	144	67.6	45.9	47.5	21.7	33.5	32.4	20.1	33.1	32.8
15	142	68.7	45.5	47.4	23.2	34.4	32.6	21.3	33.7	33.0
16	148	67.7	44.9	46.7	22.8	33.4	32.2	21.1	32.8	32.6
17	150	65.4	43.8	45.3	21.6	32.9	32.7	20.0	32.3	33.0
18	149	55.8	41.8	43.5	14.0	30.0	33.2	12.3	29.6	33.4
19	148	40.9	38.8	41.1	2.2	25.4	31.9	- 0.1	25.0	31.8
20	142	29.3	37.3	38.9	- 8.0	21.9	27.9	- 9.5	22.5	28.4
21	137	22.7	35.3	36.9	-12.7	22.4	25.1	-14.3	23.3	25.7

TABLE 3. (continued)

DATE - HOUR	n	$R_{\bar{c}_{ob}}$ (ppb)	$R_{\bar{c}_{p0}}$ (ppb)	$R_{\bar{c}_{p1}}$ (ppb)	$R_{\bar{d}_0}$ (ppb)	$R_{\lvert d_0 \rvert}$ (ppb)	$R_{S_{d0}}$ (ppb)	$R_{\bar{d}_1}$ (ppb)	$R_{\lvert d_1 \rvert}$ (ppb)	$R_{S_{d1}}$ (ppb)
22	128	20.2	33.6	35.0	-13.5	22.0	24.0	-14.8	22.8	24.4
23	118	19.4	33.4	34.5	-14.0	20.7	22.2	-15.1	21.5	22.6
79215 ALL	2489	38.6	36.2	37.7	2.4	21.2	26.5	0.9	21.4	26.7
79216 ALL	3239	39.2	36.9	38.5	2.3	24.0	29.8	0.7	24.4	30.1
79215-79216 ALL	5728	38.9	36.6	38.1	2.3	22.8	28.4	0.8	23.1	28.7

respectively. These values represent a 5.9% underprediction for layer 0 and a 2.1% underprediction for layer 1. Since these average O_3 levels are near tropospheric background values the significance of this analysis over all hourly values in the simulation period is not particularly great.

The next step was to perform an hourly analysis with a subset of the data values already used. The criterion for choosing the subset was based, in part, on the tropospheric background value of near 40 ppb O_3 used in the ROM1's initial and boundary conditions and the fact that many of the surface monitoring site locations showed O_3 predictions near this value. Therefore the data subset is based on only those receptor points where the observed value and the level 0 and 1 predicted values of O_3 are greater than 50 ppb. This should limit the data to those sites most affected by source emissions within the NEROS region. In fact the number of sites used in the analysis dropped from near 150 during the midday hours to around 30, and from around 120 during the nighttime hours to 0, after this criterion was applied.

The choice of criterion for the data subset might not seem to be the most obvious at first. Perhaps a more logical subset would be formed from choosing all points where only the observed O_3 concentration was greater than 50 ppb. In practice, this was the first subset produced for the analysis. It was found that this subset still contained far too many model predictions near tropospheric background levels to be useful in the restricted subset analysis. A number of factors could account for this including error in the location of source plumes within the model domain through transport uncertainty or source emission uncertainties. The overriding factor however is the assumption of tropospheric O_3 concentration values everywhere at the boundaries and initially when, in fact, areas of higher O_3 concentrations were observed. In any case the more restrictive criterion that was ultimately chosen produced the desired effect of reducing the data subset to those concentration values above the level of tropospheric background O_3, and presumably produced data points more affected by local and transported photochemical effects.

The histogram of observed O_3 concentrations in this data subset is presented in Figure 13. The concentration values along the axis of the plot are midpoints of the range for each class. The distribution peaks in the range 55-65 ppb and then falls off rapidly. The distribution slowly diminishes in the range above 75 ppb. This distribution does not contain the broad plateau of lower values of O_3 shown in Figure 9 for the full data set. The effect of eliminating the low data values is apparent in comparing the two figures. The reason for the lower maximum value in the data subset histogram is that we have screened out data points where either the observed or predicted values are less than 50 ppb. Thus the station that observed nearly 160 ppb showed a corresponding prediction of less than 50 ppb and was not included in the data subset.

Figures 14a and 14b present the histograms of the ROM1 O_3 predictions for layers 0 and 1, respectively, for the data subset. The predictions are skewed toward the lower end of the concentration range in the data subset. The number of model predictions above about 65 ppb is markedly lower, although the higher values extend to the 120 - 130 ppb range, nearly matching that on the observed concentration histogram. Comparing these histograms with those for the full set shown in Figure 10, it can be seen that the large number of predictions near the tropospheric background O_3 value are now eliminated, although the effect of this background value still persists to some extent in the peak for the range of 50-60 ppb of the data subset.

Histograms of d_0 and d_1 on the data subset are shown in Figures 15a and 15b. These distributions are Gaussian shaped with a peak at the zero range residual. In general, both layers 0 and 1 residuals are symmetrically distributed except for the larger tail on the underpredictive side. These histograms show a similar distribution to those in Figure 11 for the full data set, except they are not as asymmetrical as those in the latter figure.

OBSERVED OZONE

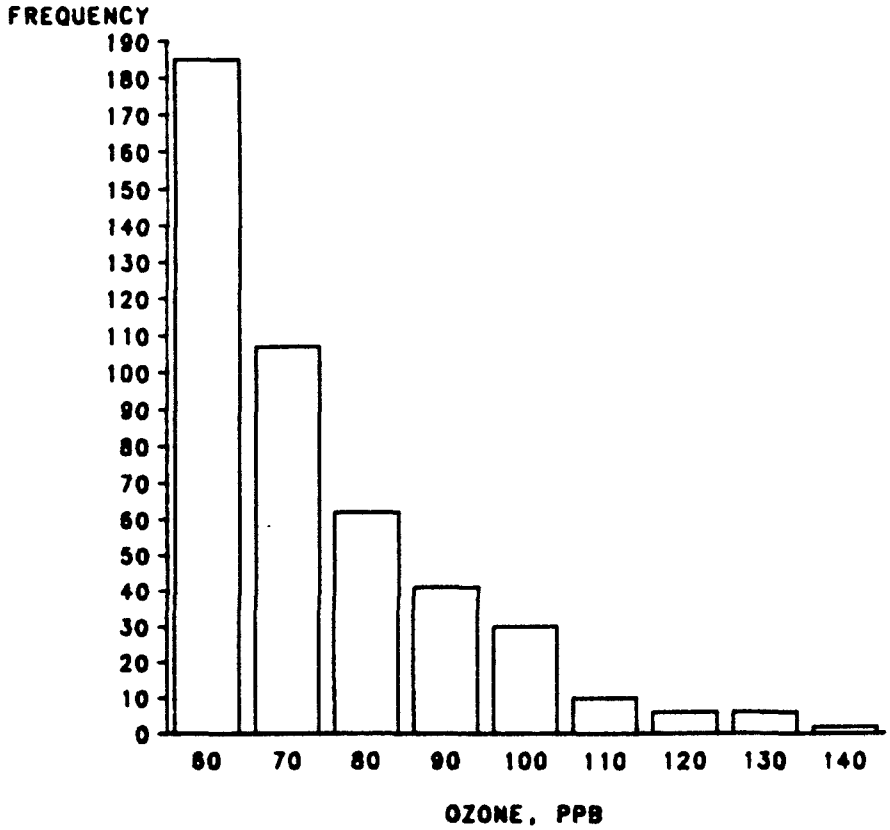

Figure 13. Histogram of observed O_3 concentrations at surface monitoring sites (where obs. and pred. O_3 > 50 ppb) on 3-4 August 1979.

PREDICTED LAYER ZERO OZONE

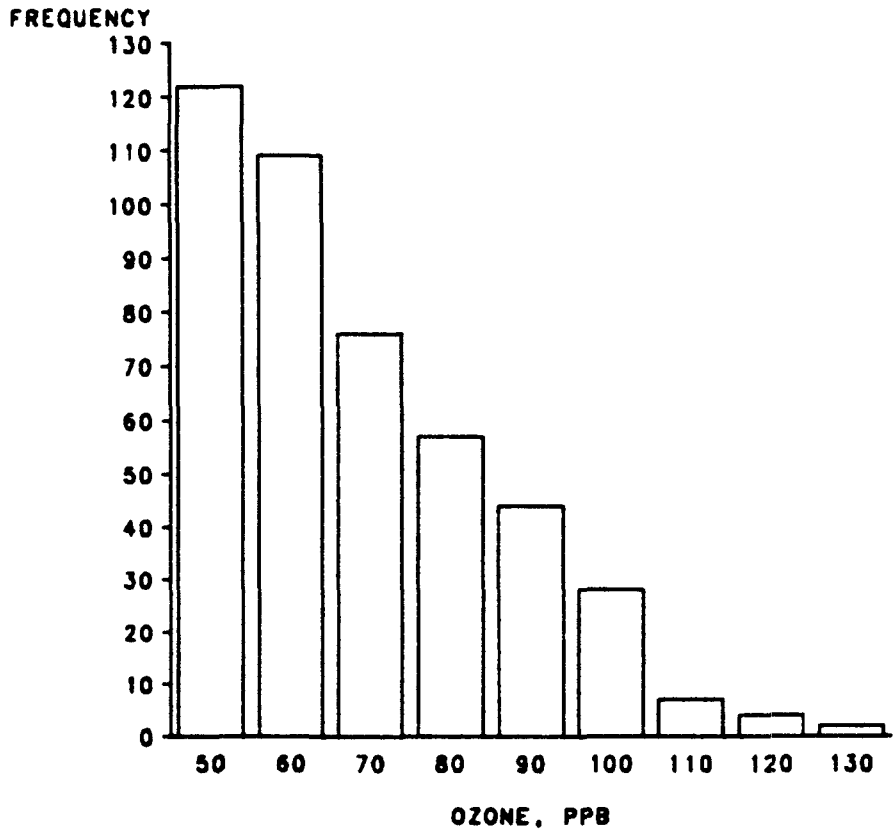

Figure 14a. Histogram of O_3 concentrations predicted by ROM1 at monitoring site locations (where obs. and pred. O_3 > 50 ppb) for 3-4 August 1979 (ROM1 layer 0).

PREDICTED LAYER ONE OZONE

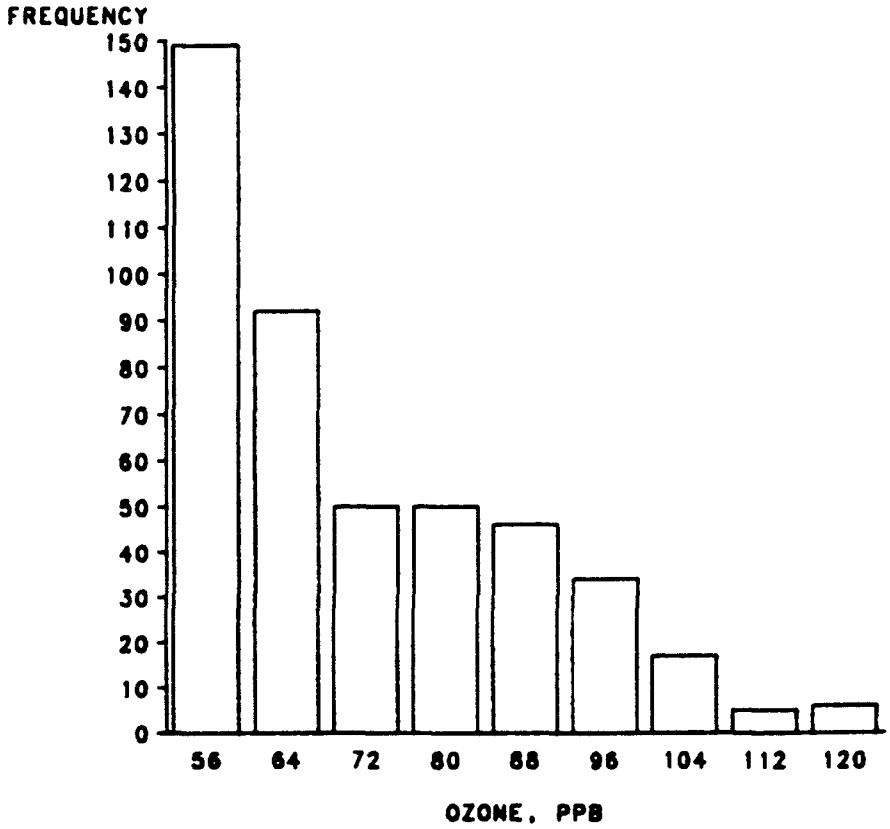

Figure 14b. Histogram of O_3 concentrations predicted by ROM1 at monitoring site locations (where obs. and pred. O_3 > 50 ppb) for 3-4 August 1979 (ROM1 layer 1).

OBSERVED MINUS PREDICTED OZONE, LEVEL ZERO

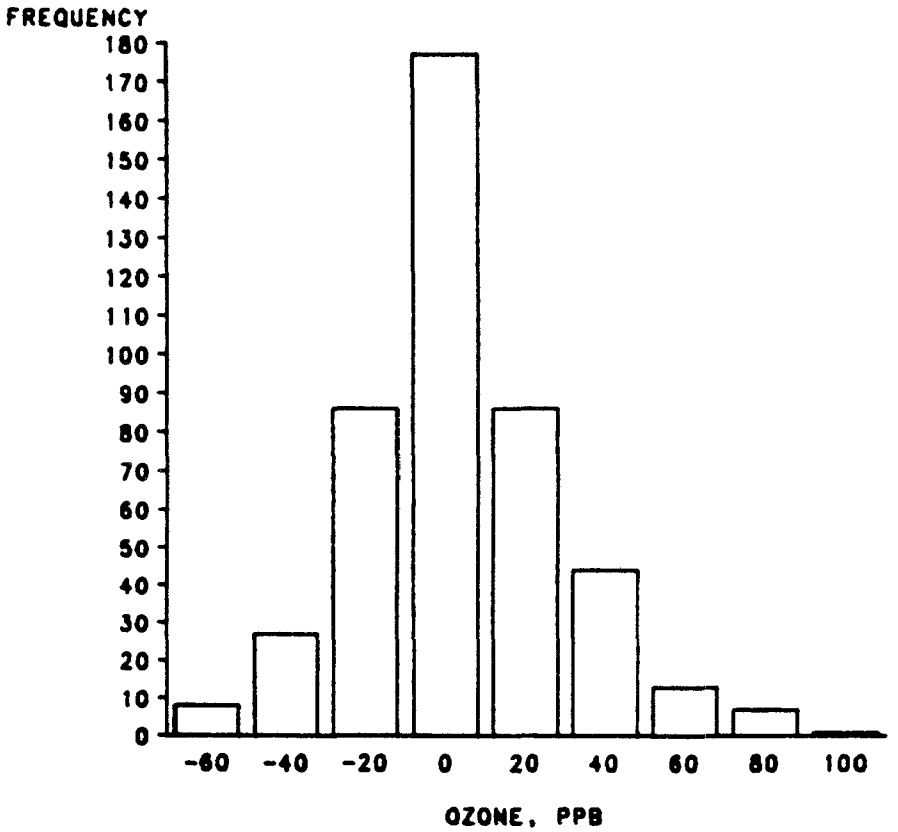

Figure 15a. Histogram of residual O_3 concentrations at monitoring site locations (where obs. and pred. O_3 > 50 ppb) for 3-4 August 1979 (ROM1 layer 0).

OBSERVED MINUS PREDICTED OZONE, LEVEL ONE

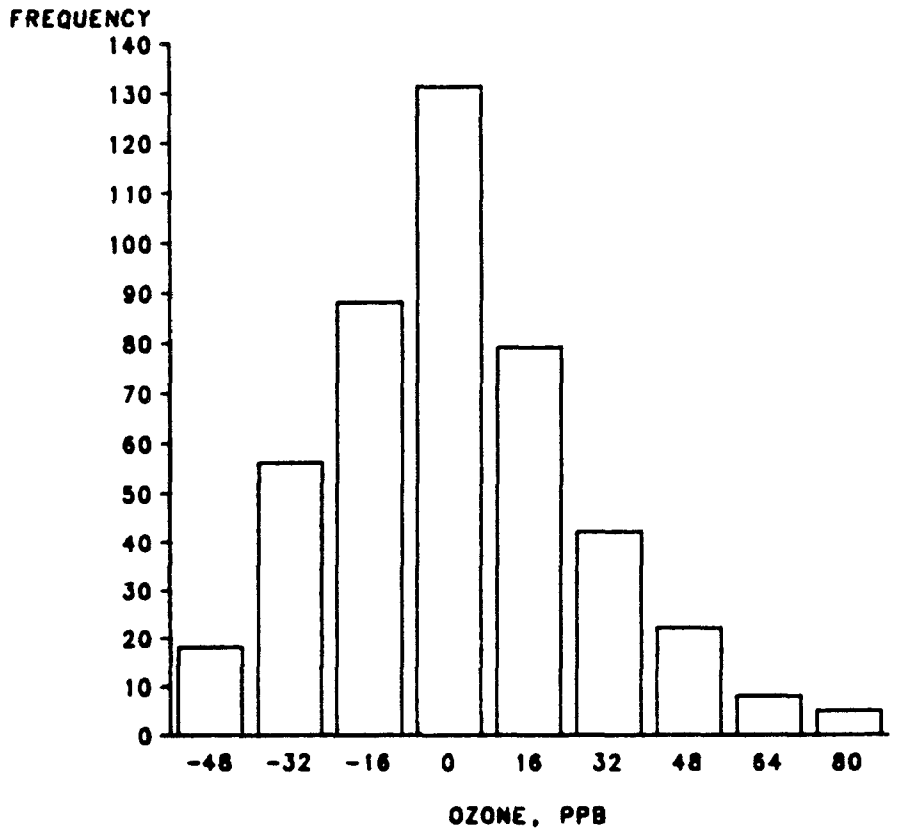

Figure 15b. Histogram of residual O_3 concentrations at monitoring site locations (where obs. and pred. O_3 > 50 ppb) for 3-4 August 1979 (ROM1 layer 1).

Plots of the time series of the concentration bias at the surface monitoring sites in the data subset are shown in Figure 16. The bias is depicted in Figure 16a and the percent bias in Figure 16b, with the 95% confidence interval about each point. It is immediately obvious that at certain hours there is little, if any, data in the subset being analyzed. This effect is a result of the elimination of the low O_3 values in this data subset, most of which occur during the nighttime hours. The diurnal variation in the bias for the full data set, seen in Figure 12, is also evident for the data subset in Figure 16. There are some irregularities in the periodicity but these are near the transition times when few data values have gone into the average. The hours with underpredictions are again generally during the daytime and the hours with overpredictions are during transitional periods or at night. These latter hours however, contain very few stations with observed or predicted concentrations above 50 ppb, so the significance of their bias value is not great. The largest values of average bias shown here are about 19% underpredicted at 1300 h on 3 August, and 14% underpredicted at 1500 h on 4 August. The magnitudes of these average bias values are fairly similar for both days of simulation. Although the plots are not shown here, the time series of bias in ROM1 layer 1 for the data subset are very similar to those shown for layer 0.

Table 4 presents a tabulation of hourly averaged parameters for values in the data subset. The number of surface monitoring sites at any given hour is considerably less here than in the full data set presented in Table 3. The maximum at any hour is 38 stations, as compared to 150 in the full set. The average observed concentration at the receptor locations varies from 51.0 ppb at 2000 h to 78.0 ppb at 1300 h on 3 August, and from 50.0 ppb at 0400 h and 0800 h to 80.7 ppb at 1600 h on 4 August. The corresponding predictions for layer 0 range from 56.0 ppb at 1900 h to 70.4 ppb at 1600 h on 3 August, and from 54.4 ppb at 0400 h to 76.2 ppb at 2000 h on 4 August. The episodic average value of observed O_3 in the data subset for all hours was 72.2 ppb and the corresponding ROM1 predictions for layers 0 and 1 were 68.9 and 71.2 ppb, respectively. This represents an average O_3 underprediction of 4.6% for ROM1 layer 0 and 1.4% for layer 1, a slightly smaller degree of underpre-

BIAS AVERAGE ALL RECEPTORS, LAYER ZERO

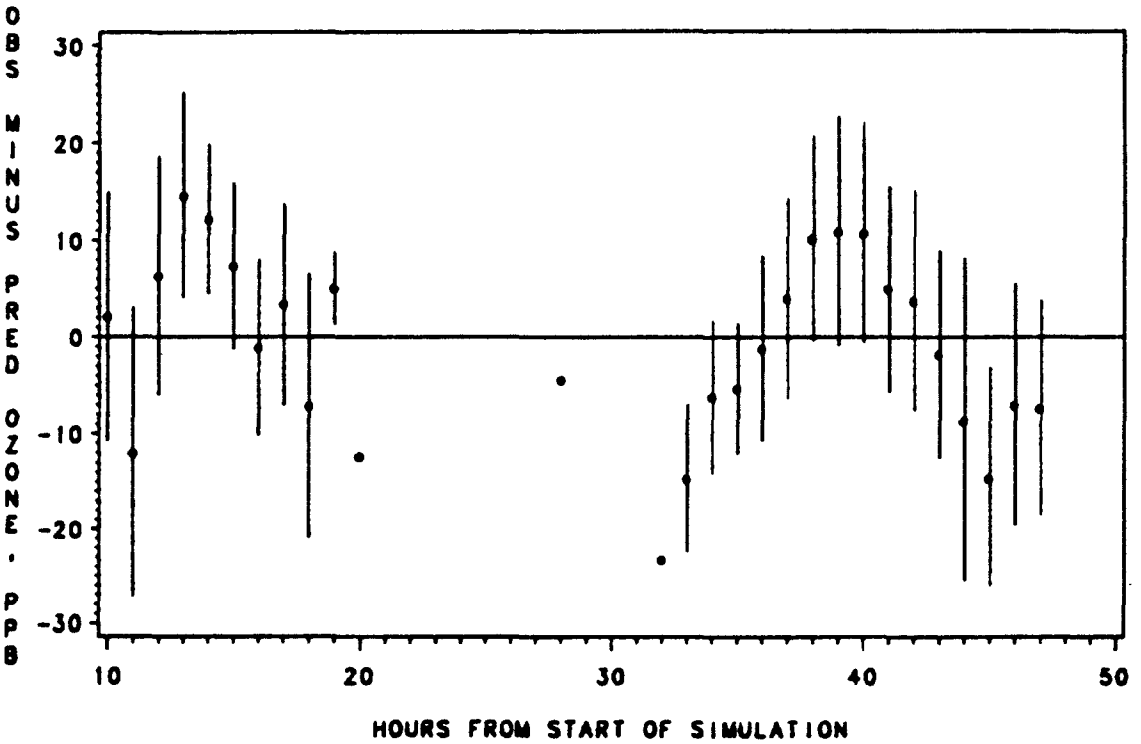

Figure 16a. Time-series over the 3-4 August 1979 simulation period of average bias over all surface receptor locations (where obs. and. pred. O_3 > 50 ppb).

PERCENT BIAS AVERAGE ALL RECEPTORS, LAYER ZERO

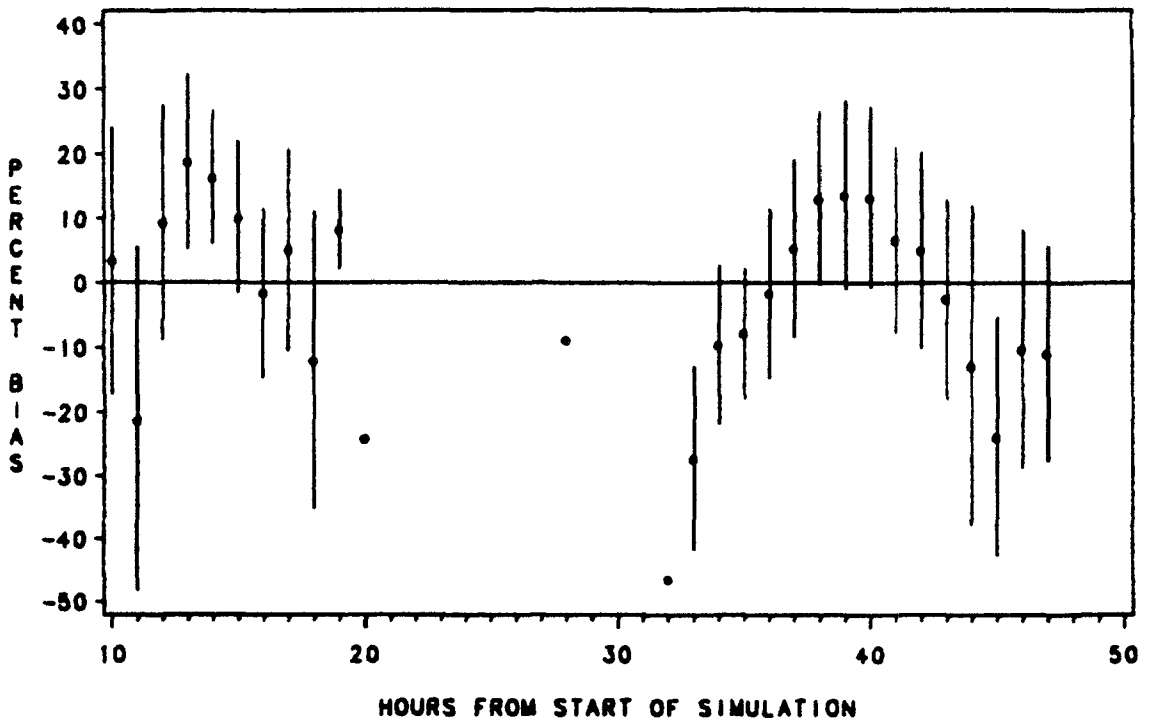

Figure 16b. Time-series over the 3-4 August 1979 simulation period of average percent bias over all surface receptor locations (where obs. and pred. O_3 > 50 ppb).

TABLE 4. SUMMARY OF ROM1 HOURLY RESULTS FOR 3-4 AUGUST 1979 WHERE OBSERVED AND PREDICTED O_3 > 50 PPB.

DATE - HOUR		n	$R_{\overline{c}_{ob}}$ (ppb)	$R_{\overline{c}_{p0}}$ (ppb)	$R_{\overline{c}_{p1}}$ (ppb)	$R_{\overline{d}_0}$ (ppb)	$R_{\overline{\lvert d_0 \rvert}}$ (ppb)	$R_{S_{d0}}$ (ppb)	$R_{\overline{d}_1}$ (ppb)	$R_{\overline{\lvert d_1 \rvert}}$ (ppb)	$R_{S_{d1}}$ (ppb)
79215	06	0	-	-	-	-	-	-	-	-	-
	07	0	-	-	-	-	-	-	-	-	-
	08	0	-	-	-	-	-	-	-	-	-
	09	0	-	-	-	-	-	-	-	-	-
	10	5	62.2	60.0	61.5	2.2	9.5	14.3	0.7	9.9	15.0
	11	6	56.2	68.1	69.4	-12.0	19.2	18.5	-13.2	20.4	18.6
	12	13	67.5	61.1	63.4	6.4	16.5	22.0	4.1	16.1	22.1
	13	21	78.0	63.3	65.4	14.7	21.6	24.1	12.6	21.6	24.8
	14	29	74.4	62.2	64.5	12.2	19.0	20.6	9.9	18.2	20.8
	15	24	73.0	65.6	67.4	7.4	17.8	20.9	5.6	17.3	21.2
	16	16	69.4	70.4	73.1	- 1.0	13.7	18.1	- 3.7	14.1	18.2
	17	13	66.7	63.3	65.9	3.5	12.6	18.7	0.7	12.8	19.1
	18	8	59.4	66.5	68.4	- 7.1	16.1	19.3	- 9.0	16.2	18.8
	19	2	61.0	56.0	58.9	5.1	5.1	2.6	2.1	2.1	0.6
	20	1	51.0	63.3	65.8	-12.3	12.3	-	-14.8	14.8	-
	21	0	-	-	-	-	-	-	-	-	-
	22	0	-	-	-	-	-	-	-	-	-
	23	0	-	-	-	-	-	-	-	-	-
79216	00	0	-	-	-	-	-	-	-	-	-
	01	0	-	-	-	-	-	-	-	-	-

TABLE 4. (continued)

DATE - HOUR	n	$R_{\bar{c}_{ob}}$ (ppb)	$R_{\bar{c}_{p0}}$ (ppb)	$R_{\bar{c}_{p1}}$ (ppb)	$R_{\bar{d}_0}$ (ppb)	$R_{\overline{\lvert d_0 \rvert}}$ (ppb)	$R_{S_{d0}}$ (ppb)	$R_{\bar{d}_1}$ (ppb)	$R_{\overline{\lvert d_1 \rvert}}$ (ppb)	$R_{S_{d1}}$ (ppb)
02	0	-	-	-	-	-	-	-	-	-
03	0	-	-	-	-	-	-	-	-	-
04	1	50.0	54.4	56.8	- 4.4	4.4	-	-6.8	6.8	-
05	0	-	-	-	-	-	-	-	-	-
06	0	-	-	-	-	-	-	-	-	-
07	0	-	-	-	-	-	-	-	-	-
08	1	50.0	73.2	85.9	-23.2	23.2	-	-35.9	35.9	-
09	8	53.7	68.3	72.2	-14.6	14.6	10.9	-18.5	18.5	12.3
10	19	64.1	70.2	72.5	- 6.2	13.6	17.1	- 8.4	15.0	17.4
11	29	66.9	72.2	74.3	- 5.3	16.0	18.1	- 7.3	16.5	18.0
12	32	72.9	74.1	76.1	- 1.2	21.7	26.9	- 3.2	22.4	26.9
13	38	75.1	71.0	73.5	4.0	23.8	31.7	1.6	23.8	31.3
14	37	78.0	67.9	70.3	10.1	26.0	31.8	7.8	25.7	31.7
15	32	80.4	69.5	72.9	10.9	27.4	33.2	7.6	26.6	33.1
16	31	80.7	70.0	72.7	10.7	23.8	31.2	8.0	22.7	31.0
17	27	74.6	69.6	72.0	5.0	18.8	27.5	2.7	18.5	27.7
18	18	75.1	71.3	74.0	3.8	19.6	24.0	1.1	20.0	24.4
19	12	69.6	71.3	74.1	- 1.8	13.6	18.5	- 4.6	13.4	17.9
20	6	67.5	76.2	77.2	- 8.7	17.4	20.5	- 9.8	17.6	20.1
21	8	61.0	75.5	77.1	-14.6	16.8	16.1	-16.1	17.6	15.7

TABLE 4. (continued)

DATE - HOUR	n	$R_{\bar{c}_{ob}}$ (ppb)	$R_{\bar{c}_{p0}}$ (ppb)	$R_{\bar{c}_{p1}}$ (ppb)	$R_{\bar{d}_0}$ (ppb)	$R_{\lvert d_0 \rvert}$ (ppb)	$R_{S_{d0}}$ (ppb)	$R_{\bar{d}_1}$ (ppb)	$R_{\lvert d_1 \rvert}$ (ppb)	$R_{S_{d1}}$ (ppb)
22	5	68.0	74.9	76.1	- 7.0	11.8	14.0	- 8.1	12.0	13.7
23	7	66.7	74.0	75.3	- 7.3	13.0	14.6	- 8.6	13.5	14.8
79215 ALL	138	70.3	64.3	66.4	6.0	17.0	21.1	3.9	16.8	21.3
79216 ALL	311	73.1	70.9	73.4	2.2	20.8	27.3	- 0.3	20.9	27.2
79215-79216 ALL	449	72.2	68.9	71.2	3.4	19.6	25.6	1.0	19.6	25.6

diction than the values computed for the full data set. The average values in the data subset are however, significantly greater than the tropospheric background O_3 value.

Maximum Values Analysis

The most significant parameter of interest for the air quality policy maker concerning ambient O_3 is the daily hourly average maximum value observed at a monitoring station. This is the value which is used, among other measures, to determine the extent of source emissions controls needed for the O_3 precursor species. The model evaluation for maximum O_3 concentration takes place in two steps here. First, in the local maxima analysis model predictions of maximum hourly average O_3 at surface monitoring site locations are compared with measured values at the sites. Second, in the global maxima analysis the concentration magnitudes and position of plumes of O_3 within the NEROS region are compared in the ROM1 predictions and in the observations at surface monitoring sites, to the extent that these sites can define such plumes. The global maxima analysis is necessary because small errors in the transport field can displace the predicted area of maximum O_3 concentrations just a short distance from the observed field, and cause large apparent underpredictions in the local maxima analysis. If the reason for the underprediction can be traced to a shift in position of the predicted O_3 plume from the observed plume, the problem could be corrected, in theory, by a more accurate description of the wind field. A model's ability to predict the correct maximum concentration, not necessarily at the right location, is the most important aspect in performance because the air quality standards apply only to the O_3 concentration level.

The local daily maximum O_3 concentration, c_{ob}^{max}, at a measuring site can be compared with the corresponding model prediction in two different ways. First, the predicted maximum at the site, c_{p0}^{max} for ROM1 layer 0 or c_{p1}^{max} for ROM1 layer 1, can be compared to c_{ob}^{max}. Second, a more restrictive measure matches the prediction occuring at the same hour

as the observed maximum, with the observed concentration ($c_{p0}(h_{ob}^{max})$ vs. c_{ob}^{max} and $c_{p1}(h_{ob}^{max})$ vs. c_{ob}^{max}). Figure 17 presents a scatterplot of the daily ROM1 layer 0 maximum O_3 concentrations vs. observations at the surface monitoring sites over the 2-day episode modeled. Figure 17a contains the plot of c_{p0}^{max} vs. c_{ob}^{max} and Figure 17b shows the plot of $c_{p0}(h_{ob}^{max})$ vs. c_{ob}^{max}. There is considerable scatter in both plots with little evidence of a strong correlation or trend. In fact the computed correlation coefficient between c_{p0}^{max} and c_{ob}^{max} is 0.08 and that between $c_{p0}(h_{ob}^{max})$ and c_{ob}^{max} is 0.00.

Looking more closely at the plots in Figure 17 it is obvious that a large cluster of the data points corresponds to an observed concentration range of 60-100 ppb and a predicted range of 30-50 ppb. These points correspond to receptor locations where the model has shown essentially only background O_3 concentrations and the monitors have detected increased levels above background. This effect may be due to a misplaced plume location in the predictions or an underestimate of the effect from precursor emissions. The plots also show a wide scatter in the data points at all concentration levels.

The values shown for c_{p0}^{max} are greater than the corresponding value of $c_{p0}(h_{ob}^{max})$ as expected, since c_{p0}^{max} is a less restrictive pairing of maximum values. The upper end of the range of values for c_{p0}^{max} is about 30 ppb greater than that for $c_{p0}(h_{ob}^{max})$, attesting to a phase lag between the time of the O_3 maxima predicted by ROM1 and the maxima observed at the monitoring stations. The results for ROM1 layer 1 are not significantly different than those shown here for layer 0.

The corresponding plots of bias versus observed maximum concentration are shown in Figure 18. The measure of bias, $d_{B0}^{max} = c_{ob}^{max} - c_{p0}^{max}$, is plotted in 18a and $d_{A0}^{max} = c_{ob}^{max} - c_{p0}(h_{ob}^{max})$ is plotted in 18b. The trends displayed in these scatterplots show a fairly strong correlation between the bias and the observed maximum concentration with increased levels of underprediction at higher ambient O_3 concentrations. Much of this trend

LAYER ZERO MAX VS RECEPTOR MAX

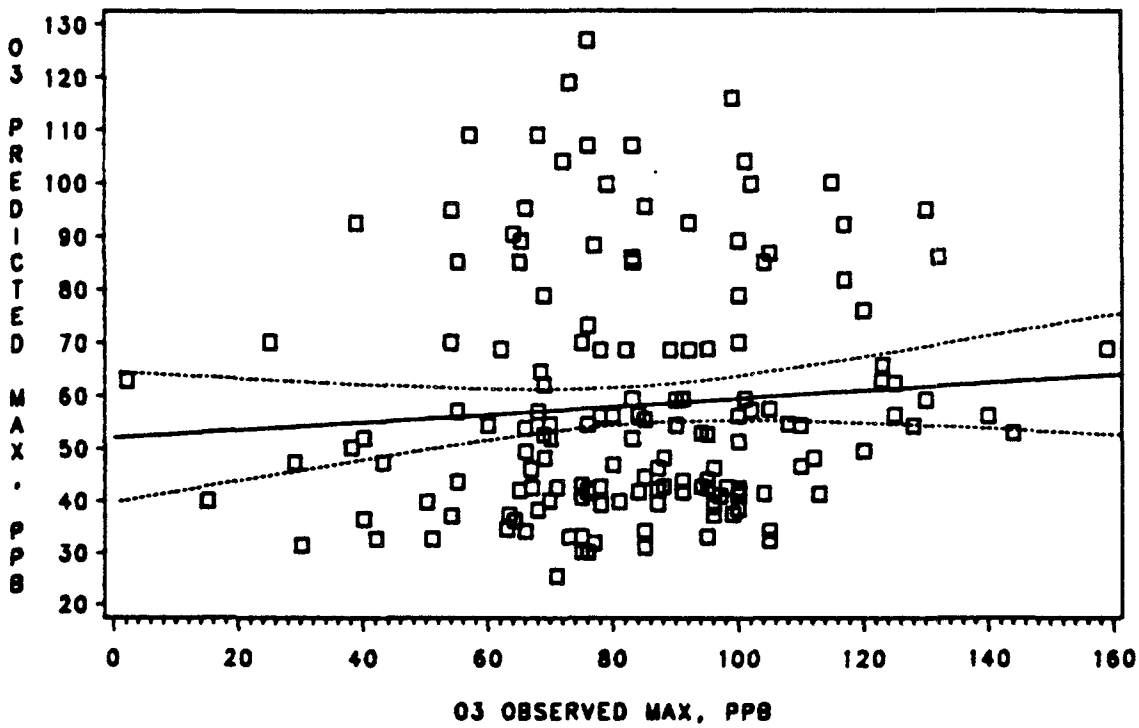

Figure 17a. Scatterplot of c_{p0}^{max} vs. c_{ob}^{max} for O_3 concentrations at all surface monitoring sites on 3-4 August 1979.

LAYER ZERO VALUE AT TIME OF OBSERVED MAX

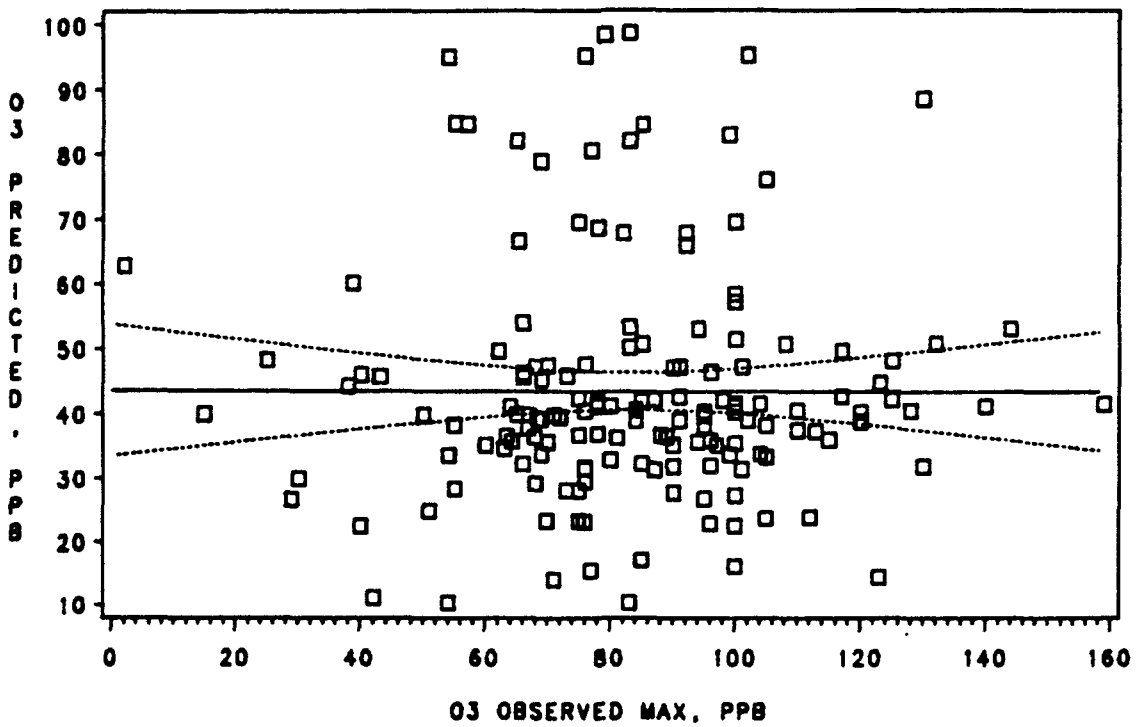

Figure 17b. Scatterplot of $c_{p0}(h_{ob}^{max})$ vs. c_{ob}^{max} for O_3 concentrations at all surface monitoring sites on 3-4 August 1979.

LAYER ZERO BIAS VS RECEPTOR MAX

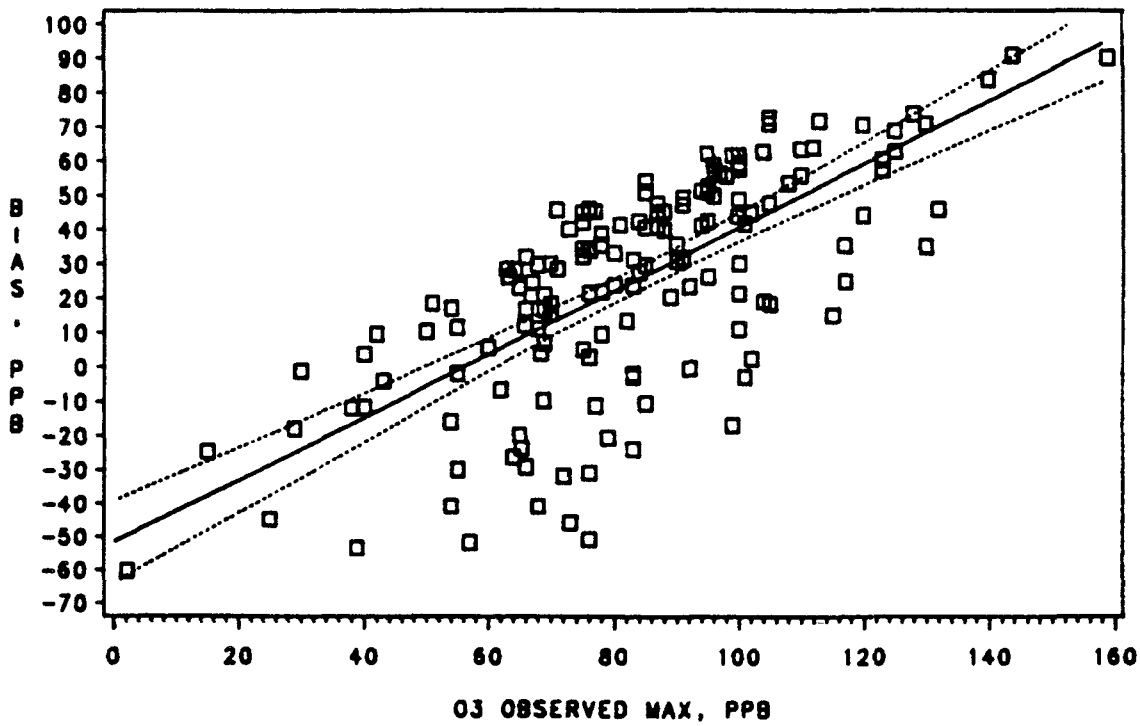

Figure 18a. Scatterplot of d_{BO}^{max} vs. c_{ob}^{max} for O_3 concentrations at all surface monitoring sites on 3-4 August 1979.

LAYER ZERO BIAS AT TIME OF RECEPTOR MAX

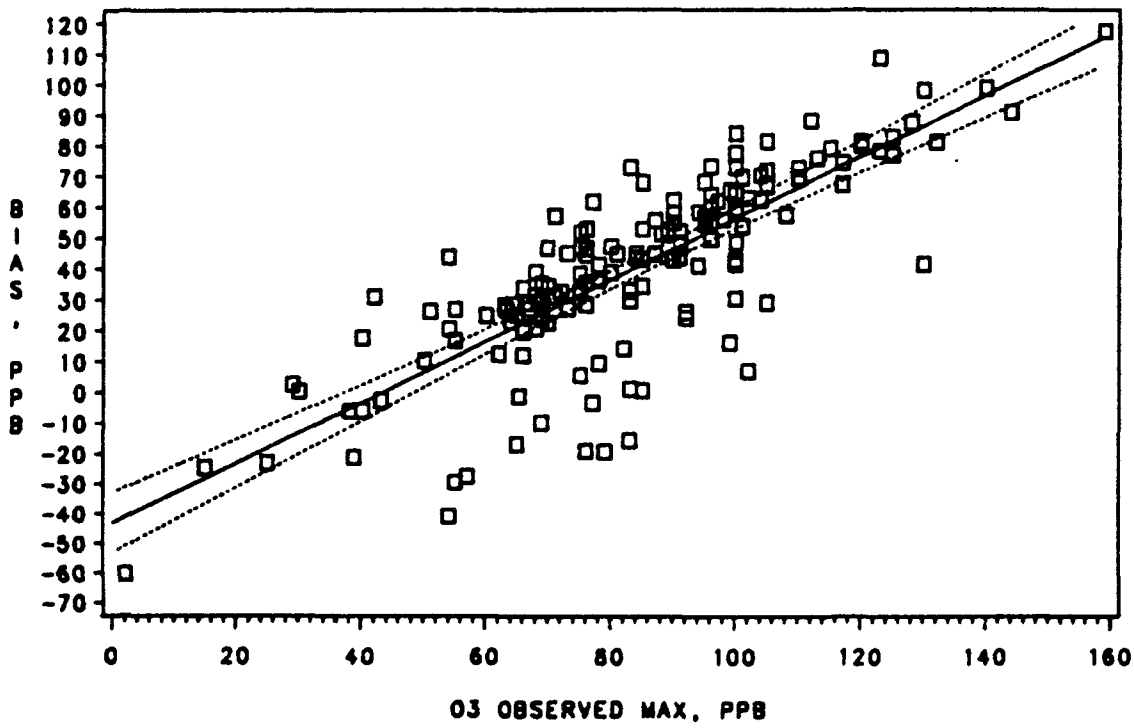

Figure 18b. Scatterplot of d_{AO}^{max} vs. c_{ob}^{max} for O_3 concentrations at all surface monitoring sites on 3-4 August 1979.

is understood to be caused by the narrow range of background concentrations predicted at many of the monitoring site locations that showed a wide range of observed maxima. Again, the problem relates to the initial and boundary O_3 tropospheric background concentration imposed on the model and the subsequent pervasiveness of this value in the predicted model results. The bias values are correspondingly larger for d_{AO}^{max} than for d_{BO}^{max} because of the more restrictive pairing implied in d_{AO}^{max}.

A summary of statistics from the local maximum values analysis for the model simulation is presented in Table 5. Results from the full data set as well as the data subset of O_3 concentrations where c_{ob}, c_{p0}, and c_{p1} are all greater than 50 ppb are given. The number of receptor stations dropped from 156 in the full data set to 47 in the data subset. Interestingly, the average observed maximum value increased by only 2-4 ppb from the data set to the subset because there were very few observed maxima less than 50 ppb at the monitoring site locations. Conversely, the average model predictions increased by 20-30 ppb from the data set to the subset because of the large number of values near the background O_3 level. For the looser pairing of observed and predicted maximum values the average bias at all receptor sites was 24.8 ppb on 3 August, representing a 34% underprediction and 25.3 ppb on 4 August, representing a 33% underprediction, for model layer 0. For layer 1 the corresponding values are 23.2 ppb (32% underprediction) on 3 August, and 23.3 ppb (30% underprediction) on 4 August. In the data subset where the lower O_3 values are excluded the results show a marked improvement. On 3 August, the average bias for layer 0 was 11.3 ppb (15% underprediction) and on 4 August, it was 5.6 ppb (7% underprediction). For layer 1 the corresponding values are 9.2 ppb (12% underprediction) on 3 August, and 2.7 ppb (3% underprediction) on 4 August. A listing of all surface monitoring sites and their respective observed and predicted maximum values on both days is given in Appendix B.

The purpose of the global maximum values analysis is to attempt to isolate individual areas or plumes of high O_3 concentrations in the model predictions and the ambient observations for comparison. The perspective

TABLE 5. SUMMARY OF ROM1 RESULTS FOR LOCAL MAXIMUM VALUES FOR 3-4 AUGUST 1979

	Full Data Set		Data Subset (c_{ob}, c_{p0}, c_{p1} > 50 ppb)	
	79215	79216	79215	79216
n	156	154	47	48
$R_{\bar{c}_{ob}^{max}}$ (ppb)	73.2	77.8	75.5	81.8
$R_{\bar{c}_{p0}^{max}}$ (ppb)	48.4	52.5	64.2	76.2
$R_{\bar{c}_{p0}(h_{ob}^{max})}$ (ppb)	40.0	43.5	60.0	68.9
$R_{\bar{c}_{p1}^{max}}$ (ppb)	50.0	54.5	66.3	79.1
$R_{\bar{c}_{p1}(h_{ob}^{max})}$ (ppb)	41.6	45.1	62.0	71.4
$R_{\bar{d}_{B0}^{max}}$ (ppb)	24.8	25.3	11.3	5.6
$R_{\bar{d}_{A0}^{max}}$ (ppb)	33.2	34.3	15.5	12.9
$R_{\bar{d}_{B1}^{max}}$ (ppb)	23.2	23.3	9.2	2.7
$R_{\bar{d}_{A1}^{max}}$ (ppb)	31.6	32.7	13.5	10.4
$R_{s_{dB0}^{max}}$ (ppb)	26.9	33.6	21.9	32.6
$R_{s_{dA0}^{max}}$ (ppb)	26.8	32.1	21.4	30.9
$R_{s_{dB1}^{max}}$ (ppb)	26.9	33.8	21.9	32.3
$R_{s_{dA1}^{max}}$ (ppb)	27.0	32.3	21.5	30.7

in this analysis is broader than that in the local maximum values analysis in that model predictions at the same location as the observation are not necessarily required. Instead, the eligible area from which the model prediction is chosen is defined to be the coherent region of concentrations, or plume, from which the observation comes. This less restrictive pairing permits us to match observations and predictions based on supposedly similar phenomenological events in the physical processes producing the maximum O_3 values. This perspective also permits us to include a larger area than the single site location where the maximum value occurred.

A number of problems arise in the implementation of this analysis. The number and spatial distribution of surface monitoring sites for O_3 is not ideal for defining plumes over the NEROS region (see Figures 1,4, and 5). The sites are primarily located in and very close to urban areas, limiting the ability to define the downwind extent of an urban plume. We shall rely on the interpolated wind field used by ROM1 to help define the projected plume location from major source areas in the NEROS region. We desire to include areas that show consistent plume transport as well as numerous monitoring sites near the projected plume path.

Figure 19 shows the 12-hour projected forward trajectories starting at 0600 h on 3 August from some of the major urban source areas in the NEROS region. The stars indicate the starting location and the dots are the monitoring site locations. The trajectories are based on the ROM1 layer 1 wind field. The analogous plot for 4 August is shown in Figure 20. On the first day the trajectories from cities in the western part of the grid show fairly consistent directions while in the east the influence of the offshore stationary front on the wind flows is evident by the varying directions, especially in the New York and Philadelphia trajectories which show recirculation patterns. On 4 August the eastern trajectories all appear from the NNW, except for Boston which shows a slower flow from the SE. The western trajectories are from the west and SW.

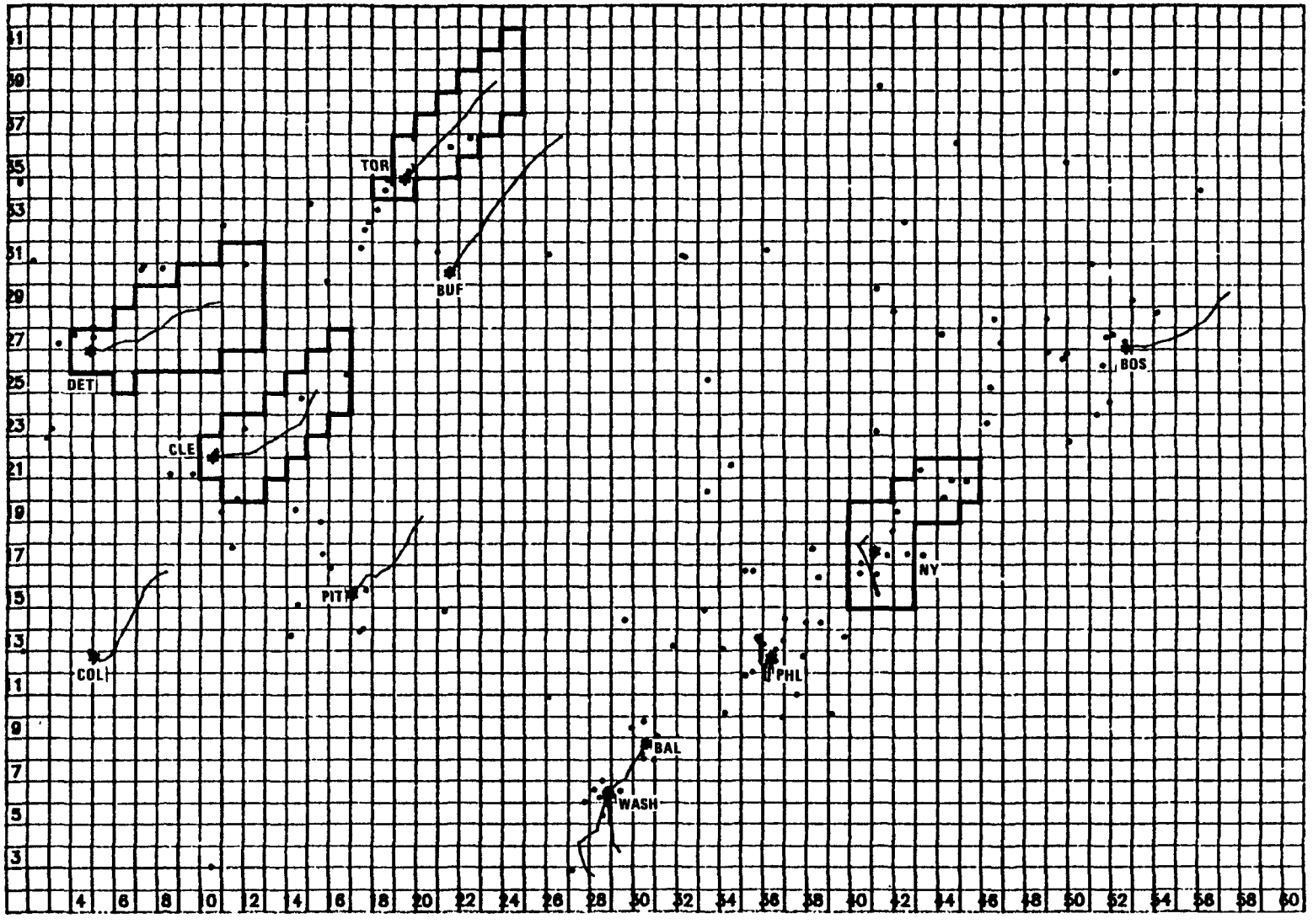

Figure 19. ROM1 grid showing projected 12-hr forward trajectories on 3 Aug. 1979 from selected urban source areas.

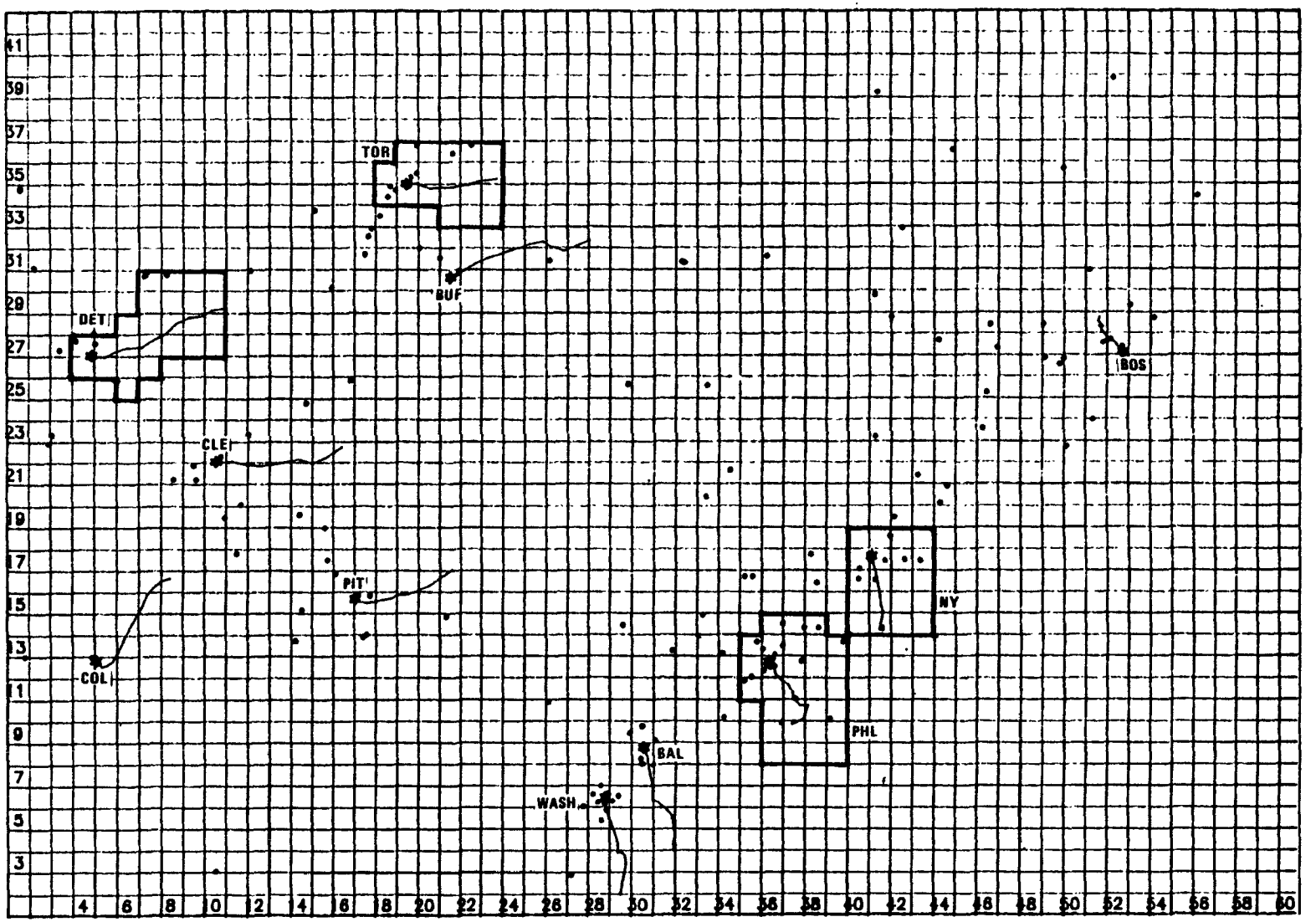

Figure 20. ROM1 grid showing projected 12-hr forward trajectories on 4 Aug. 1979 from selected urban source areas.

It is immediately apparent that few of the trajectories have sufficient monitoring sites in their vicinity to substantiate an O_3 plume. Therefore, in choosing which projected plumes to study further and determining their spatial extent we examine the contoured field of O_3 concentrations from ROM1 layer 1 on both days at 1400 h and 1600 h in Figures 21 and 22, as well as the maximum observed values of O_3 shown in Figures 4 and 5. In specific instances the aircraft sampling measurements are useful in locating O_3 plumes also. On 3 August significant O_3 plumes are projected downwind of Detroit and Toronto and near the New York area. Observed concentrations are also high along the south shore of Lake Erie so the Cleveland area will be included in the analysis also. Some relatively high O_3 values are observed also in the Washington and Philadelphia areas, although the ROM1 predictions show only minor perturbations in these areas. The variable cloud cover and occasional rain showers may have allowed just enough solar radiation through to promote some local O_3 generation there, but the hour-averaged and spatially interpolated data used by the model apparently did not allow for the same effect. The ROM1 grid areas shown in Figure 19 with the darkened borders are the plume areas chosen for further analysis on 3 August.

On 4 August significant O_3 plumes are again projected downwind of Detroit and Toronto. Since the greater portion of these plumes are over the Great Lakes, comparison with monitoring data are not easily made. However, stations near the periphery of the lakes do show higher values of O_3 (Figure 5) so these plumes will be considered for analysis. Higher O_3 areas also exist along coastal and southern New Jersey in both model predictions and observations. These areas coincide with the projected downwind extent of the New York and Philadelphia plumes, and they are included in the global maximum values analysis. Relatively high O_3 values (as high as 140 ppb) are observed in the immediate Washington, D.C. area on 4 August, although the model's predictions in this area are not much above background. The discrepancy here is unresolved and may need more simulations to determine the adequacy of the emission data and other inputs in this part of the grid. The areas with darkened borders in Figure 20 are the plume areas chosen for further analysis on 4 August.

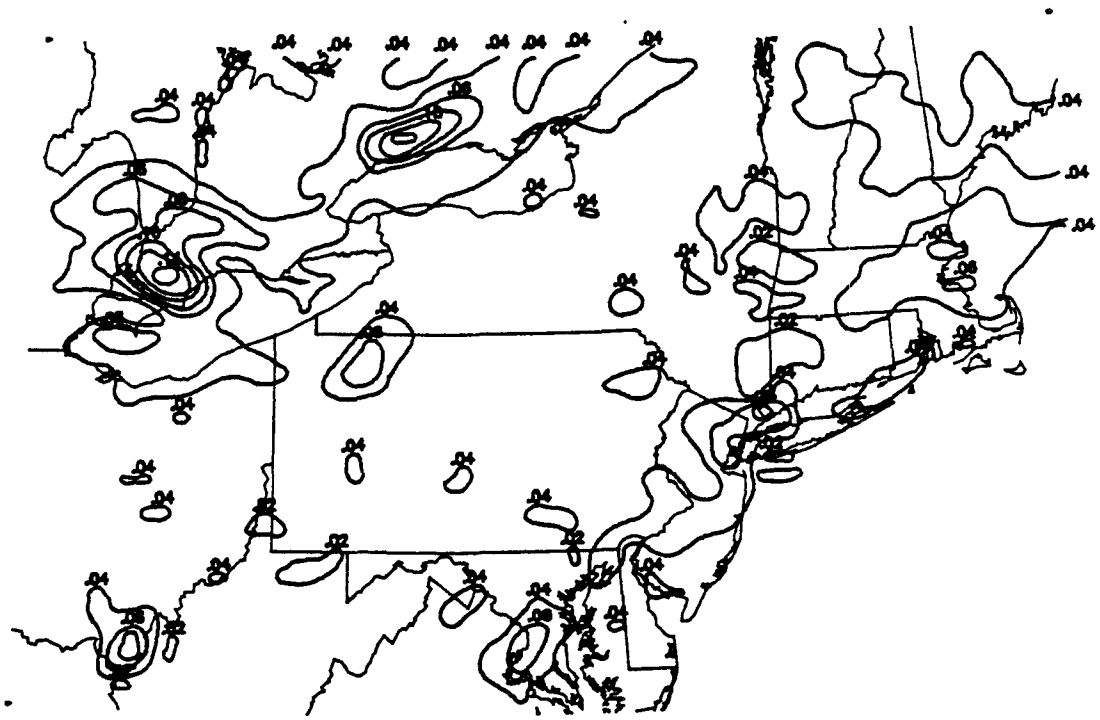

Figure 21a. Contours of hour-averaged predicted O_3 concentrations in ROM1 layer 1 on 3 Aug. 1979 at 1400 h, LST.

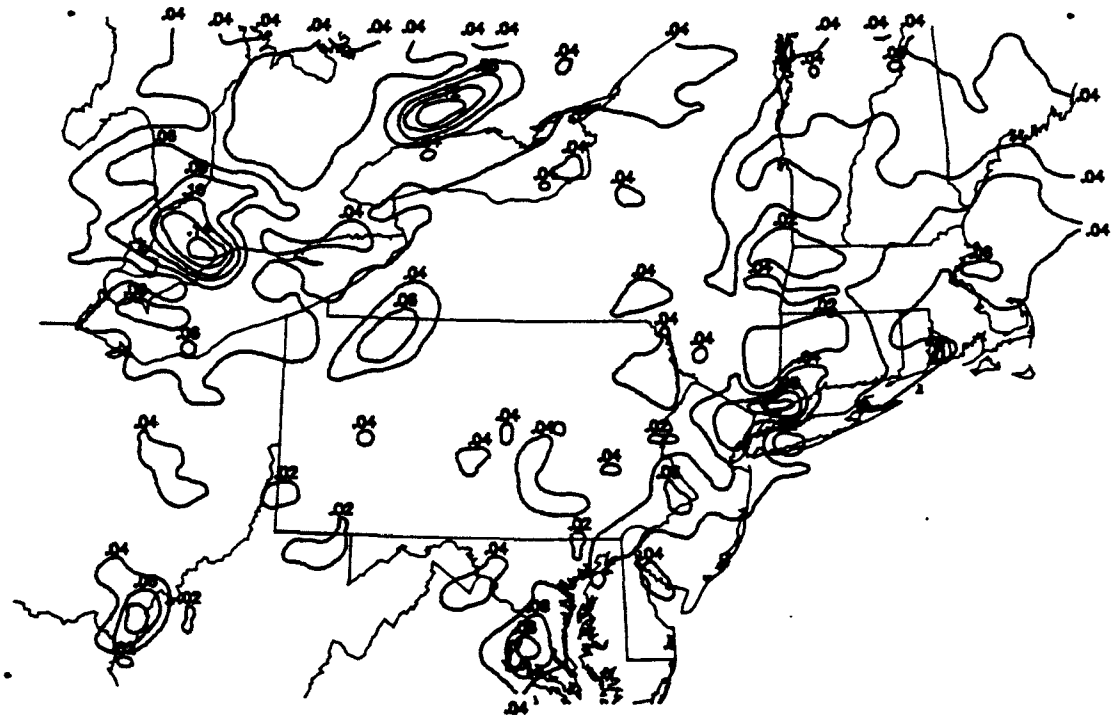

Figure 21b. Contours of hour-averaged predicted O_3 concentrations in ROM1 layer 1 on 3 Aug. 1979 at 1600 h, LST.

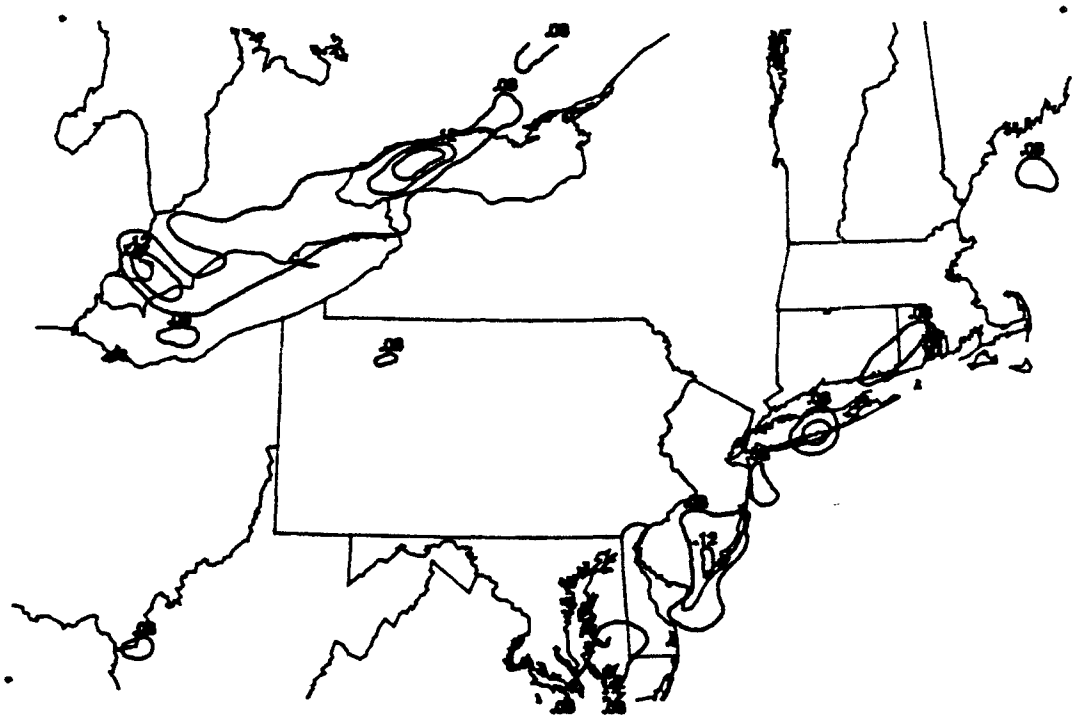

Figure 22a. Contours of hour-averaged predicted O_3 concentrations in ROM1 layer 1 on 4 Aug. 1979 at 1400 h, LST.

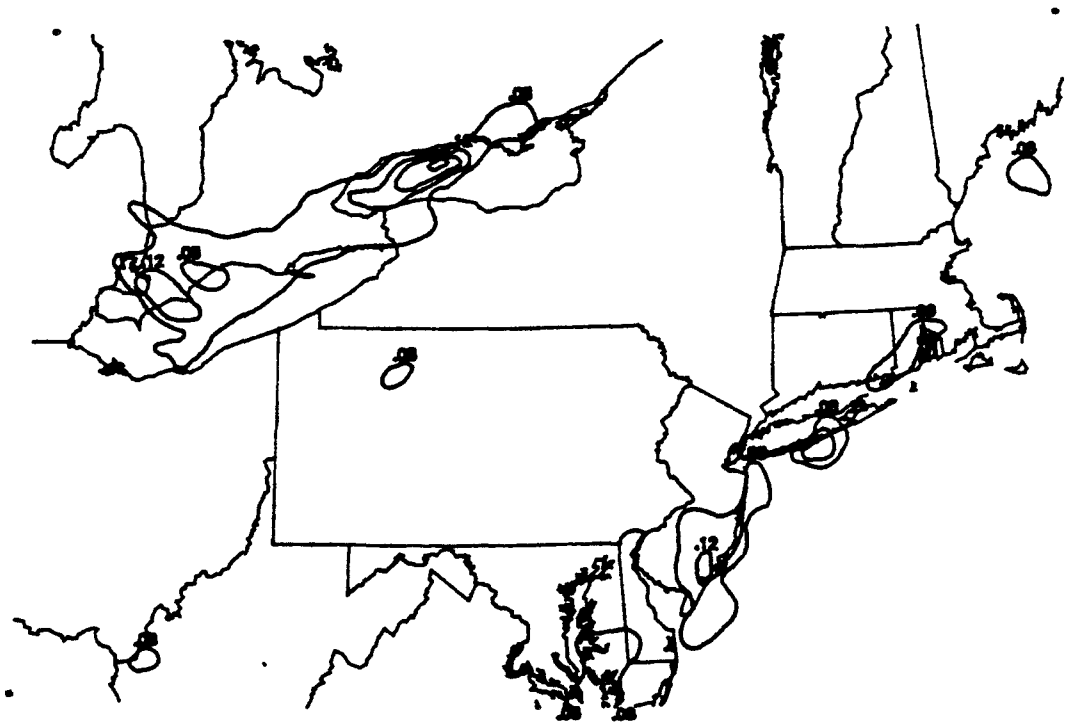

Figure 22b. Contours of hour-averaged predicted O_3 concentrations in ROM1 layer 1 on 4 Aug. 1979 at 1600 h, LST.

A more detailed depiction of the Toronto plume on 3 August is given in Figure 23. The projected O_3 plume is evident in the contoured model predictions of daily maximum O_3 downwind of the center location of Toronto, indicated by the "+". The surface monitoring sites and the maximum concentration observed at each are also shown. Two of the downwind sites observing maximum O_3 between 80 and 100 ppb show excellent agreement with model predictions at those locations. Another site located in the area of the projected plume appears to have an anomalously low maximum value of O_3 of 55 ppb. This site may have been directly affected by a nearby source of NO_x emissions during the day. There were no surface monitoring stations in the vicinity of the projected plume maximum of 144 ppb. Note that the maximum values observed at the stations nearest to the central urban area show considerable variation at close range to each other. This is not unexpected given the heterogeneous emissions patterns of a large urban area. The expected variance in concentrations within a grid cell is estimated within the formulation for model layer 0 and will be evaluated with field data using the second generation regional model, ROM2.

In estimating model performance in the global maximum perspective we define three different comparisons of model predicted concentration with the maximum observed concentration, c_{ob}^{max}, in the O_3 plume. First, there is the predicted maximum at the same location as the monitoring site of the observed maximum. Second, there is the maximum predicted concentration at any of the monitoring site locations in or near the projected plume, and finally there is the maximum concentration found in the grid cell at the center of the projected O_3 plume. These three values are designated (for ROM1 layer 1) as c_{pl-A}^{max}, c_{pl-B}^{max}, and c_{pl-C}^{max}, respectively and proceed from the most to the least strict pairing of concentrations in the global maxima analysis. For the Toronto plume on 3 August, c_{pl-A}^{max} = c_{pl-B}^{max} = 110 ppb at site ORO since the model-predicted maximum O_3 occurred at the same site as the observed maximum, and c_{pl-C}^{max} = 144 ppb at cell location (23,38). There are also corresponding values for ROM1 layer 0 that are not discussed here but will be tabulated later. The measures of bias resulting from these pairings are d_{pl-A}^{max}, d_{pl-B}^{max},

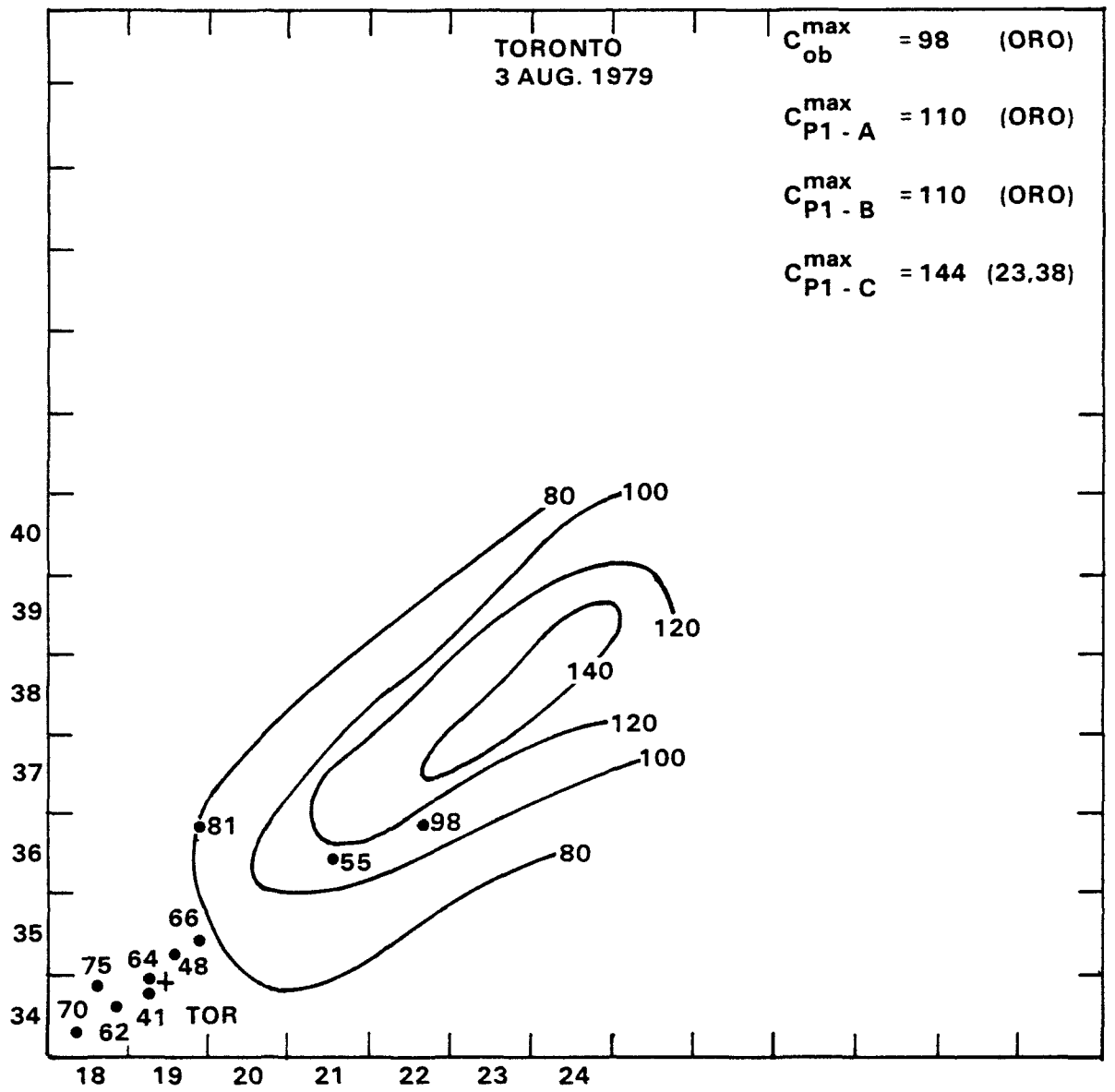

Figure 23. Predicted (ROM1 layer 1) and observed maximum O_3 concentrations (ppb) downwind of Toronto on 3 Aug. 1979.

and d_{pl-C}^{max} and have values of -12, -12, and -46 ppb, respectively, for this plume.

Figure 24 presents the time series of O_3 concentrations for station ORO on 3 August. It is evident that the predicted concentrations do not fall to the low levels that the monitoring stations observe for the dark hours. The predicted values shown here are for model layer 1, although layer 0 values are not very different. Also, the peak value is predicted earlier in the day than that observed at the station. A difference in time between the predicted and observed peak O_3 values is not uncommon in photochemical dispersion models and is often the result of the chemical kinetics in the model being more or less reactive than the existing atmospheric case. Transport and dispersion of the precursor emissions also, of course, can affect the timing of the peak at a given location. In this case the model predicts the maximum O_3 concentration within the plume to occur later in the day at 1700 h downwind of ORO. That is closer to the time of the observed maximum at ORO.

The case of the Detroit and Cleveland areas are considered together in Figure 25. The ROM1 does not develop an O_3 plume downwind of Cleveland on 3 August as can be seen by the nearly flat gradient in concentrations. Surface observations to the northeast however indicate two stations downwind, near the Lake Erie shoreline, showing maxima of 159 and 95 ppb. As discussed in Section 2, these higher concentrations are not the result of photochemical generation from Cleveland, but rather reflect the previous day's O_3 in an aged plume from Detroit or elsewhere that had been advected over Lake Erie and fumigated to the surface during the morning hours. Both the time-series records of surface concentrations at these stations and aircraft observations of O_3 aloft made by the WSU aircraft (flight 8 - see Figure 6) later in the day on 3 August over the eastern end of Lake Erie and south of Buffalo help substantiate this. Also, the maximum concentration in the model-predicted plume downwind of Detroit was 158 ppb on 3 August, very close to the value observed at the CNE station on the south shore of Lake Erie. Presumably if the maximum O_3 generated in the Detroit plume from the previous day was of a

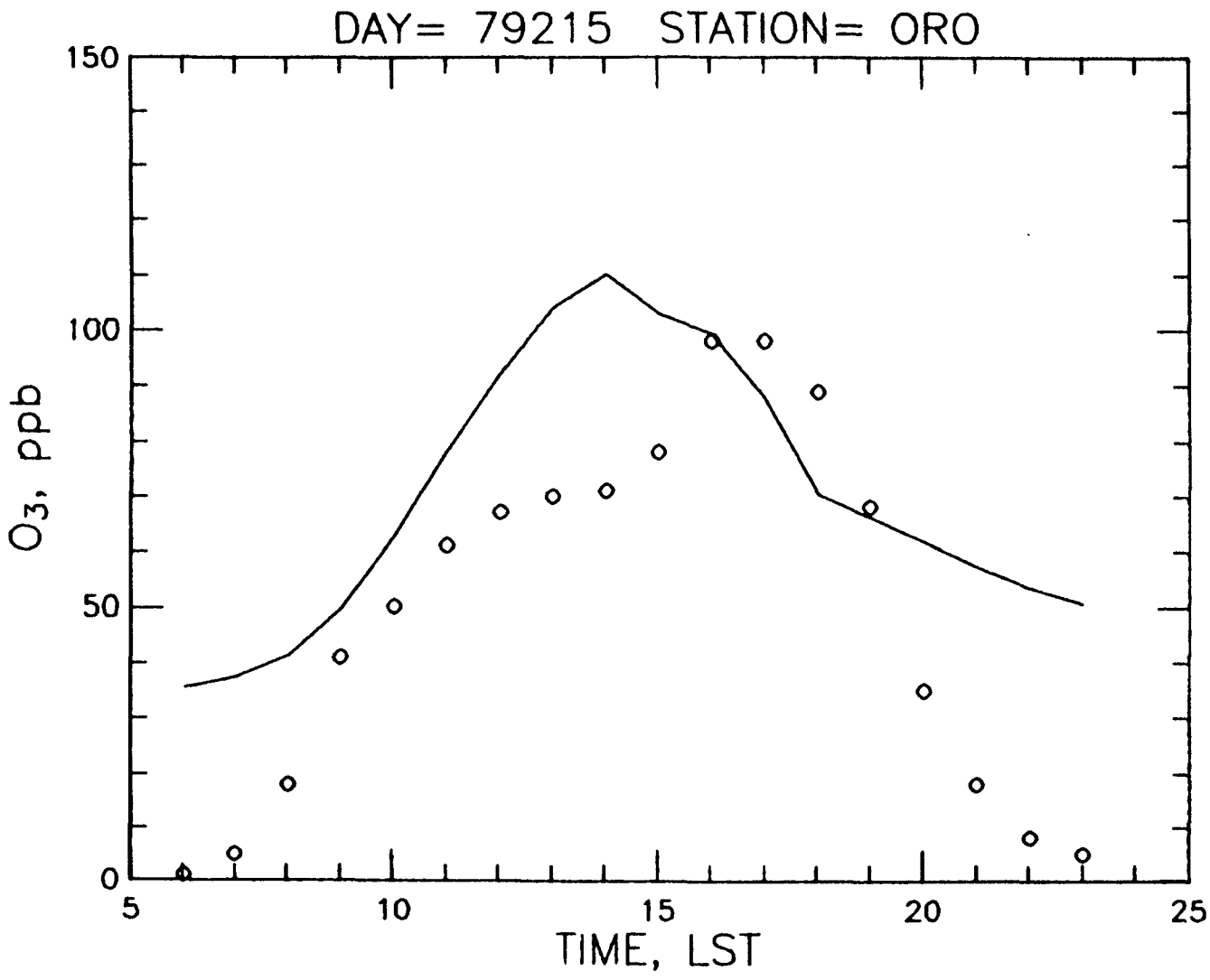

Figure 24. Time-series of predicted (ROM1 layer 1) and observed O_3 concentrations at monitoring site ORO on 3 Aug. 1979.

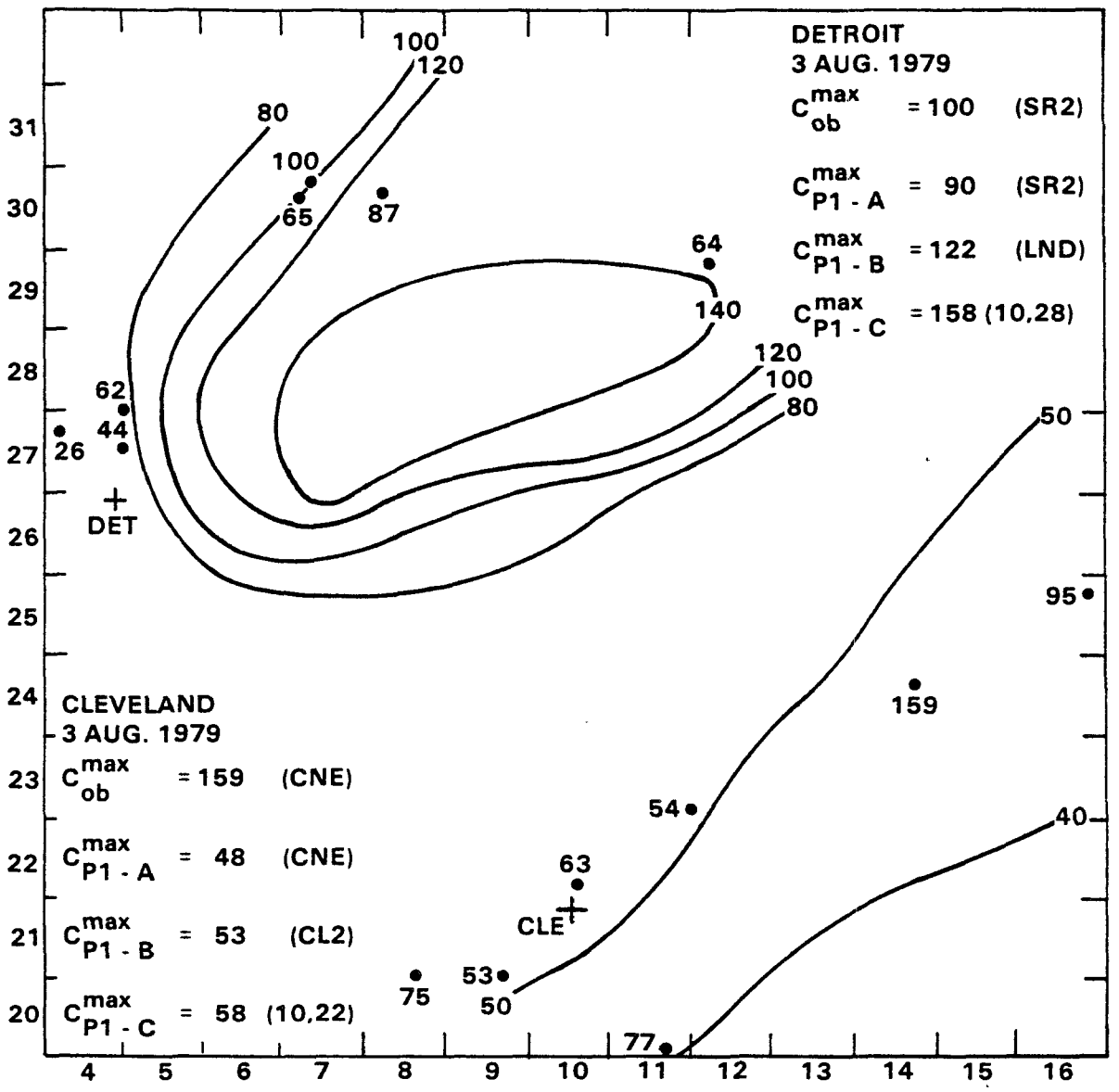

Figure 25. Predicted (ROM1 layer 1) and observed maximum O_3 concentrations (ppb) downwind of Detroit and Cleveland on 3 Aug. 1979.

similiar magnitude, the more westerly winds on 2 August would have carried the plume over Lake Erie and to the vicinity of these south shore stations. The test simulation discussed here was initialized with clean tropospheric concentrations of all species and thus does not address the issue of carry-over of concentrations from 2 August. The Cleveland area is therefore dropped from further consideration because the model predictions and the surface monitors do not support plume generation here.

The ROM1 O_3 predictions clearly show a plume emanating from the Detroit-Windsor area northeast into Ontario on 3 August. The maximum predicted concentration within this plume, c_{pl-C}^{max}, is 158 ppb at grid cell (10,28) at 1700 h, LST. The one surface station closest to the area of maximum predicted concentrations shows a measured maximum of only 64 ppb, while the model-predicted O_3 value for the site is nearly twice as much. Stations along the northern edge of the plume show somewhat closer agreement. For instance, the maximum value observed in the projected plume area, c_{ob}^{max}, was at Sarnia, Ontario (SR2) at 100 ppb and the maximum predicted value at that site was 90 ppb, a 10% underprediction. The time-series of observed and predicted O_3 concentrations for SR2 is shown in Figure 26. The observed peak is attained rather early in the day, at 1200 h, indicating the likelihood of even higher concentrations farther downwind. The model predictions again stabilize at higher levels during the nighttime hours than do the observations.

The final plume analyzed for this day is that for New York. The projected 12-hour forward trajectory for New York shown in Figure 19 indicates some looping and recirculation in the air parcels in the vicinity of the stationary front lying very close to New York. This introduces a larger degree of uncertainty in establishing an accurate trajectory path, but we do attempt to locate an O_3 plume here because observed concentrations were relatively high at several surface monitoring stations to the northeast of New York. Figure 27 shows the contoured predictions of maximum O_3 concentrations along the projected trajectory path from New York which has been expanded and lengthened somewhat for this analysis to allow for

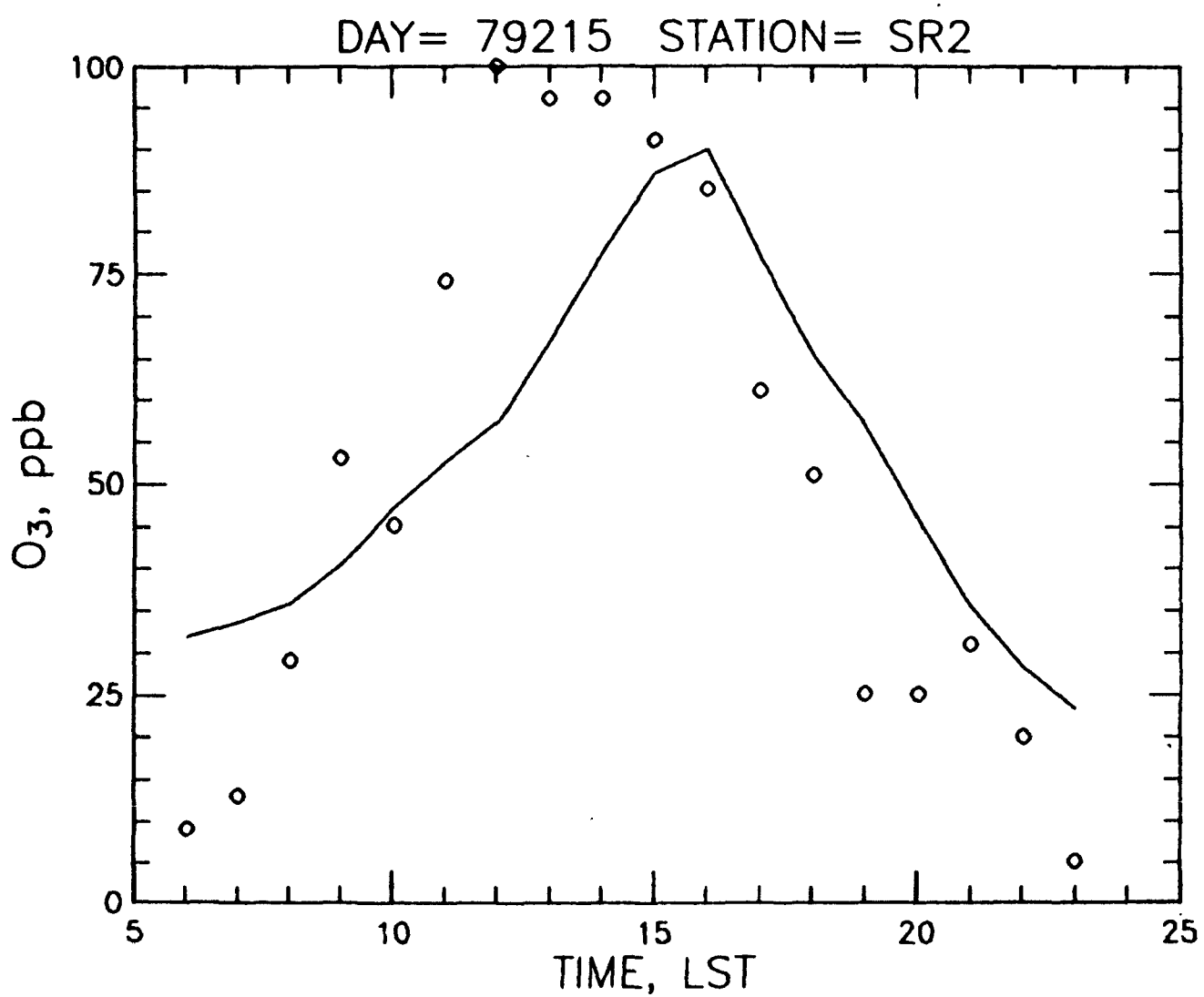

Figure 26. Time-series of predicted (ROM1 layer 1) and observed O_3 concentrations at monitoring site SR2 on 3 Aug. 1979.

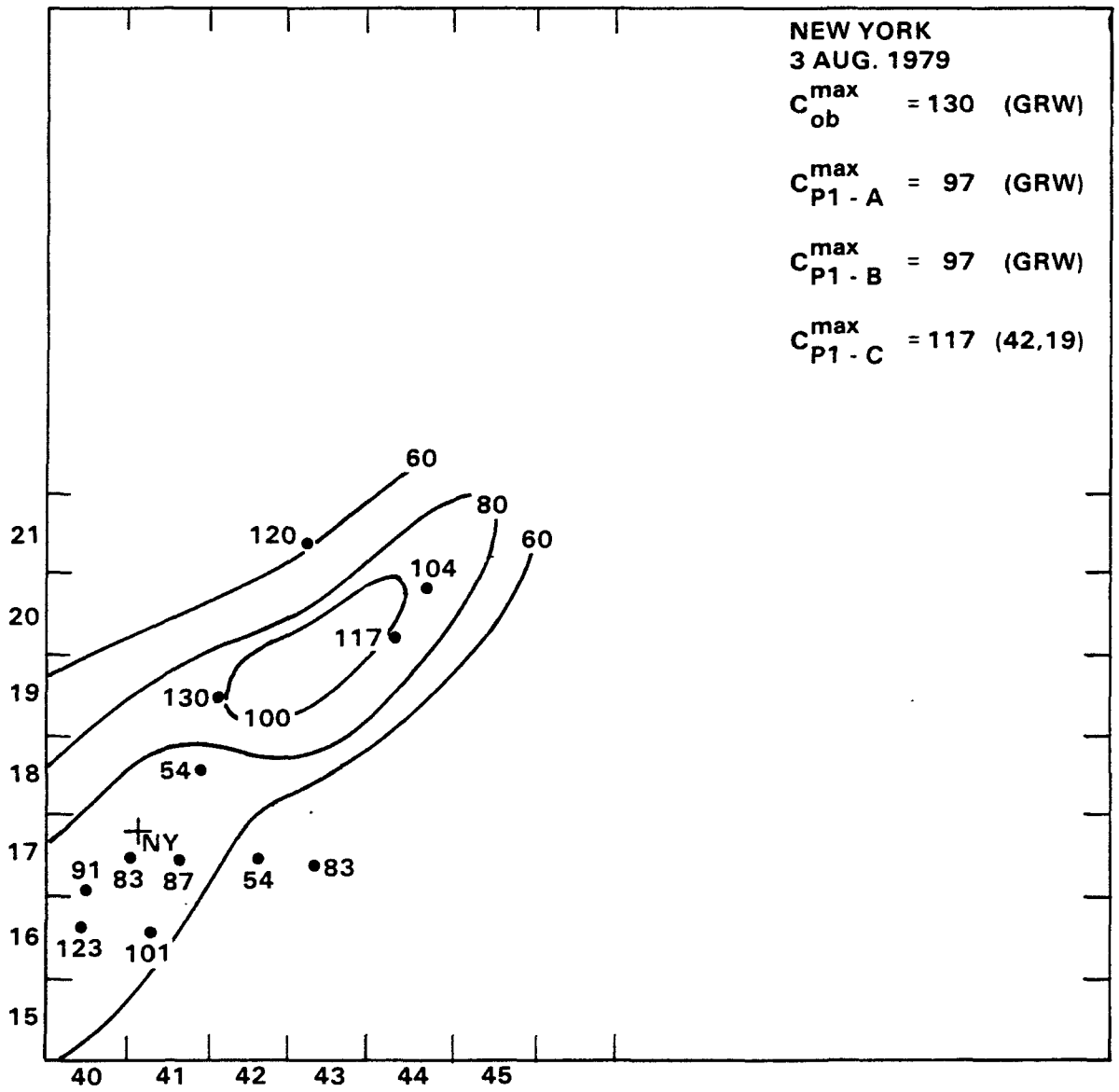

Figure 27. Predicted (ROM1 layer 1) and observed maximum O_3 concentrations (ppb) downwind of New York on 3 Aug. 1979.

the greater uncertainty in the looping path. An O_3 plume is observed in the predictions to the northeast of New York with the maximum, c^{max}_{pl-C}, of 117 ppb at grid cell (42,19). Fortuitously there are several monitoring sites in the vicinity of the predicted plume, and it appears that its predicted location is quite good. The maximum observed concentration, c^{max}_{ob}, occurred at GRW in Connecticut, located in the same grid cell as c^{max}_{pl-C}. The magnitude of the observed maximum was 130 ppb, implying a 10% underprediction when c^{max}_{ob} is paired with c^{max}_{pl-C}. The model prediction at GRW, c^{max}_{pl-A} (and c^{max}_{pl-B}), is 97 ppb, giving a 25% underprediction with the more strict pairing. A station at the northern edge of the projected O_3 plume shows a maximum concentration of 120 ppb while the prediction is around 60 ppb. Apparently, while the center portion of the plume has been well-located the breadth of the high concentration area has been underestimated. Figure 28 presents the concentration time-series at station GRW on 3 August 1979. The timing of the peak concentration coincides within one hour between observed and predicted O_3 maxima in accordance with the well-located predicted plume position. The temporal concentration gradients are smaller in the ROM1 predictions at this location than the observations and, in fact, the predicted O_3 concentration appears to level off into the evening hours while the surface monitor indicates a rapid depletion of O_3 toward evening.

Another interesting aspect of the concentration field near New York occurs to the south and southwest of the city where relatively high O_3 values (up to 123 ppb) are observed at monitoring stations there. The initial path of the trajectory from New York is in a southerly direction before looping to the northeast so it is not entirely surprising to find higher concentrations there. The model predictions, however, do not exhibit this secondary peak to the southwest, possibly because the model has advected the precursor emissions farther along the trajectory before photochemical generation could get well underway.

Over the evening and nighttime periods from 3 August into 4 August, the ROM1 advects the predicted O_3 plume from Detroit east and northeast over Lake Erie and eventually to the south of Toronto over Lake Ontario. The more stable

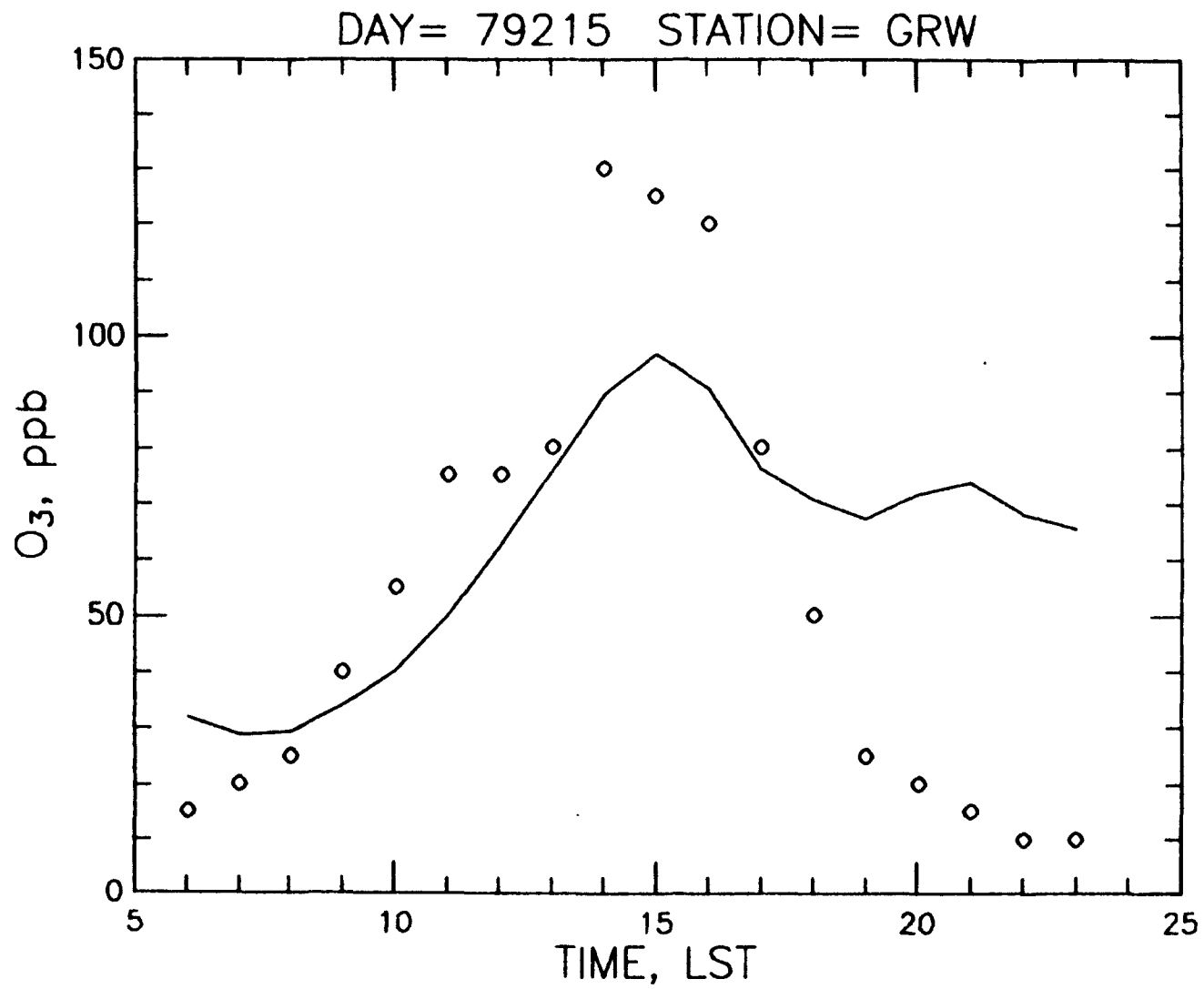

Figure 28. Time-series of predicted (ROM1 layer 1) and observed O_3 concentrations at monitoring site GRW on 3 Aug. 1979.

atmosphere over the lake waters is modeled by ROM1 and manifests in allowing the concentrations within the now-aging Detroit plume to remain rather high. The Toronto forward trajectory for 4 August shows a movement to the east of the urban area. Contours of the maximum predicted hourly O_3 for model layer 1 downwind of Toronto are shown in Figure 29. The highest predicted values, in excess of 220 ppb, are east of Toronto over Lake Ontario. The Toronto plume on 4 August is shown by the simulation to have been transported into the area of the day-old Detroit plume over the lake. The synergism between the new and older plumes has produced rather high predicted levels. None of the surface monitoring stations is located in a position to validate the highest O_3 levels. Site ORO, northeast of Toronto, had an observed maximum O_3 value of 101 ppb on 4 August. The ROM1 predictions show this site location to be just on the periphery of the O_3 plume, and the time-series of concentrations here, shown in Figure 30, clearly shows not only an underprediction, but also little correspondence in the temporal pattern. The observations appear to show that ORO was more directly affected by the Toronto plume than the predictions indicate. The maximum predicted concentration at ORO was 66 ppb.

Examining the monitoring sites upwind of Toronto might indicate the existence of the transported Detroit plume on 4 August. The results here are mixed. Two sites near the lakes, St. Catherines in Ontario and Niagara Falls in New York, indicate maximum O_3 values less than 60 ppb. The other sites show a range of 76-92 ppb, certainly more than background but not at the 100 and over ppb level of the predictions. It appears that the effect of the older transported plume has been overemphasized by the model. The highest O_3 prediction occurring at monitoring site locations, c^{max}_{pl-B}, was 107 ppb at STC and NG2, the same two sites that showed the lower maximum observed values.

WSU conducted several aircraft transects on 3-4 August that approached the area of interest of the Toronto-(old) Detroit predicted plume. The shaded grid cells in Figure 29 are those where the WSU aircraft O_3 monitor observed values between 100 and 120 ppb at about 1000 m above ground between the hours of 2000 on 3 August, and 0000 on 4 August. It thus appears that an older plume was advected into this area aloft, although judging from the sampling

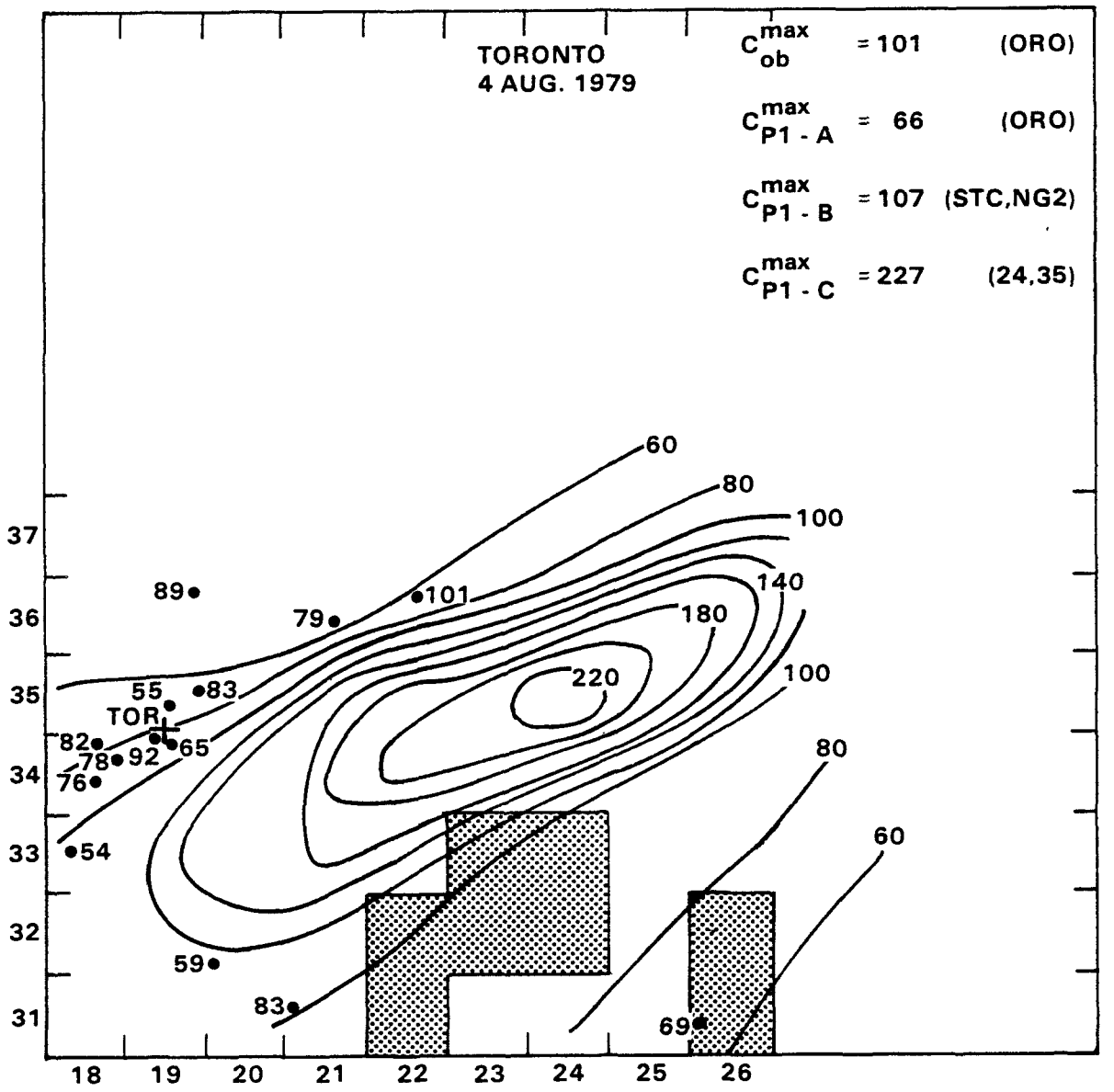

Figure 29. Predicted (ROM1 layer 1) and observed maximum O_3 concentrations (ppb) downwind of Toronto on 4 Aug. 1979.

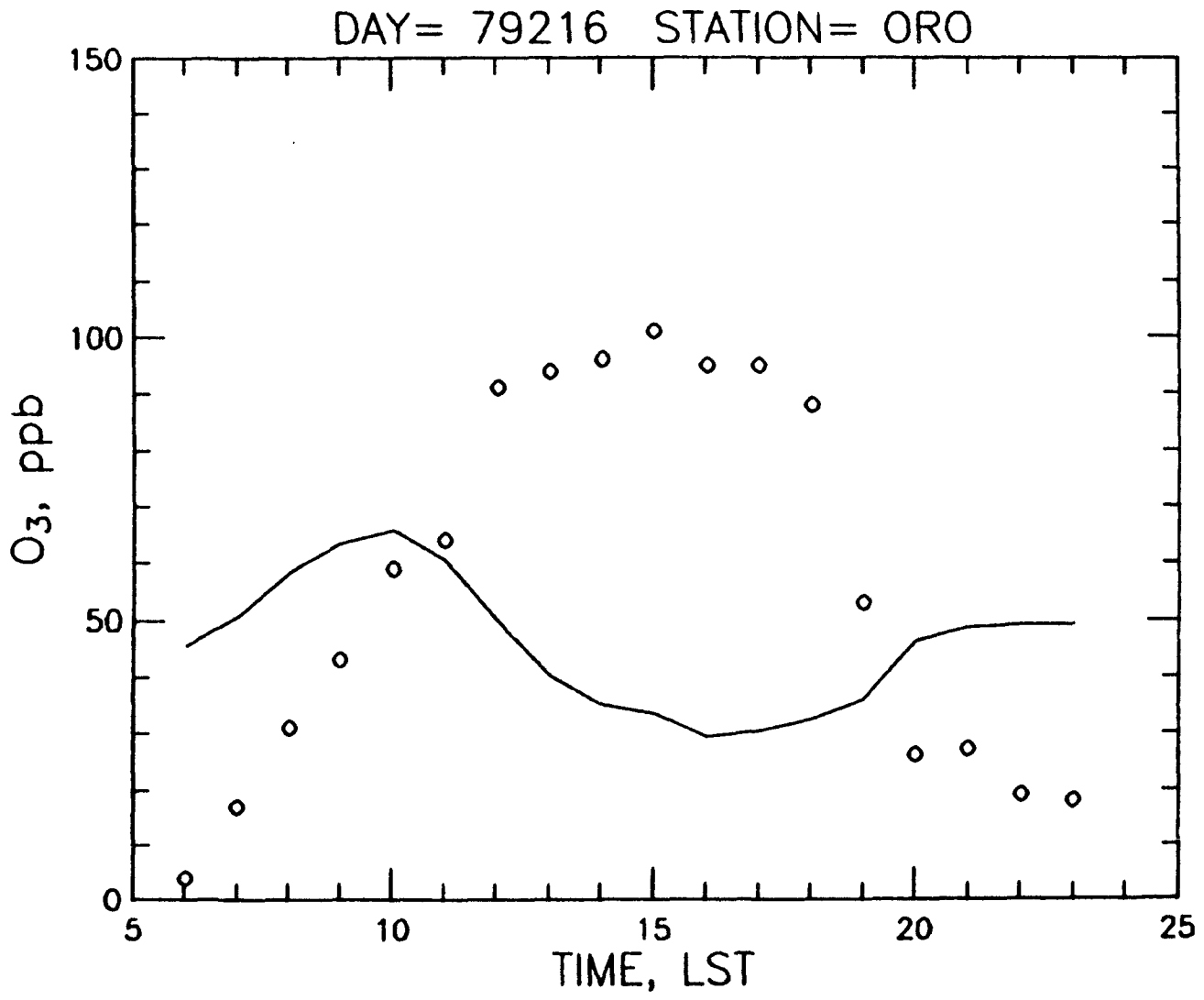

Figure 30. Time-series of predicted (ROM1 layer 1) and observed O_3 concentrations at monitoring site ORO on 4 Aug. 1979.

time and location this may have been the remnants of a plume from the Detroit area on 2 August. The surface monitoring site at Monroe, New York, near Rochester, showed maximum hourly O_3 concentrations of 61 ppb on 3 August and 69 ppb on 4 August, while the WSU aircraft sampled O_3 as high as 127 ppb aloft in the same vicinity during the night hours spanning 3-4 August. It appears that the effects of the plume aloft were not entirely felt at the surface at this particular site. If the higher observed concentrations aloft are, in fact, from the Detroit plume of 3 August, the ROM1 has predicted its location somewhat to the north of its true position.

The forward trajectory from Detroit on 4 August travels to the east of the city and later takes a northeast turn. The axis of the maximum predicted O_3 concentration area from Detroit, as seen in Figure 31, is oriented southeast from the city over Ontario and western Lake Erie. The maximum concentration, c^{max}_{pl-C}, in the plume is 162 ppb at grid cell (8,26). The surface monitoring stations showing the largest hourly level of O_3 are SR2 and PTR, northeast of Detroit, where 99 ppb was observed. There appears to be a bifurcation in the predicted plume with a secondary maximum just west of station PTR. The maximum O_3 concentration predicted at the PTR site, c^{max}_{pl-B} , is 88 ppb, an 11% underprediction. The time-series of observed and predicted O_3 concentrations at PTR is shown in Figure 32. The hourly observed values show a bimodal peak with the greater value occuring at 1800 h, LST. The predicted pattern of values is smoother with the peak occurring at 1600 h, LST. There are only 2 monitoring stations south of Detroit, near the periphery of the predicted plume. At WNS and DT4 the predicted O_3 peak values were both 94 ppb, while the observed peaks were 39 and 74 ppb, respectively. The wide variation in values at these near-by stations attests to their central urban locations. No surface monitoring sites lie close to the central area of the predicted plume.

The RTI aircraft, however, flew a sampling transect in a north-south line during the afternoon of 4 August, and measured elevated O_3 concentrations in the exact vicinity of the predicted Detroit plume. The specific flight is labeled F in Figure 7, and corresponds to a north-south run along column 8 of

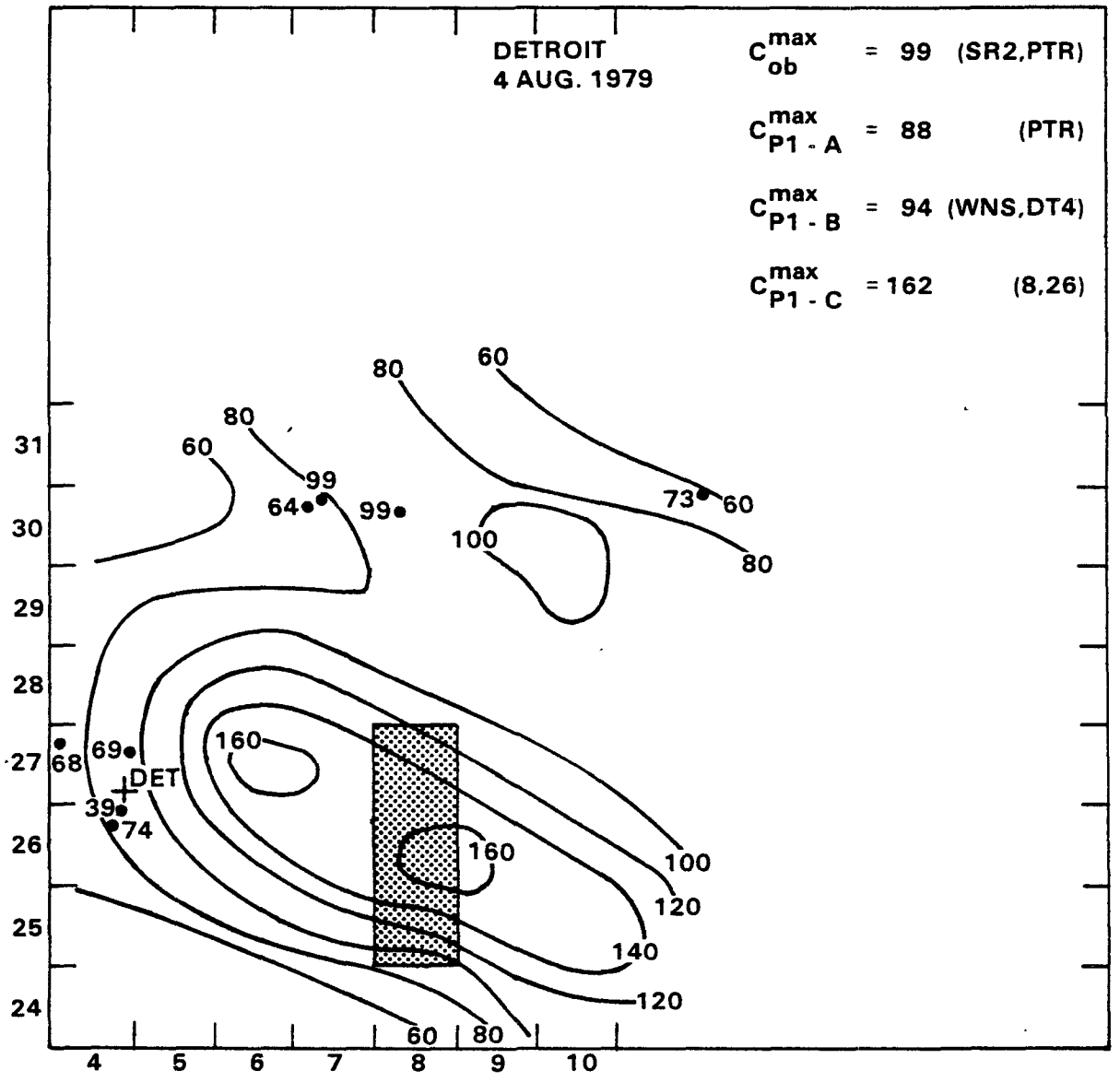

Figure 31. Predicted (ROM1 layer 1) and observed maximum O_3 concentrations (ppb) downwind of Detroit on 4 Aug. 1979.

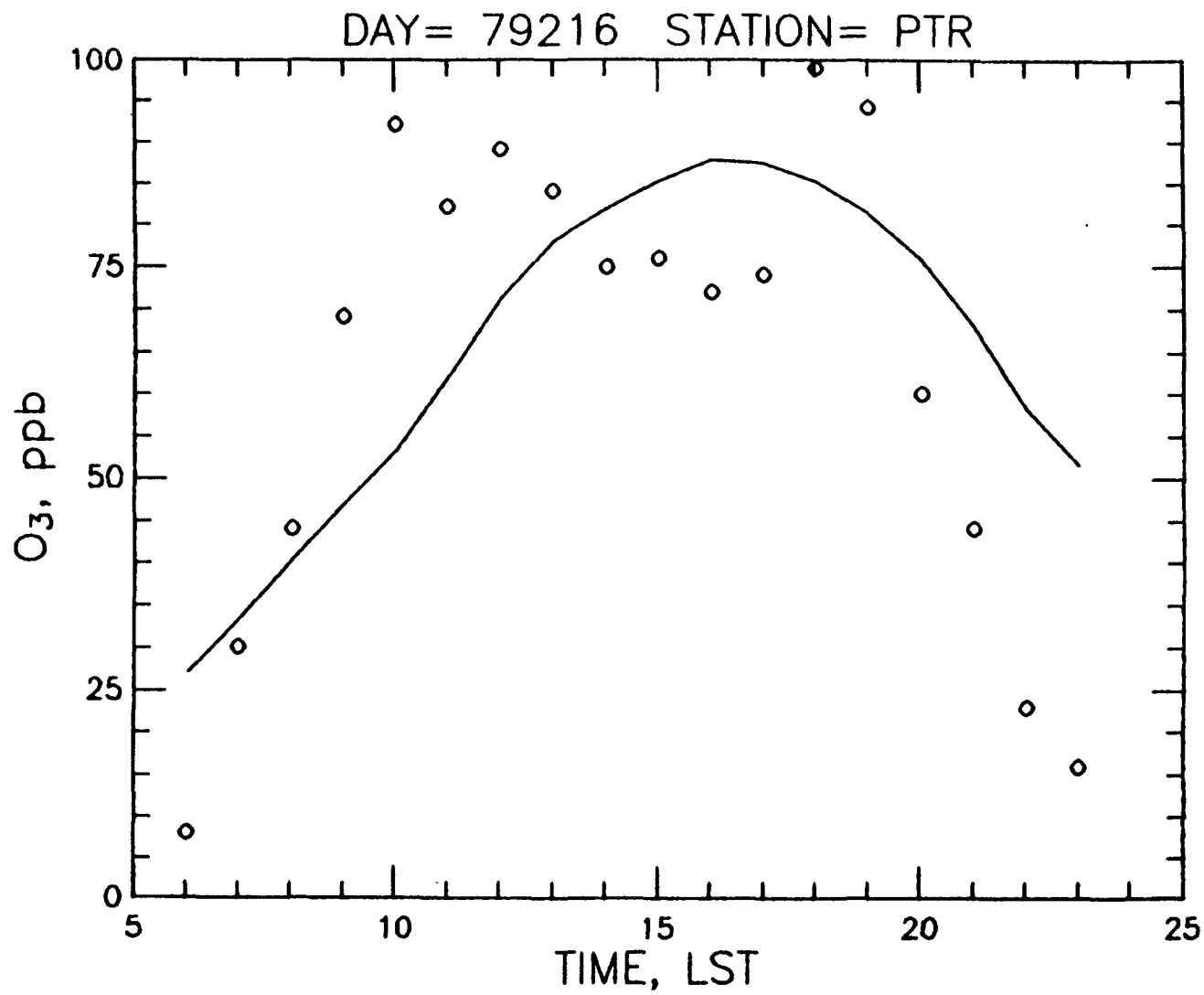

Figure 32. Time-series of predicted (ROM1 layer 1) and observed O_3 concentrations at monitoring site PTR on 4 Aug. 1979.

cells in the ROM1 model domain. The shaded cells in Figure 31 correspond to the locations where the aircraft sampled O_3 above the 60 ppb background level that existed on either side of the plume. Within the shaded cells the integrated observed values along the aircraft trajectory were about 90 ppb in cell (8,25), 105 ppb in cell (8,26), and 110 ppb in cell (8,27), although individual O_3 peak values within this sampling area reached 150 ppb. The model predictions and the aircraft observations are in rough agreement here in terms of plume location, width, and approximate O_3 concentrations. The maximum level predicted in the model (162 ppb in grid cell 8,26) occurred at 1600 h, LST while the aircraft sampling in the vicinity occurred at 1400 h, LST.

The O_3 plumes from the New York and Philadelphia areas on 4 August are shown in Figure 33. The forward trajectories for that day predict the plumes to be located SE of Philadelphia and SSE of New York. Maximum predicted O_3 concentrations in those areas are 135 ppb downwind of Philadelphia and 114 ppb downwind of New York. There is also a maximum concentration area to the east of New York that is not in a downwind direction of the city. Recirculation effects from the looped trajectory out of New York on the previous day have most likely had an additive effect with fresh emissions to the north of New York on the current day to produce this maximum concentration area off Long Island. The only surface station within this predicted plume is BAB and the maximum level recorded there was 58 ppb. There is no evidence that there was, in fact, a plume in this vicinity. The meteorological conditions of clouds and showers here on 4 August also do not support the existence of a plume. The interpolated field of cloud cover however did show some anomalous areas in the data-sparse regions over the ocean and these areas may have underestimated the cloud cover to the east of New York going into the ROM1. This would lead to an overestimate of photochemical reactivity.

The surface stations showing the highest maximum hourly O_3 concentrations near New York lie southwest in New Jersey. A maximum value of 144 ppb was recorded at site MER, while the maximum layer 1 prediction here was 59 ppb. Figure 34 presents the time-series of predicted and observed concentrations at this site. Either the predicted plume is badly positioned or recirculation

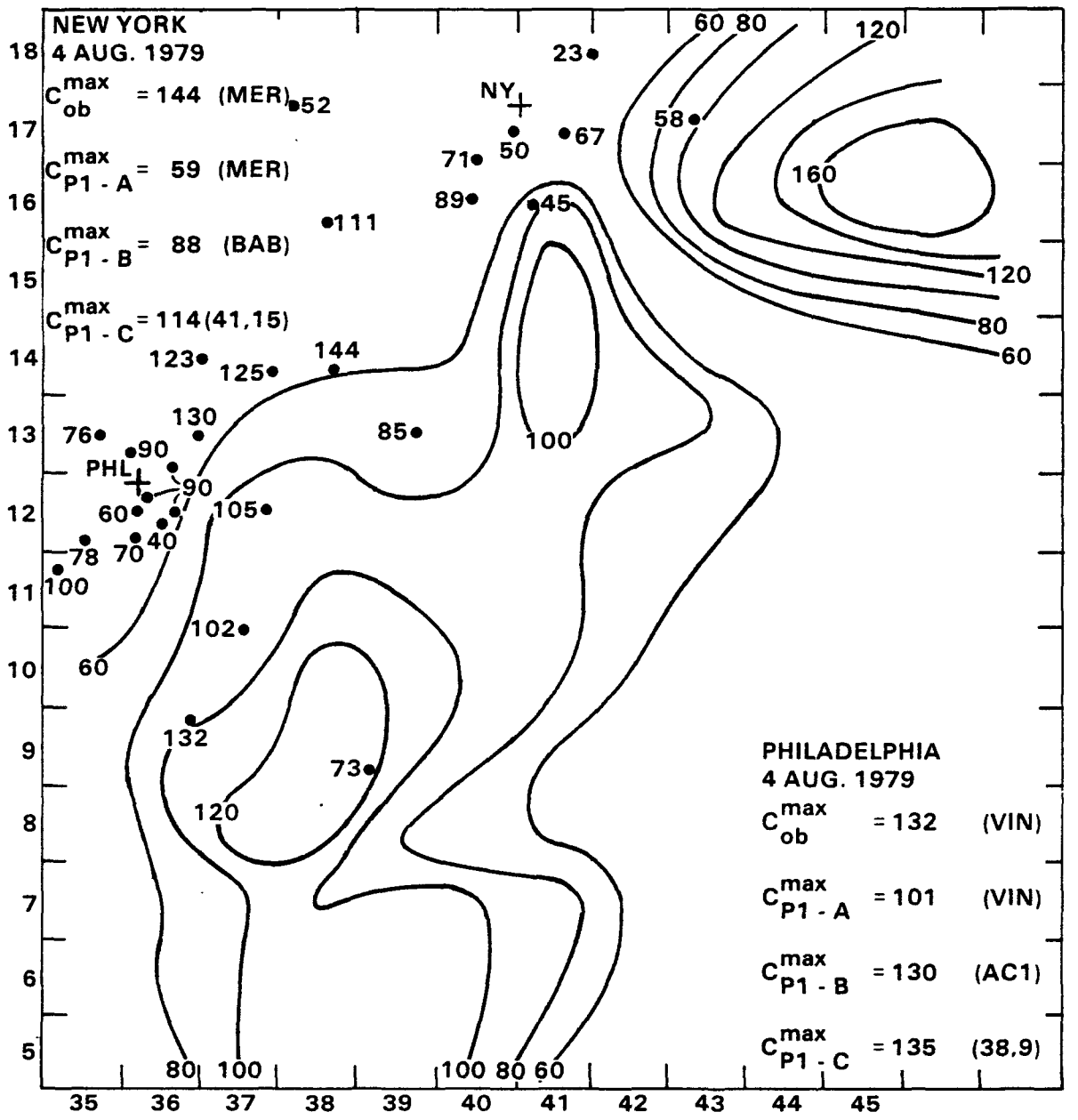

Figure 33. Predicted (ROM1 layer 1) and observed maximum O_3 concentrations (ppb) downwind of New York and Philadelphia on 4 Aug. 1979.

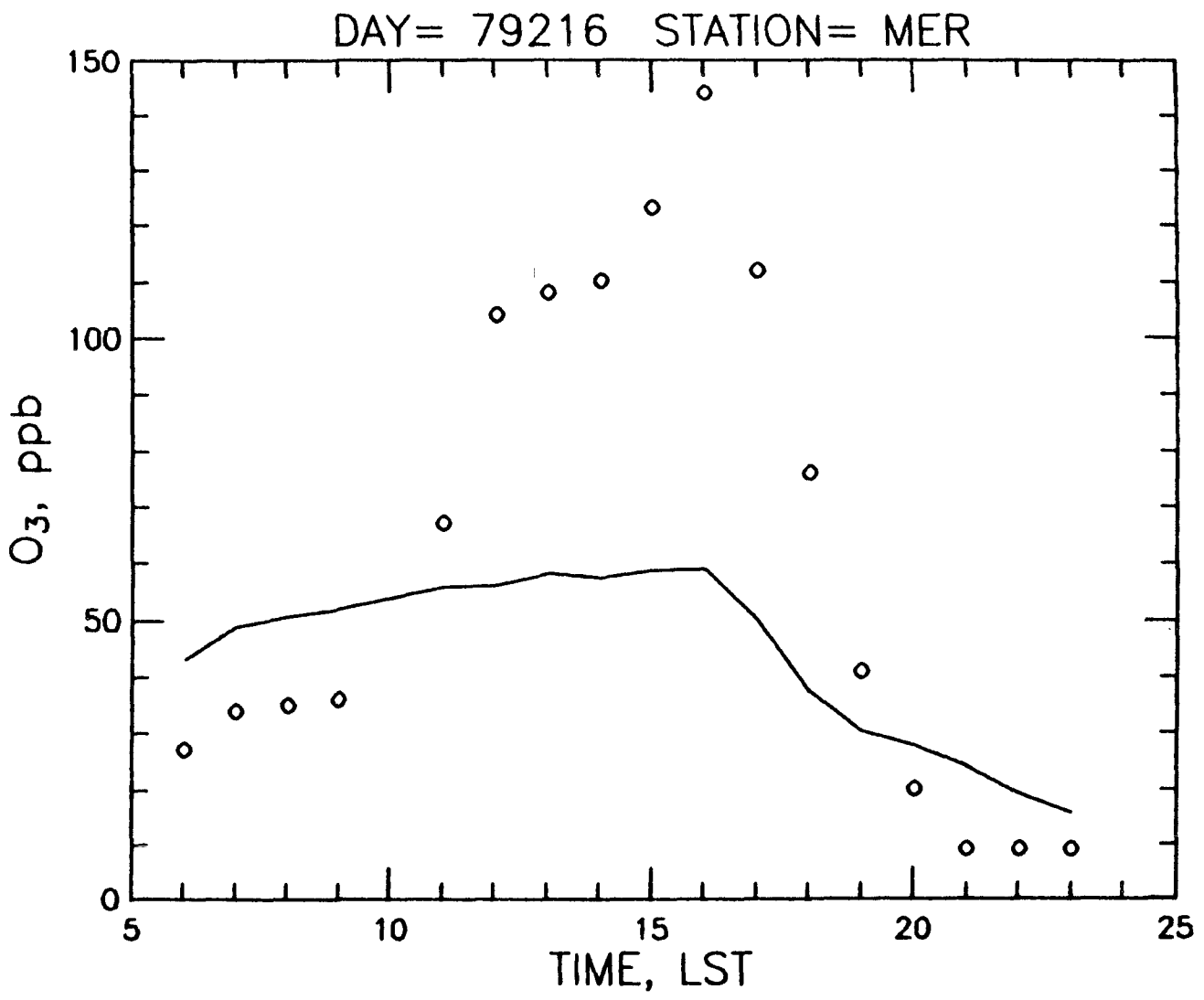

Figure 34. Time-series of predicted (ROM1 layer 1) and observed O_3 concentrations at monitoring site MER on 4 Aug. 1979.

of previous day's pollutants from Philadelphia have had an effect in this area also. It is difficult to specify because of the complex wind situation existing here during the period. Evidence of recirculation also exists upwind of Philadelphia where surface stations recorded O_3 maxima up to 100 ppb on 4 August. Downwind of Philadelphia surface monitors do indicate an O_3 plume in the vicinity of the predicted maximum. Site VIN in south-central New Jersey recorded a maximum concentration of 132 ppb on 4 August. The relatively early hour (1300 h) at which this concentration occurred may indicate that still higher concentrations existed later in the day downwind of the site. The highest concentration predicted at VIN, c^{max}_{p1-A}, was 101 ppb, while the model predicted a maximum, c^{max}_{p1-C}, of 135 ppb at cell (38,9) less than 40 km ESE of VIN. Site AC1 is located very close to the position of the ROM1 predicted maximum and shows the highest predicted O_3 maximum at a surface monitoring location, c^{max}_{p1-B}, at 130 ppb. However, the observed maximum here on 4 August was 73 ppb. Therefore, while the position of the predicted plume appears fairly good, the area of the greatest concentrations is somewhat misaligned. The time-series of predicted and observed O_3 concentrations at VIN is shown in Figure 35.

Table 6 presents a summary of statistics from the global analysis of O_3 plume maximum values discussed here. Seven plumes were considered, not including the Cleveland area on 3 August. The average value of c^{max}_{ob} recorded at surface monitoring sites in these plumes was 114.9 ppb. Three methods of pairing this observed value with ROM1 predictions were made. From the most restrictive to the least restrictive pairing the corresponding layer 1 model predictions averaged over the 7 cases are c^{max}_{p1-A} = 87.3 ppb, c^{max}_{p1-B} = 106.9 ppb, and c^{max}_{p1-C} = 151.0 ppb. The last predicted value is not restricted to measurement site locations, but can be at any grid cell within the predicted plume area. This measure has the most potential for overprediction, and in fact we would expect this to be the case because the density of measurement networks is rarely sufficient to capture the true O_3 peak value. The average bias for this pairing is -36.1 ppb, implying an average overprediction of about 31%. Note that the table shows the average of the normalized bias values over the individual days to be about 38%. The difference represents somewhat different

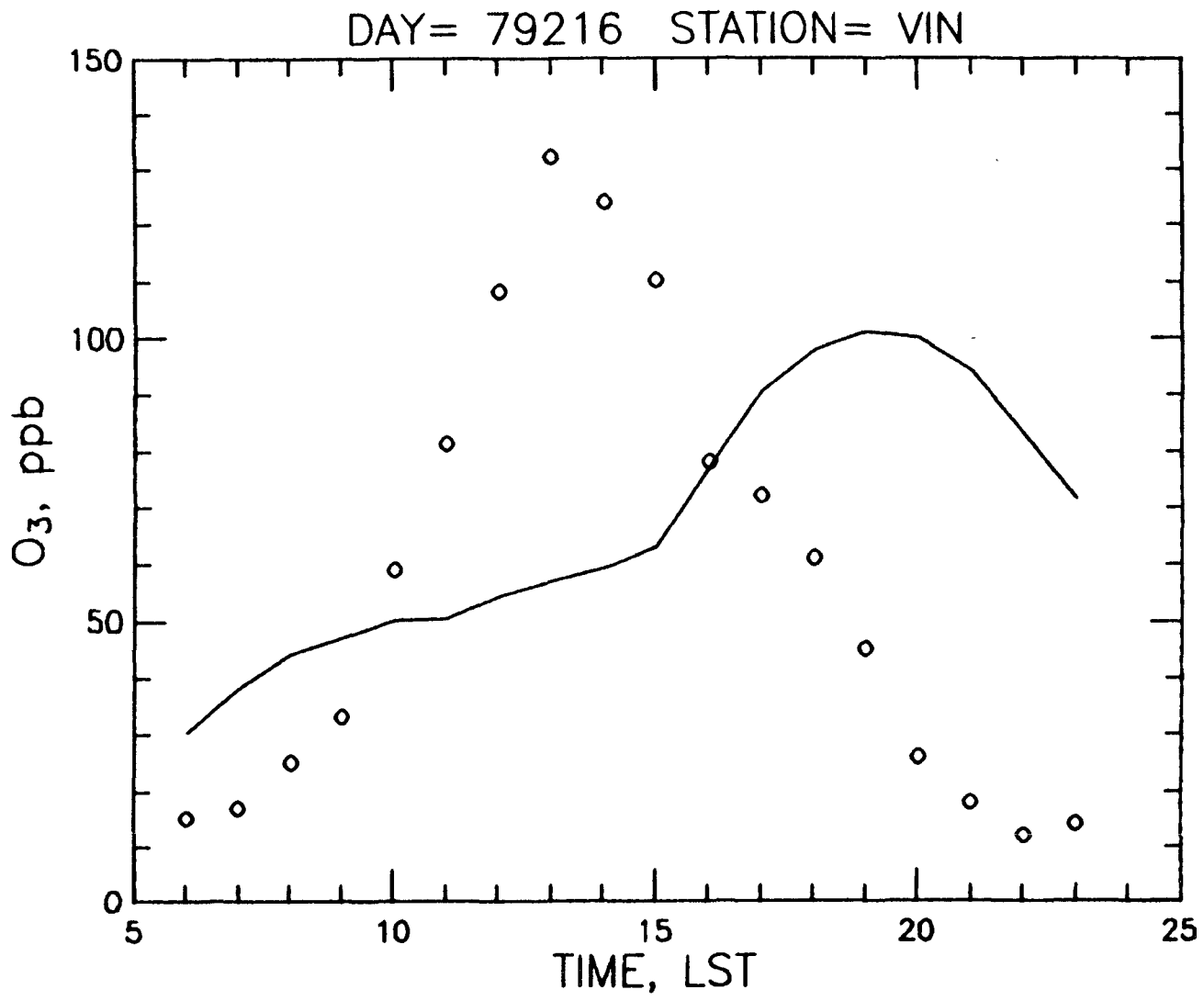

Figure 35. Time-series of predicted (ROM1 layer 1) and observed O_3 concentrations at monitoring site VIN on 4 Aug. 1979.

TABLE 6. SUMMARY OF ROM1 RESULTS FOR GLOBAL MAXIMUM VALUES FOR 3-4 AUGUST 1979.*

	DET 3 Aug	TOR 3 Aug	NY 3 Aug	DET 4 Aug	TOR 4 Aug	NY 4 Aug	PHL 4 Aug	AVG	S.D.
c_{ob}^{max}	100	98	130	99	101	144	132	114.9	19.7
(site-hr)	(SR2-12)	(ORO-16)	(GRW-14)	(PTR-18)	(ORO-15)	(MER-16)	(VIN-13)		
c_{pl-A}^{max}	90	110	97	88	66	59	101	87.3	18.5
(site-hr)	(SR2-16)	(ORO-14)	(GRW-15)	(PTR-16)	(ORO-10)	(MER-16)	(VIN-19)		
d_{pl-A}^{max}	10	-12	33	11	35	85	31	27.6	30.4
$\lvert d_{pl-A}^{max} \rvert$	10	12	33	11	35	85	31	31.0	26.3
$(d_{pl-A}^{max}/c_{ob}^{max})$x100	10%	-12.2%	25.4%	11.1%	34.7%	59%	23.5%	21.6%	22.3%
c_{pl-B}^{max}	122	110	97	94	107	88	130	106.9	15.2
(site-hr)	(LND-21)	(ORO-14)	(GRW-15)	(WNS-10) (DT4-10)	(STC-18) (NG2-19)	(BAB-11)	(AC1-15)		
d_{pl-B}^{max}	-22	-12	33	5	-6	56	2	8.0	27.3
$\lvert d_{pl-B}^{max} \rvert$	22	12	33	5	6	56	2	19.4	19.5
$(d_{pl-B}^{max}/c_{ob}^{max})$x100	-22%	-12.2%	25.4%	5.1%	-5.9%	38.9%	1.5%	4.4%	21.3%
c_{pl-C}^{max}	158	144	117	162	227	114	135	151.0	38.2
(grid cell) (hr)	(10,28) (17)	(23,38) (17)	(42,19) (16)	(8,26) (16)	(24,35) (17)	(41,15) (17)	(38,9) (15)		
d_{pl-C}^{max}	-58	-46	13	-63	-126	30	-3	-36.1	53.6
$\lvert d_{pl-C}^{max} \rvert$	58	46	13	63	126	30	3	48.4	40.8
$(d_{pl-C}^{max}/c_{ob}^{max})$x100	-58%	-46.9%	10%	-63.6%	-125%	20.8%	-2.3%	-37.9	51.2

*All concentrations are O_3 (ppb); all times are hours, LST.

ways to calculate the average degree of variation of the predicted from the observed maximum value. Note that if we drop the Toronto plume on 4 August from consideration the average overprediction changes to about 23%. The very high predicted value over Lake Ontario, out of the range of the surface monitors, lends some support for this action.

The average bias in the most restrictive pairing where the model prediction is interpolated to the same location as the monitoring station is 27.6 ppb here, and the corresponding degree of underprediction is 21.6%. For the middle case, where the maximum model prediction is restricted to monitoring site locations in or near the O_3 plume, but not necessarily at the site of the observed maximum, the average bias is 8.0 ppb with a corresponding degree of underprediction of 4.4%.

The variance in the values of over- or underprediction among the 7 plume cases considered is indicated by the standard deviation (s.d.) about the average. For the 2 most restrictive pairings the s.d. is about the same in each case, 21-22%. For the least restrictive pairing the s.d. is about 54%, although much of that variance is attributable to the 4 August Toronto plume case. Although layer 0 predicted values were not considered in the global maximum values analysis the results would not have been very different from those shown for layer 1. The layer 0 predicted maximum values were typically only a few ppb less than the corresponding layer 1 values.

SECTION 4

SUMMARY AND CONCLUSIONS

The first generation Environmental Protection Agency Regional Oxidant Model (ROM1) has been evaluated for O_3 concentrations using the 2-day test period, 3-4 August 1979, from the NEROS data base. Relatively high O_3 concentrations were measured at the surface and aloft during this period near the Great Lakes area of the United States and southern Ontario. Cloudy and showery conditions along the immediate East coast held O_3 production to low levels except for isolated times and locations in the period. The highest measured surface O_3 values were about 160 ppb south of Lake Erie on 3 August. Aircraft monitoring also confirmed about the same concentration levels aloft late on that day. An earlier study (Clarke and Ching, 1983) indicated that this large area of O_3 over the Great Lakes probably had its genesis earlier than 3 August west of the NEROS region.

The ROM1 was initialized with a chemically equilibrated mix of tropospheric background species concentrations, including about 40 ppb of O_3. The rationale behind the clean initialization was that the model would start simulation sufficiently ahead of the time of prime interest so that source emissions within the model domain would have time to accumulate and participate in photochemical smog reactions producing O_3. A relatively long lead time is required with this methodology. We have used 6 hours in this 2-day test episode, but 24-48 hours of lead time would be preferable in a longer period of simulation. This lead time is a buffer during which the initial conditions are advected out of the system and model results more properly reflect the outcome of physical and chemical processes occurring within the model domain. The purpose of this is to minimize the effect of initial conditions on model results and allow us to initialize with a spatially homogeneous field of background concentrations. If this were not the case, an initial concentration field accurately reflecting the existing ambient concentrations would need to be established. This is a particularly difficult task to accomplish on the regional scale with relatively sparse data observations.

In retrospect, the 2-day episode modeled here was not long enough to justify initialization with clean conditions. Apparently the aged O_3 plume existing in the western model domain at the start of model simulation, but not represented in the initial concentration field, caused the ROM1 to overlook a major contribution to the high concentrations observed in the southern Great Lakes area during the first day of simulation. This preliminary model evaluation exercise is therefore more a test of the procedures that will be used in later evaluations of the second generation model, ROM2, than it is of the ability of the current model to accurately simulate plumes of O_3 on the regional scale. Future evaluations will simulate over an extended period of time (up to 4 weeks), circumventing the initial condition problem.

The evaluation of ROM1 on the test episode proceeded in two stages. First, an overall analysis of O_3 observations and predictions at receptor monitoring locations in the model domain was made for all hours of the simulation except the first six. Next an analysis of the model to predict daily maximum values of O_3 was performed. In the first stage where all data were involved, results showed that the ROM1 predictions averaged under 6% less than measurements at monitoring sites. There is, however not much significance to this result since averaging data over all monitoring stations for all hours weights the result near the tropospheric background level. We are more concerned with the model's ability to predict higher values of O_3. Therefore in a second part to the first stage of analysis the same manner of evaluation was applied to a subset of the data where only simultaneous O_3 values above 50 ppb were included for observed and predicted concentrations at monitoring sites. In this case the average observed O_3 concentration over all receptors and hours was 72.2 ppb, above the level of general background O_3. The average ROM1 performance for the data subset showed a 4.6% underprediction for layer 0 and a 1.4% underprediction for layer 1. Beyond these averaged statistics, the graphical analyses used in interpreting model evaluation results were extremely useful. These analyses included histograms of observed, predicted, and residual data as well as time series of the model bias. The inherent structure of the data as well as trends in model bias can be seen from these type plots.

The second stage of model evaluation, using daily O_3 maxima, also proceeded in 2 steps. In the first step the daily maximum value at each receptor location was compared to the predicted maximum at that location as well as the prediction at the same time as the observed maximum. For layer 1, the ROM1 performance showed an average 31% underprediction for the first comparison and a 43% underprediction for the second comparison. Results for layer 0 were similar. When data were restricted to those observed and predicted O_3 pairs above 50 ppb the model performance for the local maximum analysis improved by showing average underpredictions of 8% and 15%, respectively for the above layer 1 comparisons. The improvement in model predictions in this case is principally due to restricting the analysis to comparisons at monitoring station locations where source emissions had a larger effect on O_3 levels than material that was present initially and overlooked by the clean initialization procedure.

The second step of evaluating the ROM1's performance for O_3 maxima predictions involves an analysis of individual plumes of O_3 from major source areas within the NEROS region. This is perhaps the most challenging and potentially, the most rewarding aspect of the model evaluation for it addresses the major aspect of the regional model's function, resolving plumes of pollution from urban scale and smaller sources on a regional scale grid. A difficult aspect of this step in the evaluation is determining the location and magnitude of the source plumes from a monitoring network that was not designed specifically for regional scale purposes. Monitors are most often located close to urban areas and downwind spatial coverage is usually very limited. Nevertheless, 7 cases of such plumes were identified and analyzed for the 3-4 August 1979 episode. The evaluation used three types of comparisons of O_3 maxima; only layer 1 model predictions were considered in this part of the analysis. The first comparison matched the observed daily maximum O_3 level at any monitoring site within a plume with the daily maximum O_3 prediction at that site. The second comparison matched the observed O_3 maximum with the predicted maximum at any site within or near the plume, and the third comparison matched the observed maximum with the predicted maximum at any grid cell within or near the plume. Results averaged over the 7

plumes in the test case showed a 22% underprediction for the first comparison, a 4% underprediction for the second comparison, and a 38% overprediction for the third comparison. In interpreting these results one must bear in mind that the monitoring network is probably not sufficently dense to capture the actual ambient maximum O_3 value within a plume, and also the predicted plume location and magnitudes of O_3 may not be quite accurate.

There are numerous reasons why the ROM1 may not have performed well for a given plume. We have already discussed the fact that the model was initialized with precursor species concentrations considerably below ambient conditions for some areas of the grid. Another condition likely to cause problems in model performance is a wind field with poorly defined organization. This can lead to large uncertainties in the transport and dispersion of a plume. A third condition under which the ROM1 may perform poorly is that of "patchy" cloudiness, or large spatial variability in cloud cover. This condition has the potential for calculated errors in the amount of sunlight available to the photochemical precursor species for O_3 formation. Examining the ROM1 performance for O_3 in light of these 3 conditions may provide an interesting perspective.

Both the surface data and aircraft sampling have shown that the location and magnitude of the predicted O_3 plume from Detroit on 4 Aug. is fairly accurate. The wind field in this part of the domain is well-organized with a predominant flow from the WNW during the early part of the day, shifting to more westerly and WSW directions later. Likewise, the skies were mostly clear throughout this part of the simulation period here. An examination of the ambient concentration levels of O_3 and precursor species on 2 Aug. near and upwind of Detroit does not show the presence of high concentration levels, indicating that the assumption of clean tropospheric initial concentrations was probably not in gross error. We might speculate then that the good performance of ROM1 in this case is not due to chance, but rather because certain identifiable physical conditions that are associated with the likelihood of consistent model behavior have been met. The concurrent aircraft sampling of O_3 in this plume with high levels of photochemical activity

provides a definitive measure of the model performance. Similar conditions of steady flow and mostly clear skies also existed with the Detroit plume of 3 Aug. and the Toronto plumes on both days. Model performance for O_3 in these plumes was also quite good at the monitoring station locations.

The flow field along the East coast was much less organized during the period than it was in the Great Lakes area because of the presence of a stationary front. Highly variable cloud cover was also seen to exist there. The rather poor performance of the model in the vicinity of the New York plume on 4 Aug. is not surprising in view of this. The predicted plume location and magnitude is not supported by any of the monitoring data. Model performance for the New York plume on 3 Aug. is mixed, with apparently reasonable agreement to the northeast in Connecticut and poor performance to the south and southwest. The looping trajectory of this plume, shown in Figure 19, indicates some of the disorganization of the flow. The fairly good agreement shown between O_3 observations and predictions in the Philadelphia plume on 4 Aug. is one case that may be ascribed to chance as several of the conditions described above associated with potentially poor model performance were in effect. Also, model performance for O_3 was seen to be poor for the first day of simulation where heavier O_3 or precursor concentrations were relatively high on 2 Aug., such as to the south of Lake Erie, between Cleveland, OH and Erie, PA and also on the East coast between New York and Philadelphia.

Overall, the performance of ROM1 for O_3 on this test episode is quite good. Judging from the performance of the model in the vicinity of the analyzed O_3 plumes for maximum O_3 concentrations the model performance is within the range of 4-22% underprediction, corresponding to the 2 stricter methods of paired comparison between model prediction and observation. The least strict pairing is more appropriate for a denser monitoring network, but it is useful for examining the full predictive photochemical potential from a source emissions region. The model results for prediction of maximum O_3 at receptor sites where both the observed and predicted values were over 50 ppb were also quite good, in the range of 3-15% underprediction. These are the sites most likely to have been affected by plumes generated from emissions sources within the model domain.

In summary, the ROM1 performed well and in a consistent pattern in areas of the domain least affected by high boundary or initial species concentrations, by large spatial gradients in meteorological factors, and in areas most affected by large emissions source areas within the domain. Applications with the second generation regional model, ROM2, will address some of the deficiencies found with this test application of the ROM1. The ROM2 applications will begin at a time of relatively clean conditions throughout the model domain so the assumption of clean tropospheric conditions will be fair. Also the simulation period will be one of several weeks duration to minimize the impact of the initial conditions. The probabilistic capability of the model's wind field processor will be explored in the ROM2 evaluation. This capability may address some of the concerns about model performance in regions of less organized flow.

The ROM2 will also incorporate a newer and more complete chemical kinetic mechanism than ROM1 allowing it to include biogenic organic species in the emissions inventory, a possibly important component in the photochemical smog equation on the regional scale. The vertical depth of the grid cells in ROM2 will be variable in space and time and will respond to the physical phenomena influencing the depth and stability of the boundary layer. Terrain features and cell-specific cloud fluxes will be more accurately treated. The ability of ROM2 to estimate sub-grid scale concentration fluctuations near the surface will be explored. Current plans include modeling approximately 4 weeks from the summer 1980 period of the NEROS and SAROAD data bases.

REFERENCES

Clarke, J.F. and J.K.S. Ching, 1983: Aircraft observations of regional transport of ozone in the northeastern United States. Atmospheric Environment, 17(9): 1703-1712.

Freas, W.P., 1983: Northeast corridor modeling project-data base description. EPA-450/4-83-015a, U.S. Environmental Protection Agency, Research Triangle Park, NC.

Lamb, R.G., 1983: A regional scale (1000 km) model of photochemical air pollution. Part I - Theoretical formulation. EPA-600/3-83-035, U.S. Environmental Protection Agency, Research Triangle Park, NC.

Lamb, R.G., 1984: A regional scale (1000 km) model of photochemical air pollution. Part II - Input processor network design. EPA-600/3-84-085, U.S. Environmental Protection Agency, Research Triangle Park, NC.

Lamb, R.G. and G.F. Laniak, 1985: A regional scale (1000 km) model of photochemical air pollution. Part III - Tests of the numerical algorithms. EPA/600/3-85/037, U.S. Environmental Protection Agency, Research Triangle Park, NC.

Possiel, N.C. and W.P. Freas, 1982: Northeast corridor regional modeling project-description of the 1980 urban field studies. EPA-450/4-82-018, U.S. Environmental Protection Agency, Research Triangle Park, NC.

Schere, K.L. and A.J. Fabrick, 1985: EPA Regional Oxidant Model: description and evaluation plan. EPA/600/3-85/068, U.S. Environmental Protection Agency, Research Triangle Park, NC.

Vaughan, W.M., 1985: Transport of pollutants in plumes and PEPES. EPA/600/3-85/033, U.S. Environmental Protection Agency, Research Triangle Park, NC.

APPENDIX A

LISTING OF SURFACE MONITORING STATIONS

This appendix contains a list of all surface monitoring sites for O_3 in the SAROAD and NEROS programs that were in operation during any part of 1979 and 1980. Ontario (Canada) sites are also included. The listing is limited to those sites within and just outside of the ROM modeling domain for the NEROS application. Site locations are listed both by latitude-longitude and grid coordinates.

SITE	LOCATION	STATE OR PROVINCE	LATITUDE (deg, N)	LONGITUDE (deg, W)	X-GRID	Y-GRID
AA1	ANNE ARUNDEL CO	MD	39.21	76.65	29.4	7.3
AA2	ANNE ARUNDEL CO	MD	39.17	76.63	29.5	7.0
AA3	ANNE ARUNDEL CO	MD	38.90	76.65	29.4	5.4
AA4	ANNE ARUNDEL CO	MD	39.10	76.73	29.1	6.6
AC1	ATLANTIC CO	NJ	39.52	74.46	38.2	9.1
AC2	ATLANTIC CITY	NJ	39.36	74.44	38.2	8.1
AG1	ALLEGHENY CO	PA	40.38	80.19	15.3	14.3
AG2	ALLEGHENY CO	PA	40.44	79.95	16.2	14.6
AG3	ALLEGHENY CO	PA	40.44	79.99	16.0	14.7
AG4	ALLEGHENY CO	PA	40.47	79.82	16.7	14.8
AGA	AGAWAM	MA	42.04	72.64	45.5	24.2
AK1	AKRON	OH	41.08	81.52	9.9	18.5
AK2	AKRON	OH	41.11	81.50	10.0	18.6
ALC	ALLEN CO	OH	40.76	84.07	OUTSIDE ROM GRID	
ALN	ALLENTOWN	PA	40.62	75.45	34.2	15.7
ALP	ALLEN PARK	MI	42.23	83.21	3.2	25.4
ALT	ALTOONA	PA	40.51	78.39	22.4	15.1
ALX	ALEXANDRIA	VA	38.81	77.04	27.8	4.9
AMH	AMHERST	NY	42.99	78.78	20.9	30.0
AMR	AMHERST	MA	42.39	72.52	45.9	26.3
ARL	ARLINGTON CO	VA	38.86	77.06	27.8	5.1
AS1	ASHLAND	KY	38.44	82.61	5.5	2.7
AS2	ASHLAND	KY	38.48	82.52	5.9	2.9
AS3	ASHLAND	KY	38.46	82.64	5.4	2.8
ASB	ASBURY PARK	NJ	40.22	74.01	39.9	13.3
ATL	ATTLEBORO	MA	41.93	71.26	50.9	23.6
BAB	BABYLON	NY	40.74	73.41	42.4	16.4
BAC	BAY COUNTY	MI	43.64	83.85	0.6	33.9
BAD	BADEN	PA	40.64	80.23	15.1	15.8
BAR	BARBERTON	OH	41.00	81.63	9.5	18.0
BAY	BAYONNE	NJ	40.68	74.12	39.5	16.1
BC1	BOONE CO	KY	38.92	84.85	OUTSIDE ROM GRID	
BC2	BOONE CO	KY	39.05	84.88	OUTSIDE ROM GRID	
BCK	BRACKENRIDGE	PA	40.61	79.75	17.0	15.7
BER	BEREA	OH	41.37	81.85	8.6	20.2
BET	BETHLEHEM	PA	40.62	75.36	34.5	15.7
BF1	BUFFALO	NY	42.88	78.81	20.8	29.3
BF2	BUFFALO	NY	42.93	78.87	20.5	29.6
BF3	BUFFALO	NY	42.89	78.89	20.4	29.3
BGR	BANGOR	ME	44.80	68.77	OUTSIDE ROM GRID	
BL1	BALTIMORE	MD	39.30	76.61	29.5	7.8
BL2	BALTIMORE	MD	39.24	76.58	29.7	7.4
BL3	BALTIMORE	MD	39.31	76.61	29.5	7.9
BL4	BALTIMORE	MD	39.29	76.63	29.5	7.7
BL5	BALTIMORE	MD	39.29	76.61	29.6	7.7
BL6	BALTIMORE CO	MD	39.41	76.77	28.9	8.4
BL7	BALTIMORE CO	MD	39.51	76.43	30.3	9.1
BLG	BURLINGTON	ON	43.32	79.80	16.8	31.9
BN1	BERLIN	NH	44.48	71.18	51.3	38.9
BN2	BERLIN	NH	44.47	71.18	51.3	38.8

SITE	LOCATION	STATE OR PROVINCE	LATITUDE (deg, N)	LONGITUDE (deg, W)	X-GRID	Y-GRID
BNG	BINGHAMTON	NY	42.10	75.89	32.4	24.6
BNW	BINBROOK WEST	ON	43.12	79.88	16.5	30.7
BR1	BRIDGEPORT	CT	41.18	73.19	43.2	19.1
BR2	BRIDGEPORT	CT	41.19	73.18	43.3	19.1
BRI	BRISTOL (BOROUGH)	PA	40.25	75.00	36.0	13.5
BRL	BURLINGTON	NJ	40.08	74.86	36.6	12.5
BS1	BOSTON	MA	42.35	71.10	51.6	26.1
BS2	BOSTON	MA	42.37	71.04	51.8	26.2
BS3	BOSTON	MA	42.38	71.03	51.9	26.3
BS4	BOSTON	MA	42.35	71.06	51.7	26.1
BTH	BETHESDA	MD	39.00	77.11	27.6	6.0
BU1	BURLINGTON	VT	44.48	73.21	43.2	38.9
BU2	BURLINGTON	VT	44.46	73.19	43.2	38.7
BUL	BURLINGTON CO.	NJ	39.96	74.79	36.8	11.8
BUT	BUTLER CO	PA	41.01	79.72	17.1	18.0
BVF	BEAVER FALLS	PA	40.75	80.32	14.7	16.5
CAN	CANTON	OH	40.80	81.38	10.5	16.8
CAR	CARIBOU	ME	46.87	68.01	OUTSIDE ROM GRID	
CB1	COLUMBUS	OH	40.00	83.04	3.8	12.0
CB2	COLUMBUS	OH	40.06	82.98	4.1	12.4
CB3	COLUMBUS	OH	39.96	82.99	4.0	11.8
CB4	COLUMBUS	OH	39.96	82.99	4.0	11.8
CB5	COLUMBUS	OH	40.09	82.96	4.2	12.5
CBN	CARBONDALE	PA	41.57	75.51	34.0	21.4
CCL	CECIL CO	MD	39.72	76.11	31.6	10.3
CHL	CHARLEROI	PA	40.15	79.90	16.4	12.9
CHP	CHESAPEAKE	VA	36.67	76.33	OUTSIDE ROM GRID	
CHR	CHARLTON	MA	42.31	71.97	48.1	25.9
CHS	CHARLESTON	WV	38.34	81.62	9.5	2.1
CHT	CHESTER	PA	39.84	75.37	34.5	11.0
CHV	CHEVERLY	MD	38.92	76.90	28.4	5.5
CKY	COCKEYSVILLE	MD	39.46	76.63	29.5	8.8
CL1	CLEVELAND	OH	41.50	81.62	9.5	21.0
CL2	CLEVELAND	OH	41.55	81.57	9.7	21.3
CLK	CLARK CO	OH	40.00	83.80	0.8	12.0
CLN	CLINTON CO	OH	39.43	83.79	0.9	8.6
CLO	CALLOWAY CO	KY	36.73	88.12	OUTSIDE ROM GRID	
CLR	CLERMONT CO	OH	39.08	84.18	OUTSIDE ROM GRID	
CM1	CAMDEN	NJ	39.92	75.10	35.6	11.5
CM2	CAMDEN	NJ	39.95	75.12	35.5	11.7
CM3	CAMDEN CO	NJ	39.67	74.86	36.6	10.0
CMB	CUMBERLAND	MD	39.65	78.76	20.9	9.9
CN1	CINCINNATI	OH	39.14	84.55	OUTSIDE ROM GRID	
CN2	CINCINNATI	OH	39.21	84.48	OUTSIDE ROM GRID	
CN3	CINCINNATI	OH	39.14	84.51	OUTSIDE ROM GRID	
CNE	CONNEAUT	OH	41.96	80.57	13.7	23.8
CNS	CONSHOHOCKEN	PA	40.07	75.30	34.8	12.4
CPE	CAPE ELIZABETH	ME	43.57	70.20	55.2	33.4
CPM	CAPE MAY CO	NJ	39.10	74.82	36.7	6.6

SITE	LOCATION	STATE OR PROVINCE	LATITUDE (deg, N)	LONGITUDE (deg, W)	X-GRID	Y-GRID
CR1	CORUNNA	ON	42.88	82.45	6.2	29.3
CR3	CORUNNA	ON	42.91	82.45	6.2	29.5
CTF	CHESTERFIELD CO	VA	37.36	77.59	OUTSIDE ROM GRID	
CUM	CUMBERLAND CO	ME	43.91	70.23	55.1	35.5
CV1	COVINGTON	KY	39.07	84.53	OUTSIDE ROM GRID	
CV2	COVINGTON	KY	39.09	84.51	OUTSIDE ROM GRID	
DA1	DAYTON	OH	39.77	84.21	OUTSIDE ROM GRID	
DA2	DAYTON	OH	39.76	84.19	OUTSIDE ROM GRID	
DA3	DAYTON	OH	39.81	84.19	OUTSIDE ROM GRID	
DA4	DAYTON	OH	39.76	84.20	OUTSIDE ROM GRID	
DA5	DAYTON	OH	39.78	84.20	OUTSIDE ROM GRID	
DAN	DANBURY	CT	41.40	73.44	42.2	20.4
DAY	DAYTON	KY	39.11	84.48	OUTSIDE ROM GRID	
DC1	WASHINGTON	DC	38.90	77.05	27.8	5.4
DC2	WASHINGTON	DC	38.98	77.02	27.9	5.9
DC3	WASHINGTON	DC	38.89	77.01	27.9	5.3
DC4	WASHINGTON	DC	38.88	76.97	28.1	5.3
DC5	WASHINGTON	DC	38.93	77.06	27.8	5.6
DC6	WASHINGTON	DC	38.94	77.03	27.9	5.7
DMS	DAMASCUS	MD	39.27	77.22	27.1	7.6
DNR	DONORA	PA	40.17	79.86	16.5	13.0
DNV	DANVILLE	KY	37.67	84.77	OUTSIDE ROM GRID	
DOV	DOVER	DE	39.15	75.50	34.0	6.9
DOW	DOWNINGTON	PA	40.02	75.71	33.2	12.1
DRB	DERBY	CT	41.32	73.09	43.6	19.9
DT1	DETROIT	MI	42.40	83.24	3.1	26.4
DT2	DETROIT	MI	42.36	83.10	3.6	26.1
DT3	DETROIT	MI	42.43	83.00	4.0	26.6
DT4	DETROIT	MI	42.33	83.03	3.9	26.0
DT5	DETROIT	MI	42.33	83.05	3.8	26.0
DUM	DUMONT	NJ	40.94	74.00	40.0	17.6
DVR	DANVERS	MA	42.59	70.98	52.1	27.6
EAS	EASTON	PA	40.68	75.22	35.1	16.1
EB1	ETOBICOKE	ON	43.65	79.58	17.7	33.9
EB2	ETOBICOKE	ON	43.62	79.52	17.9	33.7
EDG	EDGEWOOD	MD	39.41	76.30	30.8	8.5
ELM	ELMIRA	NY	42.11	76.80	28.8	24.7
ENF	ENFIELD	CT	42.00	72.57	45.7	24.0
ERE	ERIE	PA	42.14	80.05	15.8	24.8
ESO	EAST ORANGE	NJ	40.76	74.20	39.2	16.5
ESS	ESSEXVILLE	MI	43.62	83.85	0.6	33.7
EST	EASTON	MA	42.07	71.09	51.6	24.4
ESX	ESSEX	MD	39.35	76.48	30.1	8.1
EXC	ESSEX CO	NY	44.37	73.90	40.4	38.2
EY1	ELYRIA	OH	41.37	82.11	7.6	20.2
EY2	ELYRIA	OH	41.37	82.11	7.6	20.2
EZ1	ELIZABETH	NJ	40.66	74.21	39.1	16.0
EZ2	ELIZABETH	NJ	40.64	74.21	39.2	15.8
FAY	FAYETTE CO	KY	38.13	84.47	OUTSIDE ROM GRID	

SITE	LOCATION	STATE OR PROVINCE	LATITUDE (deg, N)	LONGITUDE (deg, W)	X-GRID	Y-GRID
FDR	FREDERICKSBURG	VA	38.31	77.45	26.2	1.9
FLM	FLEMINGTON	NJ	40.52	74.81	36.8	15.1
FLN	FLINT	MI	43.02	83.69	1.3	30.1
FLO	FLORENCE	KY	39.00	84.63	OUTSIDE ROM GRID	
FOL	FOLCROFT	PA	39.89	75.28	34.9	11.3
FRD	FREDERICK CO	MD	39.48	77.23	27.1	8.9
FRE	FREEHOLD	NJ	40.26	74.27	38.9	13.6
FX1	FAIRFAX	VA	38.84	77.31	26.8	5.1
FX2	FAIRFAX CO	VA	38.73	77.10	27.6	4.4
FX3	FAIRFAX CO	VA	38.74	77.08	27.7	4.5
GAR	GARDNER	MA	42.57	71.99	48.0	27.4
GLN	GLENS FALLS	NY	43.32	73.62	41.5	31.9
GLO	GLOUCESTER	MA	42.62	70.71	53.2	27.7
GMT	GREEN MOUNTAIN NAT.	VT	43.93	73.03	43.9	35.6
GNB	GREENBRIER CO	WV	37.77	80.33	OUTSIDE ROM GRID	
GNS	GENESEE CO	MI	43.17	83.46	2.2	31.0
GRD	GARDINER	ME	44.22	69.79	56.8	37.3
GRE	GREENFIELD	MA	42.57	72.60	45.6	27.4
GRG	GEORGETOWN	MA	42.72	70.99	52.1	28.3
GRN	GREENBELT	MD	39.02	76.83	28.7	6.1
GRR	GRAND RAPIDS	MI	42.97	85.68	OUTSIDE ROM GRID	
GRW	GREENWICH	CT	41.08	73.71	41.2	18.5
HAK	HACKENSACK	NJ	40.88	74.04	39.8	17.3
HAM	HAMILTON	MA	42.63	70.82	52.7	27.8
HAR	HARRISBURG	PA	40.24	76.85	28.6	13.5
HEN	HENRICO CO	VA	37.59	77.42	OUTSIDE ROM GRID	
HF1	HARTFORD	CT	41.77	72.68	45.3	22.6
HF2	HARTFORD	CT	41.76	72.68	45.3	22.6
HGR	HAGERSTOWN	MD	39.65	77.72	25.1	9.9
HM1	HEMPSTEAD	NY	40.75	73.59	41.7	16.5
HM2	HEMPSTEAD	NY	40.89	73.60	41.6	17.4
HML	HAMILTON	ON	43.26	79.84	16.6	31.6
HMP	HAMPTON	VA	37.00	76.40	OUTSIDE ROM GRID	
HN1	HENDERSON	KY	37.86	87.58	OUTSIDE ROM GRID	
HN2	HENDERSON	KY	37.88	87.57	OUTSIDE ROM GRID	
HNC	HANCOCK CO	KY	37.94	86.90	OUTSIDE ROM GRID	
HNR	HENRICO CO	VA	37.59	77.50	OUTSIDE ROM GRID	
HNV	HANOVER CO	VA	37.64	77.32	OUTSIDE ROM GRID	
HOP	HOPKINS CO	KY	37.53	87.35	OUTSIDE ROM GRID	
HOW	HOWARD CO	MD	39.17	76.90	28.4	7.0
HRD	HARDIN CO	KY	37.76	85.72	OUTSIDE ROM GRID	
HRF	HARFORD CO	MD	39.63	76.33	30.7	9.8
HRO	HARRODSBURG	KY	37.76	84.83	OUTSIDE ROM GRID	
HRP	HURON PARK	ON	43.29	81.49	10.0	31.7
HT1	HAMILTON CO	OH	39.28	84.37	OUTSIDE ROM GRID	
HT2	HAMILTON CO	OH	39.28	84.37	OUTSIDE ROM GRID	
HT3	HAMILTON CO	OH	39.16	84.80	OUTSIDE ROM GRID	
JF1	JEFFERSON CO	KY	38.14	85.58	OUTSIDE ROM GRID	
JF2	JEFFERSON CO	KY	38.31	85.58	OUTSIDE ROM GRID	

SITE	LOCATION	STATE OR PROVINCE	LATITUDE (deg, N)	LONGITUDE (deg, W)	X-GRID	Y-GRID
JF3	JEFFERSON CO	KY	38.11	85.87	OUTSIDE ROM GRID	
JF4	JEFFERSON CO	KY	38.17	85.88	OUTSIDE ROM GRID	
JNS	JOHNSTOWN	PA	40.31	78.92	20.3	13.9
JRS	JERSEY CITY	NJ	40.73	74.07	39.7	16.4
KCH	KITCHENER	ON	43.46	80.47	14.1	32.7
KEE	KEENE	NH	42.92	72.32	46.7	29.5
KEN	KENT CO	MI	43.04	85.41	OUTSIDE ROM GRID	
KNT	KENT CO	RI	41.62	71.72	49.1	21.7
KUT	KUTZTOWN	PA	40.51	75.79	32.9	15.1
LAN	LANCASTER CITY	PA	40.04	76.29	30.9	12.3
LAW	LAWRENCE	MA	42.71	71.17	51.3	28.2
LCH	LITCHFIELD CO	CT	41.67	73.14	43.4	22.0
LEB	LEBANON	OH	39.43	84.20	OUTSIDE ROM GRID	
LEW	LEWISTON	ME	44.10	70.22	55.1	36.6
LEX	LEXINGTON	MA	42.45	71.22	51.1	26.7
LF1	LEXINGTON-FAYETTE	KY	38.05	84.50	OUTSIDE ROM GRID	
LF2	LEXINGTON-FAYETTE	KY	38.06	84.50	OUTSIDE ROM GRID	
LF3	LEXINGTON-FAYETTE	KY	38.06	84.46	OUTSIDE ROM GRID	
LIC	LINCOLN	MA	42.43	71.30	50.8	26.6
LIN	LINDEN	NJ	40.60	74.25	39.0	15.6
LIV	LIVONIA	MI	42.38	83.40	2.4	26.3
LND	LONDON	ON	42.99	81.22	11.1	29.9
LOG	LOGAN	OH	39.53	82.38	6.5	9.2
LOW	LOWELL	MA	42.65	71.31	50.8	27.9
LPT	LONG POINT PARK	ON	42.58	80.39	14.4	27.5
LS1	LANSING	MI	42.74	84.55	OUTSIDE ROM GRID	
LS2	LANSING	MI	42.74	84.54	OUTSIDE ROM GRID	
LV1	LOUISVILLE	KY	38.25	85.81	OUTSIDE ROM GRID	
LV2	LOUISVILLE	KY	38.23	85.70	OUTSIDE ROM GRID	
LV3	LOUISVILLE	KY	38.26	85.71	OUTSIDE ROM GRID	
LV4	LOUISVILLE	KY	38.26	85.76	OUTSIDE ROM GRID	
LV5	LOUISVILLE	KY	38.23	85.76	OUTSIDE ROM GRID	
MAC	MACOMB CO	MI	42.72	82.79	4.8	28.3
MAH	MAHONING CO	OH	41.11	80.98	12.1	18.7
MAM	MAMARONECK	NY	40.93	73.76	40.9	17.6
MAR	MARION	VA	36.85	81.51	OUTSIDE ROM GRID	
MC1	MC CRACKEN CO	KY	37.16	88.79	OUTSIDE ROM GRID	
MC2	MC CRACKEN CO	KY	37.14	88.80	OUTSIDE ROM GRID	
MCG	MC GUIRE AFB	NJ	40.05	74.58	37.7	12.3
MCL	MC LEAN	VA	38.93	77.20	27.2	5.6
MDD	MIDLAND	PA	40.63	80.44	14.2	15.8
MDL	MIDDLETOWN	CT	41.55	72.63	45.5	21.3
MDN	MEDINA CO	OH	41.15	81.90	8.4	18.9
MED	MEDFIELD	MA	42.21	71.34	50.7	25.3
MER	MERCER CO.	NJ	40.22	74.59	37.6	13.3
MFD	MEDFORD	MA	42.40	71.08	51.7	26.4
MG1	MONTGOMERY CO	OH	39.80	84.13	OUTSIDE ROM GRID	
MG2	MONTGOMERY CO	OH	39.80	84.12	OUTSIDE ROM GRID	
MID	MIDDLETOWN	OH	39.53	84.39	OUTSIDE ROM GRID	

SITE	LOCATION	STATE OR PROVINCE	LATITUDE (deg, N)	LONGITUDE (deg, W)	X-GRID	Y-GRID
MK1	MUSKEGON	MI	43.24	86.20	OUTSIDE ROM GRID	
MK2	MUSKEGON	MI	43.24	86.25	OUTSIDE ROM GRID	
MK3	MUSKEGON CO	MI	43.28	86.22	OUTSIDE ROM GRID	
MN1	MANCHESTER	NH	42.99	71.46	50.1	30.0
MN2	MANCHESTER	NH	42.99	71.46	50.1	30.0
MNR	MONROE CO	NY	43.07	77.71	25.2	30.4
MNT	MONTAGUE	MA	42.57	72.53	45.9	27.4
MON	MONMOUTH CO	NJ	40.33	74.27	38.9	14.0
MRC	MORRIS CO	NJ	40.79	74.68	37.3	16.7
MRL	MERLIN	ON	42.25	82.22	7.1	25.5
MRQ	MARQUETTE CO	MI	46.81	87.73	OUTSIDE ROM GRID	
MRT	MORRISTOWN	NJ	40.80	74.48	38.1	16.8
MSG	MISSISSAUGA	ON	43.57	79.61	17.6	33.4
MU1	MUHLENBERG CO	KY	37.21	86.94	OUTSIDE ROM GRID	
MU2	MUHLENBERG CO	KY	37.22	87.05	OUTSIDE ROM GRID	
MU3	MUHLENBERG CO	KY	37.31	87.00	OUTSIDE ROM GRID	
N10	NEW YORK CITY	NY	40.60	74.13	39.5	15.6
N11	NEW YORK CITY	NY	40.78	73.91	40.4	16.7
N12	NEW YORK CITY	NY	40.67	73.98	40.1	16.0
NBR	NEW BRITAIN	CT	41.67	72.78	44.9	22.0
NC1	NEW CASTLE CO	DE	39.81	75.45	34.2	10.8
NC2	NEW CASTLE CO	DE	39.78	75.52	33.9	10.7
NC3	NEW CASTLE CO	DE	39.70	75.68	33.3	10.2
NC4	NEW CASTLE CO	DE	39.53	75.69	33.3	9.2
NCL	NEW CASTLE	PA	41.00	80.35	14.6	18.0
NG1	NIAGARA CO	NY	43.22	78.48	22.1	31.3
NG2	NIAGARA FALLS	NY	43.09	79.00	20.0	30.5
NH1	NEW HAVEN	CT	41.31	72.92	44.3	19.8
NH2	NEW HAVEN	CT	41.31	72.92	44.3	19.8
NHP	NORTHAMPTON CO	VA	37.29	75.97	OUTSIDE ROM GRID	
NKS	NEW KENSINGTON	PA	40.55	79.76	17.0	15.3
NOR	NORWALK	CT	41.11	73.41	42.4	18.7
NPN	NEWPORT NEWS	VA	37.07	76.49	OUTSIDE ROM GRID	
NRF	NORFOLK	VA	36.85	76.28	OUTSIDE ROM GRID	
NRS	NORRISTOWN	PA	40.11	75.31	34.8	12.7
NRT	NORTHAMPTON	PA	40.69	75.49	34.0	16.1
NWB	NEW BRUNSWICK	NJ	40.48	74.44	38.2	14.9
NWR	NEWARK	NJ	40.73	74.18	39.3	16.4
NY1	NEW YORK CITY	NY	40.83	73.90	40.4	17.0
NY2	NEW YORK CITY	NY	40.74	73.82	40.7	16.4
NY3	NEW YORK CITY	NY	40.77	73.97	40.1	16.6
NY4	NEW YORK CITY	NY	40.59	73.94	40.3	15.6
NY5	NEW YORK CITY	NY	40.74	73.99	40.1	16.4
NY6	NEW YORK CITY	NY	40.73	73.95	40.2	16.4
NY7	NEW YORK CITY	NY	40.67	73.97	40.1	16.0
NY8	NEW YORK CITY	NY	40.75	73.98	40.1	16.5
NY9	NEW YORK CITY	NY	40.72	74.00	40.0	16.3
NYK	NORTH YORK	ON	43.72	79.34	18.6	34.3
OCN	OCEAN CO.	NJ	40.11	74.31	38.8	12.6

SITE	LOCATION	STATE OR PROVINCE	LATITUDE (deg, N)	LONGITUDE (deg, W)	X-GRID	Y-GRID
OH1	OHIO CO	KY	37.32	86.93	OUTSIDE ROM GRID	
OH2	OHIO CO	KY	37.30	86.95	OUTSIDE ROM GRID	
OH3	OHIO CO	KY	37.56	86.77	OUTSIDE ROM GRID	
OK1	OAKVILLE	ON	43.42	79.70	17.2	32.5
OK2	OAKVILLE	ON	43.42	79.70	17.2	32.5
ONI	ONEIDA CO	NY	43.30	75.72	33.1	31.8
ORN	ORONO, MAINE	ME	44.90	68.67	OUTSIDE ROM GRID	
ORO	ORONO	ON	43.97	78.62	21.5	35.8
OSH	OSHAWA	ON	43.90	78.85	20.6	35.4
OWN	OWENSBORO	KY	37.78	87.07	OUTSIDE ROM GRID	
P10	PHILADELPHIA	PA	39.96	75.17	35.3	11.7
P11	PHILADELPHIA	PA	39.95	75.16	35.3	11.7
PAI	PAINESVILLE	OH	41.72	81.24	11.0	22.3
PAT	PATERSON	NJ	40.93	74.16	39.4	17.6
PAU	PAULSBORO	NJ	39.83	75.24	35.0	11.0
PB1	PENOBSCOT CO	ME	45.01	68.63	OUTSIDE ROM GRID	
PB2	PENOBSCOT CO	ME	44.73	68.98	OUTSIDE ROM GRID	
PB3	PENOBSCOT CO	ME	45.25	68.57	OUTSIDE ROM GRID	
PD1	PADUCAH	KY	37.08	88.60	OUTSIDE ROM GRID	
PD2	PADUCAH	KY	37.09	88.60	OUTSIDE ROM GRID	
PD3	PADUCAH	KY	37.06	88.57	OUTSIDE ROM GRID	
PEN	PENNS GROVE	NJ	39.73	75.47	34.1	10.4
PH1	PHILADELPHIA	PA	40.01	75.10	35.6	12.1
PH2	PHILADELPHIA	PA	40.05	75.24	35.0	12.3
PH3	PHILADELPHIA	PA	39.98	75.10	35.6	11.9
PH4	PHILADELPHIA	PA	39.88	75.23	35.1	11.3
PH5	PHILADELPHIA	PA	39.92	75.19	35.2	11.5
PH6	PHILADELPHIA	PA	39.91	75.15	35.4	11.4
PH7	PHILADELPHIA	PA	40.08	75.01	36.0	12.5
PH8	PHILADELPHIA	PA	39.95	75.16	35.3	11.7
PH9	PHILADELPHIA	PA	40.01	75.15	35.4	12.1
PLN	PLAINFIELD	NJ	40.60	74.44	38.2	15.6
PLS	PULASKI CO	KY	37.16	84.48	OUTSIDE ROM GRID	
PLY	PLYMOUTH	NH	43.78	71.75	49.0	34.7
PO1	PORTSMOUTH	NH	43.08	70.76	52.9	30.5
PO2	PORTSMOUTH	NH	43.08	70.76	53.0	30.5
POR	PORTLAND	ME	43.66	70.26	55.0	34.0
POU	POUGHKEEPSIE	NY	41.70	73.94	40.3	22.2
PRB	PREBLE CO	OH	39.84	84.72	OUTSIDE ROM GRID	
PRH	PORT HURON	MI	42.95	82.44	6.2	29.7
PRY	PERRY CO	PA	40.46	77.17	27.3	14.7
PSB	PHILLIPSBURG	NJ	40.68	75.19	35.3	16.1
PSQ	PRESQUE ISLE	ME	46.69	68.00	OUTSIDE ROM GRID	
PT1	PITTSBURGH	PA	40.44	80.00	16.0	14.6
PT2	PITTSBURGH	PA	40.47	79.96	16.2	14.8
PT3	PITTSBURGH	PA	40.44	79.95	16.2	14.6
PTG	PORTAGE CO	OH	41.18	81.33	10.7	19.1
PTH	PERTH AMBOY	NJ	40.51	74.27	38.9	15.1
PTR	PETROLIA	ON	42.96	82.19	7.2	29.7

SITE	LOCATION	STATE OR PROVINCE	LATITUDE (deg, N)	LONGITUDE (deg, W)	X-GRID	Y-GRID
PTS	PITTSFIELD	MA	42.45	73.20	43.2	26.7
PV1	PROVIDENCE	RI	41.82	71.41	50.4	22.9
PV2	PROVIDENCE	RI	41.82	71.41	50.4	22.9
PV3	PROVIDENCE	RI	41.83	71.41	50.3	23.0
PV4	PROVIDENCE	RI	41.83	71.41	50.4	23.0
PWM	PRINCE WILLIAM CO	VA	38.64	77.53	25.9	3.9
QIN	QUINCY	MA	42.24	70.97	52.1	25.5
RC1	ROCHESTER	NY	43.16	77.60	25.6	31.0
RC2	ROCHESTER	NY	43.17	77.52	25.9	31.0
RCK	ROCKVILLE	MD	39.11	77.11	27.6	6.7
RDG	READING	PA	40.32	75.93	32.3	13.9
REN	RENSSELAER	NY	42.63	73.75	41.0	27.8
RIC	RICHMOND	VA	37.54	77.43	OUTSIDE ROM GRID	
RIM	RICHMOND	VA	37.49	77.47	OUTSIDE ROM GRID	
RVB	RIVIERA BEACH	MD	39.16	76.51	30.0	7.0
SAG	SAGINAW	MI	43.45	83.91	0.4	32.7
SAL	SALINE	MI	42.16	83.78	0.9	24.9
SC1	SCRANTON	PA	41.44	75.62	33.5	20.7
SC2	SCRANTON	PA	41.59	76.07	31.7	21.6
SCH	SCHENECTADY	NY	42.80	73.94	40.2	28.8
SCR	SCARBOROUGH	ON	43.75	79.27	18.9	34.5
SDB	SUDBURY	MA	42.38	71.39	50.4	26.3
SHP	SHEPHERDSVILLE	KY	38.00	85.70	OUTSIDE ROM GRID	
SLM	SALEM	VA	37.29	80.05	OUTSIDE ROM GRID	
SMC	SIMCOE	ON	42.86	80.27	14.9	29.1
SMT	ST MATTHEWS	KY	38.25	85.81	OUTSIDE ROM GRID	
SMV	SOMERVILLE	NJ	40.57	74.61	37.5	15.4
SOM	SOMERVILLE	MA	42.40	71.11	51.6	26.4
SP1	SPRINGFIELD	MA	42.09	72.59	45.6	24.5
SP2	SPRINGFIELD	MA	42.14	72.49	46.0	24.8
SR2	SARNIA	ON	42.98	82.41	6.4	29.9
STC	ST. CATHERINES	ON	43.17	79.24	19.0	31.0
STF	STAFFORD	CT	41.98	72.39	46.5	23.9
STH	SOUTHFIELD	MI	42.45	83.22	3.1	26.7
STK	STARK CO	OH	40.87	81.33	10.7	17.2
STM	STAMFORD	CT	41.06	73.54	41.8	18.3
STR	STRATFORD	CT	41.15	73.15	43.4	18.9
STU	STEUBENVILLE	OH	40.36	80.62	13.5	14.2
STV	STOUFFVILLE	ON	43.97	79.27	18.9	35.8
SUS	SUSSEX CO	DE	38.58	75.27	34.9	3.5
SUT	SUITLAND-SILVER HILL	MD	38.85	76.93	28.3	5.1
SVC	SEVEN CORNERS	VA	38.87	77.14	27.4	5.2
SY1	SYRACUSE	NY	43.05	76.15	31.4	30.3
SY2	SYRACUSE	NY	43.06	76.18	31.3	30.4
SY3	SYRACUSE	NY	43.06	76.13	31.5	30.4
SY4	SYRACUSE	NY	43.06	76.18	31.3	30.4
SYB	STONY BROOK	NY	40.91	73.13	43.5	17.5
TEW	TEWKSBURY	MA	42.61	71.22	51.1	27.6
TL1	TOLEDO	OH	41.65	83.53	1.9	21.9

SITE	LOCATION	STATE OR PROVINCE	LATITUDE (deg, N)	LONGITUDE (deg, W)	X-GRID	Y-GRID
TL2	TOLEDO	OH	41.66	83.53	1.9	21.9
TL3	TOLEDO	OH	41.66	83.57	1.7	22.0
TL4	TOLEDO	OH	41.72	83.48	2.1	22.3
TOM	TOMS RIVER	NJ	39.95	74.20	39.2	11.7
TR1	TORONTO	ON	43.66	79.39	18.4	34.0
TR2	TORONTO	ON	43.65	79.37	18.5	33.9
TRE	TRENTON	MI	42.14	83.19	3.3	24.8
TRM	TRIMBLE CO	KY	38.71	85.42	OUTSIDE ROM GRID	
TRN	TRENTON	NJ	40.22	74.76	36.9	13.3
TV2	TIVERTON	ON	44.30	81.58	9.7	37.8
UTC	UTICA	NY	43.10	75.20	35.2	30.6
VAB	VIRGINIA BEACH	VA	36.89	76.18	OUTSIDE ROM GRID	
VIN	VINELAND	NJ	39.49	75.02	35.9	9.0
WAT	WATERTOWN	MA	42.37	71.18	51.3	26.2
WAY	WAYNE CO	NY	43.23	77.17	27.3	31.4
WCH	WINCHESTER	KY	38.00	84.17	OUTSIDE ROM GRID	
WH1	WHEELING	WV	40.07	80.72	13.1	12.4
WH2	WHEELING	WV	40.12	80.70	13.2	12.7
WIL	WILMINGTON	DE	39.73	75.55	33.8	10.4
WL1	WILLIAMSPORT	PA	41.25	76.99	28.0	19.5
WL2	WILLIAMSPORT	PA	41.25	76.99	28.0	19.5
WLK	WILKES-BARRE	PA	41.24	75.90	32.4	19.4
WLO	WILLOUGHBY	OH	41.64	81.41	10.4	21.8
WNS	WINDSOR	ON	42.32	83.04	3.8	25.9
WO1	WORCESTER	MA	42.26	71.80	48.8	25.6
WO2	WORCESTER	MA	42.30	71.75	49.0	25.8
WPL	WHITE PLAINS	NY	41.05	73.76	40.9	18.3
WRN	WARREN	MI	42.51	83.01	4.0	27.1
WSL	WESTLAKE	OH	41.48	81.88	8.5	20.9
YG1	YOUNGSTOWN	OH	41.10	80.65	13.4	18.6
YG2	YOUNGSTOWN	OH	41.10	80.65	13.4	18.6
YOR	YORK	PA	39.97	76.70	29.2	11.8

APPENDIX B

MAXIMUM O_3 VALUES AT SURFACE MONITORING STATIONS

This appendix contains a list of the surface monitoring sites operating during the 3-4 August 1979 period along with the observed and predicted maximum O_3 values at these sites for each of the days and the hour that the maximum value occurred. All concentrations are in units of ppb and times are in hours, LST.

DATE	SITE	c_{ob}^{max}	h_{ob}^{max}	$c_{p0}(h_{ob}^{max})$	$c_{p1}(h_{ob}^{max})$	c_{p0}^{max}	h_{p0}^{max}	c_{p1}^{max}	h_{p1}^{max}
79215	AA1	69.0	14	36.4	38.5	42.8	17	46.0	18
79215	AA2	71.0	14	36.4	38.5	42.8	17	45.9	16
79215	AC1	76.0	12	31.6	32.1	37.0	9	37.5	9
79215	AG4	57.0	15	33.9	33.9	35.1	13	35.1	13
79215	AGA	100.0	16	16.0	16.2	37.7	13	38.3	13
79215	AK1	58.0	18	37.6	38.0	40.0	16	40.4	16
79215	ALN	59.0	17	20.8	22.3	33.1	9	35.1	8
79215	ALX	75.0	14	69.5	72.0	70.0	15	72.3	15
79215	AMH	69.0	18	39.8	41.4	40.4	17	41.5	17
79215	AMR	99.0	14	33.6	33.9	37.5	17	37.9	17
79215	ARL	100.0	14	69.5	72.0	70.0	15	72.3	15
79215	ATL	87.0	11	42.1	43.7	42.1	11	43.7	11
79215	BAB	83.0	11	10.2	10.6	24.6	20	25.1	20
79215	BAD	31.0	14	23.1	23.5	26.4	17	26.9	17
79215	BAY	91.0	12	47.1	47.8	59.4	16	59.8	16
79215	BER	53.0	9	32.3	34.5	47.5	17	49.8	17
79215	BET	55.0	17	18.4	19.5	30.2	9	31.4	9
79215	BL1	37.0	14	26.0	26.3	28.2	10	28.3	10
79215	BL3	38.0	14	26.0	26.3	31.0	8	31.2	8
79215	BL6	70.0	14	31.8	33.0	36.3	17	38.8	18
79215	BLG	55.0	13	40.3	40.5	48.0	22	48.8	22
79215	BN1	41.0	16	40.7	41.6	41.3	18	41.9	17
79215	BNG	79.0	14	37.8	38.0	38.5	15	38.4	15
79215	BNW	66.0	16	45.6	48.3	55.6	20	57.3	20
79215	BR2	117.0	14	42.6	43.0	92.2	18	93.0	18
79215	BRI	100.0	14	46.4	49.1	62.8	17	67.8	17
79215	BTH	61.0	14	52.5	55.0	56.2	13	58.9	13
79215	BUL	87.0	12	36.9	39.5	51.2	15	53.5	15
79215	BVF	29.0	18	26.6	27.2	26.6	18	27.2	18
79215	CAN	55.0	16	38.2	38.4	38.2	16	38.4	16
79215	CB1	85.0	19	32.2	33.2	34.2	14	34.8	14
79215	CB4	66.0	19	32.2	33.2	34.2	14	34.8	14
79215	CHL	79.0	16	24.8	25.0	31.1	8	32.0	8
79215	CHR	100.0	17	51.3	52.0	51.3	17	52.0	17
79215	CHS	60.2	12	29.2	33.8	31.9	13	35.3	9
79215	CHT	83.0	13	50.1	54.3	51.9	14	55.9	14
79215	CHV	64.0	14	52.5	55.0	56.2	13	58.9	13
79215	CKY	66.0	15	33.5	36.4	33.5	15	36.4	15
79215	CL2	63.0	12	39.1	39.9	51.7	18	52.8	18
79215	CLK	105.0	15	33.2	36.0	34.2	20	36.2	9
79215	CM1	89.0	13	41.3	45.1	59.2	15	64.5	16
79215	CM3	84.0	14	32.0	33.7	41.2	12	43.4	12
79215	CNE	159.0	16	41.5	41.4	47.7	19	47.7	19
79215	CPE	105.0	18	38.1	38.5	42.2	23	42.8	23
79215	DAN	120.0	16	38.7	38.8	49.5	17	49.7	17
79215	DC1	15.0	10	39.9	41.1	39.9	10	41.1	10
79215	DC4	10.0	15	70.0	72.3	70.0	15	72.3	15
79215	DC5	125.0	16	41.4	43.9	56.2	13	58.9	13
79215	DC6	100.0	17	40.2	42.0	56.2	13	58.9	13
79215	DNR	95.0	16	26.7	27.3	33.1	7	34.5	7

DATE	SITE	c_{ob}^{max}	h_{ob}^{max}	$c_{p0}(h_{ob}^{max})$	$c_{p1}(h_{ob}^{max})$	c_{p0}^{max}	h_{p0}^{max}	c_{p1}^{max}	h_{p1}^{max}
79215	DOW	96.0	14	31.9	37.1	33.2	15	37.5	15
79215	DRB	104.0	15	33.7	34.1	85.0	19	86.0	19
79215	DT3	43.9	15	44.5	44.9	72.7	10	73.4	10
79215	DT4	25.0	15	30.1	30.2	70.2	9	71.1	9
79215	EB1	75.0	15	46.0	46.9	59.0	10	61.0	10
79215	EB2	62.0	15	46.0	46.9	59.0	10	61.0	10
79215	ERE	95.0	14	39.6	39.7	40.0	15	40.1	16
79215	ESS	63.3	17	36.5	36.5	37.2	7	37.2	8
79215	ESX	80.0	15	25.3	25.4	31.0	6	31.6	7
79215	EXC	67.0	23	36.1	38.5	38.8	18	39.3	17
79215	EY1	75.0	17	40.2	42.3	42.8	16	45.4	15
79215	FDR	100.0	13	35.3	37.0	38.5	15	40.9	16
79215	FLN	57.7	12	35.7	37.3	35.7	11	37.4	11
79215	FX1	92.3	14	52.4	52.9	54.3	13	54.8	13
79215	FX2	115.0	14	68.2	71.7	81.7	17	87.1	16
79215	GAR	78.0	14	41.7	42.7	42.6	17	43.3	17
79215	GLN	65.0	15	43.8	45.3	43.8	15	45.3	15
79215	GLO	102.0	14	38.9	40.1	50.0	17	50.9	17
79215	GMT	45.0	10	35.0	37.5	39.2	18	40.5	17
79215	GRE	38.0	18	22.5	22.6	36.4	6	36.8	6
79215	GRG	69.0	12	39.1	40.4	52.6	16	53.4	16
79215	GRW	130.0	14	88.5	89.7	95.0	15	96.7	15
79215	HAR	69.0	17	41.8	43.6	44.5	18	44.6	18
79215	HF2	100.0	14	27.2	27.5	38.0	11	38.6	11
79215	HGR	46.0	13	31.0	35.3	32.6	9	36.2	16
79215	HM1	54.0	11	10.2	10.6	24.6	20	25.1	20
79215	HML	68.0	17	47.2	47.9	48.0	22	48.8	22
79215	HRP	63.0	12	34.6	37.6	34.6	12	37.6	12
79215	JNS	65.0	16	26.3	27.6	30.1	9	33.6	9
79215	KCH	76.0	17	31.4	33.9	64.9	21	68.2	21
79215	KNT	115.0	13	35.9	36.2	40.7	17	41.0	17
79215	LAN	56.0	16	33.5	40.7	43.1	20	45.9	20
79215	LEX	70.0	14	47.4	49.1	54.6	15	55.3	15
79215	LIC	76.0	16	47.5	48.4	54.6	15	55.3	15
79215	LIV	39.8	12	38.0	38.5	39.3	16	39.9	16
79215	LND	64.0	13	66.6	72.8	119.0	21	122.0	21
79215	MAM	54.0	15	95.0	96.7	95.0	15	96.7	15
79215	MCL	50.0	13	38.3	40.9	38.3	13	41.3	12
79215	MED	50.0	9	39.8	40.9	39.8	9	40.9	9
79215	MER	102.0	12	31.7	35.3	40.1	15	44.0	16
79215	MFD	66.0	14	53.9	56.0	53.9	14	56.0	14
79215	MN1	75.0	17	33.2	34.1	37.3	15	37.7	15
79215	MNR	61.0	17	33.2	35.4	34.4	12	36.3	11
79215	MRC	69.0	14	33.7	37.7	33.8	13	37.7	13
79215	MSG	70.0	15	48.9	48.6	56.8	10	56.4	10
79215	N10	123.0	12	44.7	45.7	65.7	15	67.3	15
79215	NC1			MISSING	DATA				
79215	NC4	92.0	12	35.1	36.6	45.9	20	48.6	20
79215	NCL	31.0	18	35.6	37.9	37.0	17	39.2	17

DATE	SITE	c_{ob}^{max}	h_{ob}^{max}	$c_{p0}(h_{ob}^{max})$	$c_{p1}(h_{ob}^{max})$	c_{p0}^{max}	h_{p0}^{max}	c_{p1}^{max}	h_{p1}^{max}
79215	NG2	72.0	17	40.0	40.1	40.0	17	40.3	18
79215	NH2	30.0	8	29.9	30.7	31.4	7	32.1	7
79215	NRS	110.0	14	37.4	41.8	46.6	18	52.9	18
79215	NY2	87.0	13	31.3	31.9	39.5	18	40.0	18
79215	NY4	101.0	12	47.1	47.8	59.4	16	59.8	16
79215	NY5	83.0	13	53.2	53.9	59.4	16	59.8	16
79215	NYK	48.0	13	53.8	53.6	72.2	11	72.4	11
79215	OCN	95.0	11	38.0	42.7	42.5	15	45.3	15
79215	OK1	64.0	13	41.1	42.7	42.0	16	43.8	16
79215	ORO	98.0	16	92.5	99.3	104.0	14	110.0	14
79215	OSH	55.0	16	58.0	57.6	93.7	12	93.6	12
79215	P10	80.0	16	48.7	55.3	54.4	15	55.5	15
79215	PAI	54.0	13	41.2	41.3	47.7	19	48.2	19
79215	PH1	80.0	12	35.3	38.0	59.2	15	64.5	16
79215	PH2	90.0	12	35.1	35.9	54.4	15	55.5	15
79215	PH4	60.0	15	46.0	48.3	51.9	14	55.9	14
79215	PH5	60.0	12	35.1	35.9	54.4	15	55.5	15
79215	PH6	40.0	12	46.0	49.1	51.9	14	55.9	14
79215	PH7	110.0	12	35.3	38.0	59.2	15	64.5	16
79215	PH8			MISSING DATA					
79215	PLY	50.0	13	39.3	39.9	39.3	13	39.9	13
79215	POU	41.0	17	3.8	4.0	32.6	9	33.6	9
79215	PRH	65.3	13	66.6	67.2	89.1	16	89.9	16
79215	PT2	76.0	15	29.4	29.4	29.5	16	29.6	16
79215	PTG	77.0	14	32.2	33.3	38.8	17	40.2	17
79215	PTR	87.0	16	116.0	120.0	116.0	16	120.0	16
79215	PTS	62.0	14	10.3	10.4	23.1	7	23.5	7
79215	PV3	75.0	13	36.7	38.6	40.7	19	41.9	19
79215	RDG	36.0	14	33.5	36.7	36.7	17	40.2	17
79215	REN	78.0	15	10.9	11.4	26.1	7	26.4	7
79215	RVB	73.0	13	31.7	32.7	34.0	12	35.6	12
79215	SC1	113.0	13	37.2	39.5	41.3	16	42.4	16
79215	SCH	71.0	14	38.4	38.8	38.4	14	38.9	13
79215	SCR	66.0	15	51.0	50.9	72.2	11	72.4	11
79215	SMC	84.0	14	39.7	41.4	46.4	23	48.0	23
79215	SMV	51.0	13	41.2	43.2	46.8	23	49.1	23
79215	SR2	100.0	12	57.1	57.4	89.1	16	89.9	16
79215	STC	72.0	17	39.4	40.4	40.9	23	41.7	23
79215	STH	26.5	12	42.8	43.9	45.2	10	46.5	10
79215	STU	100.0	17	22.4	23.1	29.4	13	30.4	13
79215	STV	81.0	15	58.9	66.0	68.6	13	77.0	13
79215	SVC	97.4	14	52.4	52.9	54.3	13	54.8	13
79215	SY1	72.0	15	23.6	24.1	36.8	10	38.0	10
79215	SY2	78.0	15	23.6	24.1	36.8	10	38.0	10
79215	SY4	78.0	15	23.6	24.1	36.8	10	38.0	10
79215	TL1	70.0	19	34.9	35.9	42.5	11	43.5	11
79215	TL4	65.0	14	37.3	38.1	40.3	12	41.1	12
79215	TR1	64.0	17	40.6	41.7	59.0	10	61.0	10
79215	TR2	41.0	11	72.2	72.4	72.2	11	72.4	11

DATE	SITE	c_{ob}^{max}	h_{ob}^{max}	$c_{p0}(h_{ob}^{max})$	$c_{p1}(h_{ob}^{max})$	c_{p0}^{max}	h_{p0}^{max}	c_{p1}^{max}	h_{p1}^{max}
79215	TRN	81.0	13	36.9	37.3	55.9	17	58.4	17
79215	UTC	83.0	17	37.5	38.7	38.2	18	39.2	18
79215	VIN	77.0	13	29.4	33.6	35.6	20	38.1	20
79215	WH2	69.9	18	23.2	25.1	30.4	10	32.9	8
79215	WLK	72.0	13	29.8	31.9	33.0	9	35.2	6
79215	WNS	92.0	10	65.9	66.6	65.9	10	66.6	10
79215	WO1	52.0	15	53.7	54.4	57.0	17	57.8	17
79215	WO2	65.0	18	55.1	55.8	57.0	17	57.8	17
79215	WRN	62.2	13	53.4	53.8	57.2	12	57.8	12
79215	YG2	70.0	16	36.1	36.9	37.2	17	38.0	17
79216	AA1	94.0	13	35.6	37.1	36.7	12	38.3	12
79216	AA2	88.0	12	36.7	38.3	36.7	12	38.3	12
79216	AC1	73.0	11	85.8	87.1	127.0	14	130.0	15
79216	AG4	78.0	13	36.8	36.8	39.4	18	39.6	18
79216	AGA	90.0	13	36.6	37.6	42.5	15	43.5	15
79216	AK1	80.0	13	32.8	33.0	46.9	19	47.5	19
79216	ALN	75.0	17	28.0	29.9	32.2	7	34.5	7
79216	ALX	75.0	11	41.9	43.2	50.4	14	52.1	14
79216	AMH	77.0	22	80.5	81.5	88.3	18	90.2	18
79216	AMR	68.0	16	15.1	15.4	28.1	3	29.2	3
79216	ARL	100.0	12	45.3	46.7	50.4	14	52.1	14
79216	BAB	58.0	12	85.4	87.1	85.9	11	88.3	11
79216	BAD	43.0	14	45.7	46.9	47.2	15	48.1	15
79216	BAY	71.0	12	9.1	9.1	35.1	10	35.6	10
79216	BER	84.0	11	40.5	42.1	56.4	15	59.0	15
79216	BET	75.0	14	23.2	24.3	28.2	21	29.9	21
79216	BL1	71.0	15	39.8	40.0	42.6	17	42.9	17
79216	BL3	67.0	15	39.8	40.0	42.6	17	42.9	17
79216	BL6	96.0	12	35.8	36.6	39.0	18	39.8	19
79216	BLG	57.0	11	84.6	85.5	109.0	15	110.0	15
79216	BN1	76.0	9	40.4	41.2	41.7	14	42.8	16
79216	BNG	88.0	11	36.6	36.5	48.2	18	48.3	18
79216	BNW	50.0	15	92.9	99.8	95.3	13	102.0	12
79216	BR2	68.0	12	16.6	16.8	32.3	3	33.2	3
79216	BRI	123.0	19	14.3	16.8	42.6	0	45.9	4
79216	BTH	80.0	13	41.1	42.9	41.1	13	42.9	13
79216	BUL	105.0	17	75.9	82.7	86.7	16	93.6	16
79216	BVF	28.0	14	45.7	46.9	47.2	15	48.1	15
79216	CAN	50.0	15	38.9	39.1	43.6	18	43.9	18
79216	CB1	75.0	15	32.2	32.8	34.1	12	34.9	12
79216	CB4	64.0	16	32.6	33.4	34.1	12	34.9	12
79216	CHL	85.0	16	17.0	17.3	20.7	18	21.0	18
79216	CHR	75.0	15	19.9	20.3	22.0	11	22.4	11
79216	CHS	77.0	16	15.3	16.6	29.5	0	31.8	9
79216	CHT	78.0	15	47.8	51.4	47.8	15	51.4	15
79216	CHV	78.0	13	41.1	42.9	41.1	13	42.9	13
79216	CKY	97.0	14	35.0	37.1	41.0	17	43.4	17
79216	CL2	108.0	13	50.6	51.5	54.6	19	56.7	20
79216	CLK	90.0	17	33.7	36.5	34.0	12	37.1	13

DATE	SITE	c_{ob}^{max}	h_{ob}^{max}	$c_{p0}(h_{ob}^{max})$	$c_{p1}(h_{ob}^{max})$	c_{p0}^{max}	h_{p0}^{max}	c_{p1}^{max}	h_{p1}^{max}
79216	CM1	90.0	12	47.0	51.7	55.9	16	60.3	16
79216	CM3	102.0	17	95.2	99.7	99.7	16	105.0	16
79216	CNE	136.0	15	58.7	58.6	68.8	23	69.1	23
79216	CPE	55.0	10	45.4	47.1	57.4	13	58.2	13
79216	DAN	79.0	15	0.4	0.4	19.9	1	20.6	1
79216	DC4	25.0	13	48.2	49.7	50.4	14	52.1	14
79216	DC5	140.0	13	41.1	42.9	41.1	13	42.9	13
79216	DC6	95.0	15	38.1	39.7	41.1	13	42.9	13
79216	DNR	91.0	10	21.1	21.7	21.1	10	21.7	10
79216	DOW	80.0	13	36.5	41.7	39.6	14	44.6	15
79216	DRB	66.0	12	1.6	1.6	25.4	4	26.7	4
79216	DT3	68.9	13	78.8	79.4	78.8	13	79.4	13
79216	DT4	38.8	13	60.1	60.9	92.5	10	93.7	10
79216	EB1	82.0	12	67.8	69.7	68.6	11	70.8	11
79216	EB2	78.0	11	68.6	70.8	68.6	11	70.8	11
79216	ELM	2.0	23	62.7	65.3	62.7	23	65.3	23
79216	ERE	88.0	16	66.1	66.3	68.8	15	68.9	15
79216	ESS	62.2	13	37.2	37.2	37.3	9	37.3	9
79216	ESX	98.0	16	42.0	42.3	42.6	17	42.9	17
79216	EXC	95.0	22	40.3	44.0	44.1	17	44.6	17
79216	EY1	125.0	11	48.0	50.0	62.3	18	65.1	18
79216	FDR	100.0	13	31.1	32.6	33.9	10	35.2	10
79216	FLN	64.3	12	35.7	37.5	36.3	13	38.4	9
79216	FX1	128.0	12	40.4	40.8	40.7	13	41.4	13
79216	FX2	117.0	12	49.5	52.7	49.5	12	52.7	12
79216	GAR	78.0	14	13.6	14.1	23.9	0	24.2	0
79216	GLN	91.0	13	42.5	44.5	43.7	16	47.6	18
79216	GLO	33.0	16	56.2	57.5	57.2	17	59.0	17
79216	GMT	75.0	13	42.3	43.8	43.0	15	44.8	16
79216	GRE	40.0	1	22.4	23.7	25.6	0	26.1	0
79216	GRG	37.0	9	25.3	26.1	52.3	17	55.4	15
79216	GRW	65.0	11	15.7	15.9	58.5	0	62.0	0
79216	HAR	85.0	14	41.9	41.7	43.8	12	43.7	12
79216	HF2	85.0	14	40.5	41.7	41.6	13	42.5	13
79216	HGR	51.0	15	24.8	26.7	28.4	2	31.4	2
79216	HM1	30.0	9	70.0	72.5	70.0	9	72.5	9
79216	HML	60.0	21	68.5	69.2	109.0	15	110.0	15
79216	JNS	76.0	16	23.1	24.5	23.1	16	24.6	15
79216	KCH	75.0	23	44.1	46.5	73.2	8	86.4	7
79216	KNT	50.0	2	24.7	24.9	100.0	14	102.0	13
79216	LAN	66.0	18	46.2	49.5	49.4	16	52.5	16
79216	LEX	60.0	17	46.9	48.2	49.4	16	50.7	16
79216	LIC	69.0	17	46.9	48.2	49.4	16	50.7	16
79216	LIV	66.8	12	37.8	38.3	46.1	18	47.0	18
79216	LND	73.0	18	45.8	59.0	99.7	0	107.0	0
79216	MAM	23.0	16	2.1	2.1	35.5	3	36.5	3
79216	MCL	67.9	12	36.4	38.3	37.2	13	39.4	13
79216	MER	144.0	16	53.0	58.9	53.0	16	58.9	16
79216	MFD	29.0	15	34.8	36.8	39.2	12	40.1	12

DATE	SITE	c_{ob}^{max}	h_{ob}^{max}	$c_{p0}(h_{ob}^{max})$	$c_{p1}(h_{ob}^{max})$	c_{p0}^{max}	h_{p0}^{max}	c_{p1}^{max}	h_{p1}^{max}
79216	MN1	96.0	11	22.8	23.3	34.7	19	36.0	18
79216	MNR	69.0	14	45.2	48.7	62.1	18	66.1	18
79216	MRC	53.0	17	47.5	55.7	48.2	16	55.7	17
79216	MSG	76.0	10	95.2	94.6	107.0	17	107.0	17
79216	N10	89.0	13	25.6	26.5	45.1	10	46.2	10
79216	NC1	100.0	16	41.0	43.5	41.0	16	43.5	16
79216	NC4	94.0	14	52.9	54.7	52.9	14	55.3	15
79216	NCL	38.0	18	44.2	47.1	50.1	16	53.7	16
79216	NG2	83.0	23	98.7	99.9	107.0	19	107.0	19
79216	NRS	76.0	13	32.7	36.2	32.7	13	36.2	13
79216	NY2	67.0	11	32.5	33.2	32.5	11	33.2	11
79216	NY4	45.0	10	35.1	35.6	35.1	10	35.6	10
79216	NY5	50.0	11	27.1	27.4	35.1	10	35.6	10
79216	NYK	55.0	12	84.7	84.9	85.1	11	85.3	11
79216	OCN	85.0	13	48.5	54.2	52.7	15	59.7	15
79216	OK1	54.0	12	79.1	83.7	90.4	15	94.7	15
79216	ORO	101.0	15	31.3	33.4	62.3	10	65.7	10
79216	OSH	79.0	12	98.4	98.4	99.7	13	99.6	13
79216	P10	90.0	18	27.7	28.3	42.9	14	43.6	14
79216	PAI	62.0	15	49.6	49.8	68.7	19	71.6	20
79216	PH1	90.0	18	31.8	35.2	55.9	16	60.3	16
79216	PH2	90.0	16	32.8	33.3	42.9	14	43.6	14
79216	PH4	70.0	13	35.6	38.2	47.8	15	51.4	15
79216	PH5	60.0	18	27.7	28.3	42.9	14	43.6	14
79216	PH6	40.0	18	33.5	36.2	47.8	15	51.4	15
79216	PH7	130.0	18	31.8	35.2	55.9	16	60.3	16
79216	PLY	65.0	11	39.9	40.5	42.0	14	43.0	15
79216	POU	42.0	18	11.0	12.0	31.2	8	32.6	8
79216	PRH	63.8	18	69.4	70.0	75.3	16	77.6	16
79216	PT2	76.0	14	37.6	37.5	42.1	17	42.2	17
79216	PTG	87.0	11	31.2	32.5	46.3	23	47.6	23
79216	PTR	99.0	18	82.9	85.3	85.0	17	87.9	16
79216	PTS	71.0	14	13.9	14.3	25.4	12	26.0	12
79216	PV3	32.7	2	27.0	28.0	36.5	6	39.7	6
79216	RDG	54.0	16	33.5	35.3	37.1	10	39.3	10
79216	REN	105.0	15	23.6	24.1	32.4	19	33.2	19
79216	RVB	96.0	14	46.3	47.4	46.3	13	47.4	14
79216	SC1	99.0	14	37.2	37.9	38.3	15	39.1	15
79216	SCH	85.0	12	50.6	51.7	55.5	16	56.4	16
79216	SCR	83.0	13	82.0	82.4	85.1	11	85.3	11
79216	SMC	85.0	18	84.5	90.2	95.6	15	101.0	15
79216	SMV	112.0	17	23.8	25.5	48.1	3	49.9	2
79216	SR2	99.0	18	69.4	70.0	75.3	16	77.6	16
79216	STC	59.0	12	73.7	75.9	104.0	18	107.0	18
79216	STH	68.4	13	39.2	40.6	64.5	18	66.6	18
79216	STU	96.0	12	33.9	35.1	38.5	17	39.8	16
79216	STV	89.0	13	36.4	41.8	36.7	12	41.8	13
79216	SVC	110.0	12	40.4	40.8	40.7	13	41.4	13
79216	SY1	84.0	16	38.9	39.5	41.7	20	42.8	20

DATE	SITE	c_{ob}^{max}	h_{ob}^{max}	$c_{p0}(h_{ob}^{max})$	$c_{p1}(h_{ob}^{max})$	c_{p0}^{max}	h_{p0}^{max}	c_{p1}^{max}	h_{p1}^{max}
79216	SY2	91.0	16	38.9	39.5	41.7	20	42.8	20
79216	SY4	91.0	16	38.9	39.5	41.7	20	42.8	20
79216	TL1	95.0	14	40.0	41.0	41.7	13	42.9	13
79216	TL4	100.0	12	41.4	42.6	41.7	13	42.9	13
79216	TR1	92.0	12	67.8	69.7	68.6	11	70.8	11
79216	TR2	65.0	13	82.0	82.4	85.1	11	85.3	11
79216	TRN	125.0	17	42.1	42.5	56.3	16	57.0	16
79216	UTC	104.0	16	41.4	42.2	41.4	16	42.4	19
79216	VIN	132.0	13	50.7	56.8	86.1	20	101.0	19
79216	WH2	63.8	14	36.5	39.3	40.0	16	43.0	16
79216	WLK	73.0	13	28.0	29.2	32.4	9	33.8	9
79216	WNS	74.0	11	89.0	89.9	92.5	10	93.7	10
79216	WO1	55.0	16	28.2	28.9	29.1	17	29.7	17
79216	WO2	68.0	17	29.1	29.7	29.1	17	29.7	17
79216	WRN	100.0	15	58.3	58.9	78.8	13	79.4	13
79216	WSL	120.0	10	40.1	40.1	75.9	15	76.0	15
79216	YG2	81.0	15	36.2	37.2	39.8	19	41.2	19

GLOSSARY

Symbol	Definition
c_{ob}	Observed hour-average O_3 concentration at a given receptor at a given hour
${}^{R}\overline{c}_{ob}$	Average value of c_{ob} over all receptors at a given hour
c_{ob}^{max}	Maximum value of c_{ob} during a daily period at a given receptor
${}^{R}\overline{c}_{ob}^{max}$	Average value of c_{ob}^{max} over all receptors at a given hour
c_{po}	Predicted ROM1 layer 0 hour-average O_3 concentration interpolated to a given receptor location at a given hour
${}^{R}\overline{c}_{p0}$	Average value of c_{p0} over all receptors at a given hour
c_{p0}^{max}	Maximum value of c_{p0} during a daily period at a given receptor location
${}^{R}\overline{c}_{p0}^{max}$	Average value of c_{p0}^{max} over all receptors at a given hour
$c_{p0}(h_{ob}^{max})$	Value of c_{p0} at the hour of occurence of c_{ob}^{max}
${}^{R}\overline{c}_{p0}(h_{ob}^{max})$	Average value of $c_{p0}(h_{ob}^{max})$ over all receptors at a given hour
c_{p1}	Predicted ROM1 layer 1 hour-average O_3 concentration interpolated to a given receptor location at a given hour
${}^{R}\overline{c}_{p1}$	Average value of c_{p1} over all receptors at a given hour
c_{p1}^{max}	Maximum value of c_{p1} during a daily period at a given receptor location
${}^{R}\overline{c}_{p1}^{max}$	Average value of c_{p1}^{max} over all receptors at a given hour
$c_{p1}(h_{ob}^{max})$	Value of c_{p1} at the hour of occurrence of c_{ob}^{max}
${}^{R}\overline{c}_{p1}(h_{ob}^{max})$	Average value of $c_{p1}(h_{ob}^{max})$ over all receptors at a given hour

Symbol	Definition
c_{p1-A}^{max}	Maximum ROM1 layer 1 predicted O_3 concentration during a daily period at the same receptor location where c_{ob}^{max} occurred within a given O_3 plume
c_{p1-B}^{max}	Maximum ROM1 layer 1 predicted O_3 concentration during a daily period at any receptor location within or near a given O_3 plume
c_{p1-C}^{max}	Maximum ROM1 layer 1 predicted O_3 concentration during a daily period at any grid cell within or near a given O_3 plume
d_0	$= c_{ob}-c_{p0}$. Residual difference (bias) between observed and predicted O_3 concentrations at a given receptor location at a given hour
${}^{R}\overline{d_0}$	Average value of d_0 over all receptors at a given hour
${}^{R}\overline{\lvert d_0 \rvert}$	Average value of absolute d_0 values (gross error) over all receptors at a given hour
d_{A0}^{max}	$= c_{ob}^{max} - c_{p0}(h_{ob}^{max})$
${}^{R}\overline{d_{A0}^{max}}$	Average value of d_{A0}^{max} over all receptors at a given hour
d_{B0}^{max}	$= c_{ob}^{max} - c_{p0}^{max}$
${}^{R}\overline{d_{B0}^{max}}$	Average value of d_{B0}^{max} over all receptors at a given hour
d_1	$= c_{ob} - c_{p1}$. Residual difference (bias) betwen observed and predicted O_3 concentrations at a given receptor location at a given hour
${}^{R}\overline{d_1}$	Average value of d_1 over all receptors at a given hour
${}^{R}\overline{\lvert d_1 \rvert}$	Average value of absolute d_1 values (gross error) over all receptors at a given hour
d_{A1}^{max}	$= c_{ob}^{max} - c_{p1}(h_{ob}^{max})$
${}^{R}\overline{d_{A1}^{max}}$	Average value of d_{A1}^{max} over all receptors at a given hour
d_{B1}^{max}	$= c_{ob}^{max} - c_{p1}^{max}$
${}^{R}\overline{d_{B1}^{max}}$	Average value of d_{B1}^{max} over all receptors at a given hour

Symbol	Definition
d^{max}_{p1-A}	$= c^{max}_{ob} - c^{max}_{p1-A}$
d^{max}_{p1-B}	$= c^{max}_{ob} - c^{max}_{p1-B}$
d^{max}_{p1-C}	$= c^{max}_{ob} - c^{max}_{p1-C}$
$(d^{max}_{p1-A}/c^{max}_{ob})X\ 100$	Percent bias between c^{max}_{ob} and c^{max}_{p1-A}
$(d^{max}_{p1-B}/c^{max}_{ob})X\ 100$	Percent bias between c^{max}_{ob} and c^{max}_{p1-B}
$(d^{max}_{p1-C}/c^{max}_{ob})X\ 100$	Percent bias between c^{max}_{ob} and c^{max}_{p1-C}
h^{max}_{ob}	Hour of occurrence of c^{max}_{ob}
h^{max}_{p0}	Hour of occurrence of c^{max}_{p0}
h^{max}_{p1}	Hour of occurrence of c^{max}_{p1}
n	Number of receptor monitoring sites for O_3 reporting values at a given hour
$R_{S_{d0}}$	Standard deviation of the residual differences (noise) over all receptors at a given hour for ROM1 layer 0
$R_{S_{d1}}$	Standard deviation of the residual differences (noise) over all receptors at a given hour for ROM1 layer 1
$R_{S^{max}_{dA0}}$	Standard deviation of d^{max}_{A0} over all receptor locations
$R_{S^{max}_{dA1}}$	Standard deviation of d^{max}_{A1} over all receptor locations
$R_{S^{max}_{dB0}}$	Standard deviation of d^{max}_{B0} over all receptor locations
$R_{S^{max}_{dB1}}$	Standard deviation of d^{max}_{B1} over all receptor locations

TECHNICAL REPORT DATA
(Please read Instructions on the reverse before completing)

1. REPORT NO.	2.	3. RECIPIENT'S ACCESSION NO.
4. TITLE AND SUBTITLE EPA REGIONAL OXIDANT MODEL: ROM1 EVALUATION FOR 3-4 AUGUST 1979		5. REPORT DATE 6. PERFORMING ORGANIZATION CODE
7. AUTHOR(S) Kenneth L. Schere		8. PERFORMING ORGANIZATION REPORT NO.
9. PERFORMING ORGANIZATION NAME AND ADDRESS (same as 12.)		10. PROGRAM ELEMENT NO. CDWA1A/02-4021 (FY-86) 11. CONTRACT/GRANT NO.
12. SPONSORING AGENCY NAME AND ADDRESS ATMOSPHERIC SCIENCES RESEARCH LABORATORY - RTP, NC OFFICE OF RESEARCH AND DEVELOPMENT U.S. ENVIRONMENTAL PROTECTION AGENCY RESEARCH TRIANGLE PARK, NC 27711		13. TYPE OF REPORT AND PERIOD COVERED In-house 14. SPONSORING AGENCY CODE EPA/600/09

15. SUPPLEMENTARY NOTES

16. ABSTRACT

The first generation U.S. Environmental Protection Agency Regional Oxidant Model (ROM1) has been tested and evaluated for O_3 predictions on a two-day test case episode in the northeast U.S. during 3-4 August 1979. The period was characterized by relatively high O_3 concentrations in the southern Great Lakes area where clear skies persisted. The highest observed hour-average O_3 level monitored at a surface site during the period was 159 ppb. The ROM1 incorporates some simplifying assumptions and algorithms as compared to the second generation version, ROM2, which is in preliminary testing stages now and will eventually become the production version of the model. Evaluation results for this test episode showed that the ROM1 had approximately a 6% average underprediction of O_3 when all hours and surface monitoring sites were considered. When the data were restricted to only those observed and predicted pairs of O_3 values greater than 50 ppb the average performance improved to a 1% underprediction. The evaluation aspect concerned with estimating maximum daily O_3 values showed a 8% average underprediction of the maximum value for the restricted data subset. An analysis of individual O_3 plumes during the episode showed average model performance for predicting the plume maximum concentration level to lie between 22% underprediction and 38% overprediction.

17. KEY WORDS AND DOCUMENT ANALYSIS

a. DESCRIPTORS	b. IDENTIFIERS/OPEN ENDED TERMS	c. COSATI Field/Group

18. DISTRIBUTION STATEMENT RELEASE TO PUBLIC	19. SECURITY CLASS *(This Report)* UNCLASSIFIED 20. SECURITY CLASS *(This page)* UNCLASSIFIED	21. NO. OF PAGES 22. PRICE

EPA Form 2220-1 (Rev. 4-77) PREVIOUS EDITION IS OBSOLETE